Development of Dual Gas Diffusion-Type Biofuel Cells on the Basis of Electrochemical Understanding of Enzyme-Modified Electrodes

Keisei So

2017

Table of Contents

General Introduction

Bioelectrocatalysis, in which an enzyme reaction and an electrode reaction are coupled, is a key process for several electrochemical devices such as biofuel cells, biosensors, and bioreactors. The reaction is classified into two types: mediated electron transfer (MET) and direct electron transfer (DET). In the MET-type system, an artificial redox mediator shuttles electrons between an electrode and an enzyme. In the DET-type system, an enzyme itself directly communicates with an electrode.

Biofuel cells are sustainable and environmentally friendly energy conversion systems in which enzymes are utilized as biocatalysts. The devices are constructed with enzyme modified bioanodes and biocathodes. Due to the characteristics of the enzyme reaction, the power device can operate under very mild and safe conditions, e.g., at neutral pH, room temperature, and atmospheric pressure. Moreover, the device does not require precious metals such as Pt, since the active sites in enzymes consist of nonprecious metals (e.g., Cu, Ni, Fe, Mo, and W) or organic compounds (e.g., nicotinamide adenine dinucleotide, flavin adenine dinucleotide, and quinones).

Regarding the performance of MET-type biofuel cells, mediators can minimize the kinetic barrier in the electron transfer between redox enzymes and electrodes. However, this often incurs a thermodynamic loss in order to create a driving force for the electron transfer between an enzyme and an electrode and thus decreases the operating potential of biofuel cells. Conversely, in DET-type biofuel cells, an enzyme directly communicates with an electrode. As a result, this makes it possible to minimize the thermodynamic loss in the electron transfer between an enzyme and an electrode

In this research, the author aimed to construct a DET-type H_2/O_2 biofuel cell. Bilirubin oxidase (BOD) and two kinds of [NiFe]-hydrogenases are used for a cathodic enzyme and anodic enzymes, respectively. BOD is one of the multi copper oxidases and is a promising enzyme for DET-type biocathodes to reduce O_2 into H_2O. BOD has high bioelectrocatalytic activity even at neutral pH, and its formal potential is relatively close to that of the H_2O/O_2 redox couple. Among hydrogenases, O_2-tolerant and standard [NiFe]-hydogenases are suitable enzymes which can realize DET-type bioelectrocatalytic oxidation of H_2 oxidation with high turnover rate.

In chapter 1, the author focused on the DET-type bioelectrocatalysis with BOD. In the case of BOD, it is very important to control the orientation of BOD on the electrode surface because the interfacial electron transfer rate constant of BOD is not so fast. Since the rate constant increases exponentially upon decreasing the distance between the electrode surface and the redox site of the enzyme, the author developed some methods to achieve favorite orientation of BOD onto the electrode surface. In addition, the author investigated the electrochemical characteristics of BOD from the viewpoint of bioelectrochemisty.

In chapter 2, the author constructed gas diffusion-type electrodes. In dissolved system, the

low solubility and low diffusion coefficients of O_2 and H_2 cause limitations in the catalytic current and result in a decrease in power of H_2/O_2 biofuel cells. Gas diffusion type electrodes which can supply a gaseous substrates from the gas phase can get rid of the problems. Thus, the author created new types of gas diffusion-type electrodes with some carbon materials and improved the mass-transfer rates at bioanodes and biocathodes. Moreover, the gas diffusion-type system is also useful to solve a problem of [NiFe]-hydrogenases. When [NiFe]-hydrogenases suffer from high oxidative stress at high potentials, they form inactive state. This phenomenon is called “oxidative inactivation” and causes power decay of H_2/O_2 biofuel cells. Judging from its mechanism, the inactivation can be considered to compete with H_2 binding. Since the gas diffusion electrode can maintain high substrate concentrations near the active enzyme on the electrode, the author tried to avoid the inactivation by using the electrode.

In chapter 3, the author constructed a DET-type dual gas diffusion H_2/O_2 biofuel cell system by combining the BOD modified biocathode and the [NiFe]-hydrogenase modified bioanode. This attempt is the first example in the field of biofuel cells.

Chapter 1

Electrochemical Understanding and Improvement of Direct Electron Transfer-Type Bioelectrocatalysis with Bilirubin Oxidase

1-1. Improvement of a direct electron transfer-type fructose/dioxygen biofuel cell with a substrate-modified biocathode

Abstract

Fructose/dioxygen biofuel cell, one of the direct electron transfer (DET)-type bioelectrochemical devices, utilizes fructose dehydrogenase (FDH) on the anode and multi-copper oxidase such as bilirubin oxidase (BOD) on the cathode as the catalysts. The power density in the literature is limited by the biocathode performance. The author shows that the DET-type biocathode performance is greatly improved, when bilirubin or some related substances is adsorbed on electrodes before the BOD adsorption. Several data support that the substrate modification induces the proper orientation of BOD on the electrode surface for the DET. The substrate-modification method has successfully been applied to air-breathing gas-diffusion-type biocathodes. The author has also optimized the conditions of the FDH adsorption on carbon cryogel electrodes. Finally, a one-compartment DET-type biofuel cell without separators has been constructed, and the maximum power density has reached 2.6 mW cm^{-2} at 0.46 V of the cell voltage under quiescent (passive) and air atmospheric conditions.

1. Introduction

Biofuel cells, which are electric generators that utilize redox enzymes as catalysts, are very secure devices due to the enzyme reactions that can operate under mild conditions (room temperature, atmospheric pressure and neutral pH).[1–6] Generally, enzymes in the biofuel cells oxidize several biologically related reductants such as alcohols, sugars, amines, organic acids, or hydrogen at the anode and reduce dioxygen at the cathode. There are two types of electric connection between enzymes and electrodes to realize bioelectrocatalysis. One is mediated electron transfer (MET) type, in which the mediator shuttle the electron between the enzyme and the electrode to reduce the kinetic hindrance in the interfacial electron transfer (ET). The other is direct electron transfer (DET) type, in which the enzyme can directly transfer the electron to or from the electrode.

Although the number of redox enzymes capable of direct communication with electrodes is limited, many researchers pay attention to the DET-type enzymatic biofuel cell, since it has several advantages over the MET-type one. Mediator-less configuration does not require, in principle, any

separator or membrane between the electrodes, which leads to simplifications in the cell construction. In addition, the DET-type cell can reduce the possible health hazard problems due to artificial mediators and thermodynamic losses arising from the difference in the redox potentials between the mediator and the active site (strictly speaking, the electron donating site to or accepting site from the second redox substrate) of the (multi-redox site-having) enzyme.[1,7] In terms of the advanced application, DET-type enzymatic biofuel cells can be powering of micro–electronic devices extracting energy from biological sources and will be related to implantable biofuel cells operating *in vivo* and providing power for implantable biomedical devices. [8–12]

Fructose/dioxygen (O_2) biofuel cell is one of DET-type enzymatic devices.[13–15] It utilizes a heterotrimetric flavoprotein-cytochrome *c* complex, fructose dehydrogenase (FDH) on the anode and multi-copper oxidase (MCO) on the cathode as the catalysts. FDH catalyzes 2-electron oxidation of D-fructose to 5-keto-D-fructose[16] at the FAD catalytic center, and the electrons are transferred to electrodes via the heme C-containing subunit.[17] FDH from *Gluconobactor japonicus* NBRC3260 has been cloned and overexpressed in a *Gluconobactor oxydans* strain.[18] On the other hand, MCO is a family of the enzymes that include laccase, bilirubin oxidase (BOD) and Cu efflux oxidase (CueO), etc. They have usually four copper atoms that are classified into three types according to their spectroscopic and magnetic properties: type I (T1), type II (T2) and type III (T3) coppers.[19] MCOs can receive electrons at the T1 copper site from electrodes. The electrons are transferred to the T2–3 cluster composed of one T2 copper and two T3 copper atoms, where dioxygen is reduced to water in a four-electron reduction process.[20,21]

The fructose/O_2 biofuel cells provide relatively high power density compared to most of the DET-type devices (0.85 mW cm^{-2} under O_2 -saturated stirred conditions with laccase as an cathode catalyst at 25 °C and pH 5.0;[13] 1.8 mW cm^{-2} under O_2 -saturated stirred conditions with laccase as an cathode catalyst at 25 °C and pH 5.0, the area of the cathode being twice of the anode area;[14] 0.17 mW cm^{-2} under continuous air-bubbling conditions at 25 °C and pH 5.0),[15] but much lower than that of MET-type enzymatic biofuel cell with the best performance (10 mW cm^{-2}).[22] The cell power density of the fructose/O_2 biofuel cells reported is limited by the biocathode performance. One of the reasons is low concentrations of dissolved O_2, which limits the current density governed by the O_2 diffusion. Recently, air-breathing gas-diffusion-type biocathodes, which is able to utilize atmospheric O_2, have been developed.[23–26] A steady-state current density of 20 mA cm^{-2} was achieved by using non-glycoprotein CueO as a DET-catalyst under quiescent and O_2 atmospheric conditions.[24] Unfortunately, the redox potential of the electron-accepting site (T1) of CueO is relatively low compared with that of laccase and BOD.[20] This means that CueO inherently causes thermodynamic loss in the catalytic ET process from the T1 site to O_2. One of the superior points of BOD is that it works as a cathode catalyst even under neutral pH,[27,28] though the optimum pH is 4.0 in solution with 2,2'-azino-bis-(3-ethylbenzthioline-6-sulfonic acid, $ABTS^{2-}$ as an artificial electron donor.[29] Therefore, in this work, the

author focuses on BOD as a biocathode catalyst by supposing its broad application as an air-diffusion biocathode in future.

Unfortunately, another problem is raised here when we use BOD for gas-diffusion biocathodes. The current density of the air-breathing gas-diffusion biocathode is drastically decreased when CueO is replaced with laccase or BOD.[24] This is due in part to the fact that the redox potential of BOD (and laccase) is rather high compared to that of CueO.[30] However, we can point out another factor that the oligosaccharide chain might behave as a hindrance to the DET-type bioelectrocatalysis,[31,32] especially in inconvenient orientation on electrodes, since the ET rate constant decreases exponentially with an increase in the distance between the redox sites and electrodes.[33] Therefore, control of the enzyme orientation on the electrode surface is one of the major concerns in biocathode developments.

Several methods have been proposed to control the protein orientation on electrodes and to improve the DET kinetics. The covalent bonding between a Cys residue and gold electrodes,[34,35] the ligand formation of a His-tag on engineered proteins with Ni-linkers modified on the electrode surface[34,36,37] are utilized to control the protein orientation, but the methods do not seem to be effective in improving the DET kinetics, since the linkers used increase the distance between the redox site and the electrode surface. In contrast, the modification based on diazonium coupling reaction on the functionalized carbon electrode,[38] the modification with functionalized gold nanoparticles,[39,40] the π–π stacking between aromatic molecules modified on enzymes and carbon electrodes,[25,41] and the strong hydrophobic interaction between an enzyme (laccase) and an aromatic molecule (anthracene) modified on electrodes[42] have been reported to induce the proper orientation for the DET. In the last case, the anthracene moiety on the electrode is believed to preferentially interact with the T1 site of laccase.

In this study, the author has a hypothesis that when the electrode is modified with the substrate of BOD (or related compounds), BOD will attractively interact with the modified compound in such an orientation that the electron-accepting T1 site faces the electrode surface. The orientation seems to be convenient in the DET-type bioelectrocatalysis.

The author also attempted to create a high performance bioanode for DET-type biofuel cells with FDH. Carbon cryogel (CCG), one of the mesoporous carbon materials, was used for the adsorption of FDH in our previous study.[43] The pore size-control of the mesoporous electrode is found to be important and effective to increase the amount of the adsorbed FDH and the DET-type bioelectrocatalytic current density. However, the CCG electrode is hydrophobic and it was difficult to adsorb FDH uniformly. Thus, the author examined several pre-treatments of CCG electrodes in order to increase the electrode surface area in the mesopores available for the FDH adsorption.

Finally, the author constructed a one-compartment fructose/O_2 DET-type biofuel cell without separators. In previous reports on fructose/O_2 DET-type biofuel cells,[13–15] the cell performance was evaluated under convective conditions to increase the power. Since the author may suppose that

biofuel cells will be operated under quiescent (that is, passive) and air atmospheric conditions in practical case, the power of the biofuel cell constructed here is evaluated under such practical conditions. The highest power density of 2.6 mW cm^{-2} has been attained at 0.46 V.

2. Experimental

2.1 Materials

Ketjien Black EC300J (KB) was kindly donated from Lion Co. (Japan). Carbon cryogel gel (CCG) was synthesized according to previous papers,[43,44] and the peak value of the pore radius was 54 nm. Carbon paper (CP, TGP-H-120) was purchased from Toray Co. (Japan). Polytetrafluoroethylene fine powder (PTFE, 6-J) and poly-(vinylidene difluoride) (PVDF) were obtained from DuPont Mitsui Fluorochemicals (Japan) and Kureha (Japan), respectively. Bilirubin oxidase (BOD; EC 1.3.3.5) from *Myrothecium verrucaria* was donated from Amano Enzyme Inc. (Japan) and used without further purifications. Fructose dehydrogenase (FDH; EC 1.1.99.11) from *Gluconobacter japonicas* NBRC3260 was purified according to the literature.[18] Bilirubin was purchased from Wako Pure Chemical (Japan) and was dissolved in 30 mM NaOH aqueous solution. For experiments of atomic absorbance spectroscopy (AAS), nitric acid, perchloric acid, and hydrochloric acid of super special grade were purchased from Wako Pure Chemical (Japan), and ultra pure water was used to prepare the reagent solution. All other chemicals used in this study were of analytical grade unless otherwise specified and all solutions were prepared with distilled water.

2.2 Preparation of KB-modified glassy carbon electrode

Glassy carbon electrode (GCE, 3 mm in diameter, BAS) was polished with alumina slurry (Buehler, 1 μm), sonicated and washed with distilled water. KB powder was mixed with PTFE (KB : PTFE = 8 : 2, (w/w)) and homogenized (Heat Systems GmbH & Co.) in 2-propanol for 3 min in an ice bath to prepare KB slurry. The slurry (3 μL) was applied to a GCE and dried at 60 °C to prepare a KB-modified GC electrode (KB-GCE). Subsequently, 10 μL of bilirubin solution (3 mM) was applied on the KB-GCE, and the electrode was dried at room temperature and washed with distilled water. The electrode is named BL-KB-GCE. For comparison, the KB-GCE without modification of bilirubin was immersed in NaOH solution (30 mM), dried at room temperature, and washed. BOD solution (10 mg mL^{-1}, dissolved in 100 mM phosphate buffer (pH 7)) was then applied to the aforementioned electrodes and they were kept in water-saturated atmosphere for 1.5 h at 4 °C to be dried slowly, washed with distilled water (or 1 M citrate buffer, a buffer solution used for electrochemical characterization), and immediately served for electrochemical measurements.

2.3 Evaluation of the amount of BOD adsorbed on KB

The KB slurry (15 μL) described in Section 2.2 was applied to a sheet of parafilm (Bemis Co. Inc, U.S.A) and dried at 60 °C. Bilirubin and BOD was adsorbed on a KB-mounted parafilm sheet in a manner similar to that described in Section 2.2. After the adsorption of bilirubin and BOD, the samples were incinerated at 800 °C for 3 h. After cooling, nitric acid and perchloric acid were added, and then the samples were heated cautiously until white fumes were no longer evolved. The residue was dissolved in 0.1 M HCl under heating. The Cu concentrations were determined by AAS based on the calibration-curve method. The amount of BOD was calculated from the amount of Cu atom by considering the fact that BOD contains 4 Cu atoms.

2.4 Preparation of KB-modified CP electrode

The air-breathing gas-diffusion-type electrode without modification of bilirubin was prepared according to the literature.[24] In brief, KB powder was mixed with PTFE (KB : PTFE = 6 : 4, (w/w)) and homogenized in 2-propanol for 5 min in ice to prepare KB slurry. The slurry (100 μL) was applied to one side of CP (1.5 cm in diameter) and dried at 60 °C. The electrode is called KB-CPE. For bilirubin-modified electrodes, KB powder was mixed with PTFE in a ratio of KB : PTFE = 4 : 6, (w/w). 0.3 mL of bilirubin solution (1 mM) was then applied to a KB-CPE, which was dried at room temperature. The surface of KB-CPE was washed with phosphate buffer (pH 7) 5 times. The bilirubin-modified electrode is called BL-KB-CPE. BOD solution (5 mg mL^{-1}, dissolved in pH 7 phosphate buffer) was applied to the electrodes, which were dried for 2 h under reduced pressure at room temperature.

2.5 Preparation of CCG-modified CP electrode

CCG was mixed with PVDF (CCG : PVDF = 8 : 2, (w/w)) and homogenized in *N*-methyl-2-pyrrolidone for 10 min under water cooling to prepare CCG slurry. The slurry (200 μL) was applied to both sides of CP (1.5 cm in diameter) and dried on a hotplate at about 90 °C. The electrode was first pre-treated by plasma etching for 5 min at about 8 Pa on a soft etching device (Meiwa Fosis SEDE-GE, Japan). The pre-treated electrode was immersed in ethanol to degas from the mesopores, and then transferred to distilled water. This operation was performed twice and finally the electrode was immersed in 1 M citrate buffer (pH 5.0). The pre-treated electrode is called CCG-CPE. The CCG-CPE was immersed in an FDH solution (30 μM) for about 24 h at 4 °C. The electrodes were gently shaken during FDH adsorption on a shaker (Vortex Genie-2).

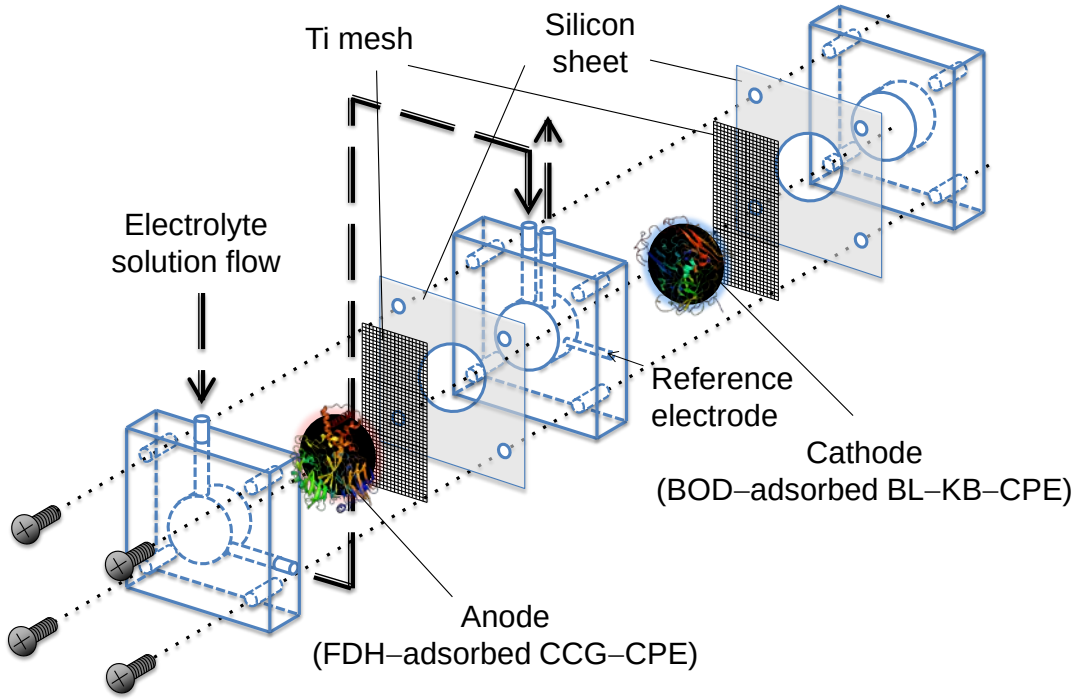

Figure 1.
A schematic illustration of one-compartment cell

2.6 DET-type biofuel cell

The BOD-adsorbed BL-KB-CPE and the FDH-adsorbed CCG-CPE were attached to a handmade one-compartment cell, as shown in Fig. 1. The projected surface area of the cathode and the anode was adjusted to be 1.0 cm^2. A titan mesh was utilized as a current collector. The cathode and the anode of the cell were connected through a variable resistor (Type 2786 Decade Resistance Box, Yokogawa Hokushin Electric., Japan). The cell voltage, the cathode potential, and the anode potential were measured against an Ag|AgCl|sat. KCl reference electrode with an electrometer at given values of the resistance in the range from 100 kΩ to 20 Ω. The current density and the power density were calculated based on the projected surface area of the electrodes used. Measurements were carried out in 1 M citrate buffer (pH 5.0 : the optimum pH of FDH[43]) containing 500 mM D-fructose at room temperature (23 ± 2 °C) under quiescent and air atmospheric conditions in a passive mode.

2.7 Electrochemical measurements

Cyclic voltammetry (CV) and chronoamperometry (CA) were performed on an electrochemical analyzer BAS CV 50 W. Steady-state measurements were carried out with rotating disk GCEs (RDE-2, BAS, Inc.) as called KB-GCE or BL-KB-GCE. A platinum wire and the

Ag|AgCl|sat. KCl electrode were used as the counter electrode and the reference electrode, respectively, and measurements were carried out at 23 ± 2 °C. For long-term stability test, KB-GCEs were stored in pH 7 phosphate buffer at 4 °C after each CA measurement. A handmade air-diffusion-type electrolysis cell, which is identical with that reported in a previous paper,[23] was used for the measurements at KB-CPE and BL-KB-CPE. The projected surface area of the working electrode was set to be 1.0 cm^2. A titan mesh was utilized as a current collector.

3. Results and discussion

3.1 Effect of bilirubin modification on biocathode reaction

The effect of the bilirubin modification on the catalytic reduction of O_2 was examined using BOD-adsorbed BL-KB-GCE and BOD-adsorbed KB-GCE on the RDE method. The result is shown in Fig. 2, panel A. Under O_2-saturated conditions, the cathodic waves were observed with both BOD-adsorbed electrodes, while such catalytic waves were not observed in the absence of either O_2 or BOD (data not shown). The results prove that the adsorbed BOD works as a DET-type catalyst to reduce O_2. The onset potential of the two kinds of the BOD-adsorbed electrodes was about 0.5 V, which is close to the formal potential of the T1 site of BOD (0.46 V).[45] The catalytic wave at the BOD-adsorbed BL-KB-GCE is much larger than that at the BOD-adsorbed KB-GCE and shows sigmoidal characteristics,

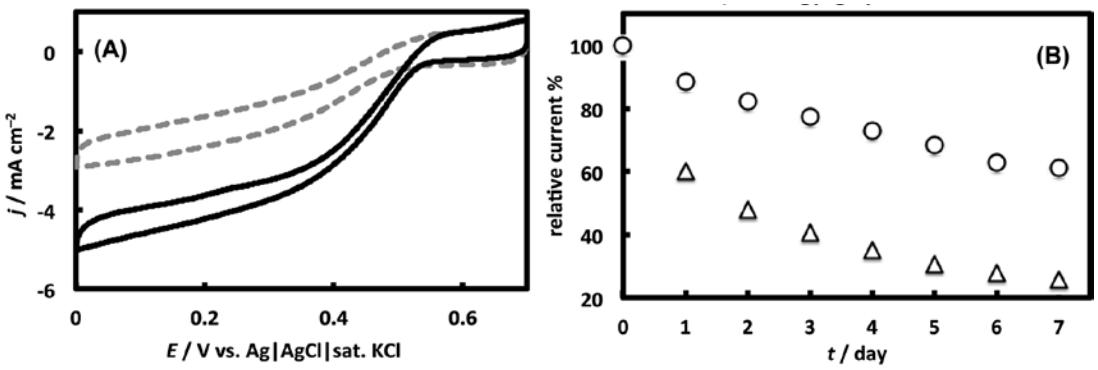

Figure 2
(A) Rotating disk voltammograms of catalytic O_2-reduction at BOD-adsorbed BL-KB-GCE (solid line) and BOD-adsorbed KB-GCE (dotted line) in an O_2-saturated phosphate buffer (pH 7). The rotating rate was 4000 rpm, and the scan rate was 20 mV s^{-1}.
(B) The long-term stability of BOD-adsorbed BL-KB-GCE (circle) and BOD-adsorbed KB-GCE (triangle). The activity was measured from the steady-state catalytic current on CA at 0 V and 60 s after the potential step in an O_2-saturated phosphate buffer (pH 7). The current is plotted as the relative value. The rotating rate was 4000 rpm. The error bars were evaluated by the Student *t*-distribution at 90% confidence level.

while the bilirubin-unmodified electrode (BOD-adsorbed KB-GCE) shows rather straight characteristics in the voltammogram. In other words, the bilirubin modification causes the shift in the half-wave potential of the catalytic wave to the direction of the positive potential. The sigmoidal and straight characteristics of the catalytic waves can be ascribed to the controlled and random orientation of the adsorbed enzyme, respectively.[46] Therefore, the author may assume that bilirubin adsorbed on the electrode can assist BOD to face the electrode surface in an orientation convenient for the DET catalysis. Considering a simple DET-type catalytic model, the current density (j) can be expressed by eqns. (1)-(4) as follows,[30]

$$j = \frac{j^{\lim}}{1+{k_{\mathrm{cat}}}/{k_{\mathrm{f}}}+{k_{\mathrm{b}}}/{k_{\mathrm{f}}}} \quad (1)$$

$$j^{\lim} = nFk_{\mathrm{cat}}\lambda\Gamma_{\mathrm{t}} \quad (2)$$

$$k_{\mathrm{f}} = k^{\circ}\exp\left[-\alpha(F/RT)\left(E-E_{\mathrm{E}}^{\circ\prime}\right)\right] \quad (3)$$

$$k_{\mathrm{b}} = k^{\circ}\exp\left[(1-\alpha)(F/RT)\left(E-E_{\mathrm{E}}^{\circ\prime}\right)\right] \quad (4)$$

where n, F, Γ_{t}, and λ are the number of electrons (n = 1 for the T1 Cu site of BOD), the Faraday constant, the total surface concentration of BOD, and the (averaged) ratio of electrochemically active enzyme to the total one, respectively. The catalytic constant k_{cat} is a function of the intramolecular ET rate constant from the T1 site to the T2–3 cluster and the intermolecular ET rate constant for the O_2 reduction at the T2–3 cluster. Here, the k_{cat} value was used as a maximum catalytic rate constant for BOD of 250 s^{-1} in solution according to a previous study.[30] $E_{\mathrm{E}}^{\circ\prime}$, k° and α are the formal potential (0.46 V vs. Ag|AgCl|sat. KCl) of the T1 site of BOD,[45] the standard surface ET rate constant, and the transfer coefficient, respectively. The value of α was set as 0.3 according to the literature.[30] The rotating disk voltammograms were fitted by eqns. (1)–(4) with k° and $\lambda\Gamma_{\mathrm{t}}$ as the adjustable parameters using a non-linear regression analysis by Excel®. Table 1 summarizes the fitted values of k° and $\lambda\Gamma_{\mathrm{t}}$. The result clearly shows that the bilirubin modification increases k° and $\lambda\Gamma_{\mathrm{t}}$.

On the other hand, AAS measurements revealed that the amount of BOD adsorbed (Γ_{t}) on the BL-KB-GCE is significantly smaller than that on the KB-GCE, the ratio being 0.34 ± 0.15. The reason of the decrease in the adsorbed BOD by the bilirubin-modification may be ascribed to the electrostatic repulsion between negatively charged bilirubin on KB and negatively charged BOD (pI = 4.1).[47] Considering this result and the data in Table 1, the bilirubin modification increases the value of λ, the ratio of λ between BL-KB-GCE and KB-GCE being 4 ± 2. Thus, the author can conclude that the substrate modification can induce the proper orientation of BOD for the DET reaction.

Table 1
Effects of bilirubin modification of the characteristics of BOD-modified electrode with KB-mounted GCE in terms of the standard ET rate constant ($k°$) and the effective amount of surface concentration of BOD ($\lambda\Gamma_t$).[a)]

Electrode	$k°$ / s^{-1}	$\lambda\Gamma_t$ / 10^{-10} mol cm^{-2}
BL-KB-GCE	240 ± 12	1.4 ± 0.1
KB-GCE	68 ± 4	0.92 ± 0.05

a) The errors were evaluated by the Student *t*-distribution at 90% confidence level.

The long-term stability of the adsorbed BOD on BL-KB-GCE was examined for one week in compared with KB-GCE. The result is shown in Fig. 2, panel B. The catalytic current decayed with time in a (pseudo)first-order kinetics. The half-life time of the decay was about one and half day at the KB-GCE, but it was drastically improved up to about 7 days by the substrate modification (that is, at BL-KB-GCE).

The author also examined the effect of bilirubin-related compounds on the BOD-catalytzed O_2-reduction. Catechol, hydroquinone, pyrogallol, hemin or ditaurobilirubin, which are catalytically oxidized by BOD in aerated solution[47], were pre-adsorbed on the KB-GCEs before the BOD adsorption. Rotating disk voltammograms of these substance–adsorbed electrodes are measured (data not shown). For all electrodes, the catalytic waves showed sigmoidal characteristics almost similar to that observed at BL-KB-GCE. Accordingly, the author can conclude that these substances also cause the positive effect on the orientation of BOD. Especially, hemin and pyrogallol modification showed good performance to give large limiting catalytic currents. However, BOD–adsorbed BL–KB–GCE showed the best characteristics in view of sigmoidal current –potential behavior (i.e. the onset characteristics) among the other substances. In addition, bilirubin modification was most stable among the substrates examined. Therefore, the author uses bilirubin as a pre-modifier in the following.

3.2 Application of substrate-modification to gas-diffusion-type biocathode (KB-CPE)

For the application to a DET-type biofuel cells, a BOD-adsorbed BL-KB-CPE as well as a BOD-adsorbed KB-CPE was fabricated as gas-diffusion-type biocathodes. Cyclic voltammograms of the BOD-adsorbed electrodes were recorded under quiescent (passive) and O_2 atmospheric conditions in 1 M citrate buffer (pH 5) and are shown in Fig. 3. The pH is the optimum one for FDH.[43] The citrate concentration is optimized in a previous paper.[23] The BL-KB-CPE provides voltammograms with a low overpotential compared with the KB-CPE (Fig. 3). In the reverse scan of the voltammograms in Fig. 3, the current density decreases due to the depletion of the O_2 concentration near the electrode surface. The depletion is caused by improved bioelectrocatalytic reaction kinetics under limited O_2 supply. Thus, in view of the enzyme-catalyzed electrode kinetics, a further increase in the current

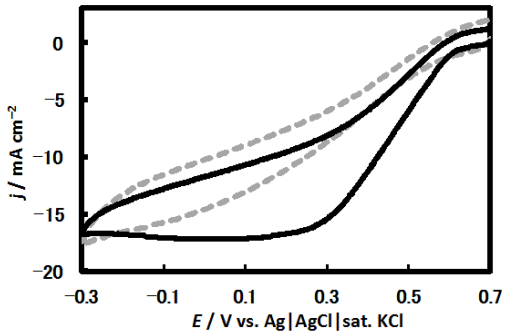

Figure 3
Cyclic voltammograms of catalytic O_2-reduction at air-diffusion BOD-adsorbed BL-KB-CPE (solid line) and BOD-adsorbed KB-CPE (dotted line) in 1 M citrate buffer (pH 5) under O_2 atmospheric condition. The scan rate was 5 mV s^{-1}.

density can be expected by improvement of the O_2 supplying system for the gas-diffusion-type electrode proposed here.

3.3 Optimization of FDH adsorption on CCG-CPE

The effects of the two pre-treatments (plasma etching and ethanol treatment) and the shaking during adsorption on the FDH-catalyzed fructose oxidation current density were evaluated from the catalytic current density in CA at 0.5 V and 100 s after the potential step as a measure (data not shown). From these results, the author can conclude that the ethanol treatment causes a drastic increase in the catalytic current density (from 5 ± 1 mA cm^{-2} up to 14 ± 6 mA cm^{-2}). Most probably, the ethanol treatment increases the effective surface area of the mesopores, since ethanol can penetrate into the mesopores and then degas in the pores. The hydrophilic treatment by the plasma etching and the shaking during adsorption are positively effective but its efficiency is not so high.

In this work, the author adopted two pretreatments before the FDH adsorption and the shaking method during the FDH adsorption. The details of the optimized method are given in Experimental section (2.5), and the final electrode is called FDH-adsorbed CCP-CPE. Cyclic voltammograms of the FDH-adsorbed CCG-CPEs recorded under quiescent (passive) conditions in 1 M citrate buffer (pH 5) containing 500 mM D-fructose is shown in Fig. 4 (solid line). The current density reached about 38 mA cm^{-2} at –0.5 V. The value is about 10 times higher than that obtained at CCG-mounted CPE without the two pre-treatments and the shaking method (data not shown).

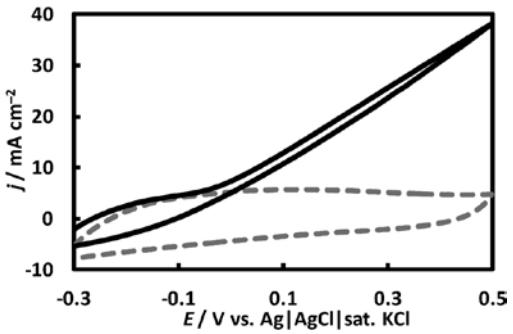

Figure 4
Cyclic voltammograms of FDH-adsorbed CCG-CPEs in 1 M citrate buffer (pH 5) under quiescent conditions in the presence (solid lines) and absence (dotted lines) of 500 mM D-fructose. The scan rate was 20 mV s^{-1}.

3.4 DET-type biofuel cell

A DET-type biofuel cell without separators was constructed. The biocathode was BOD-adsorbed BL-KB-CPE, and the bioanode was FDH-adsorbed CCG-CPE. These enzyme adsorbed electrodes were set in the biofuel cell assembly illustrated in Fig. 1.

The biofuel cell was operated in 1 M citrate buffer (pH 5) containing 500 mM D-fructose under quiescent and air atmospheric conditions at room temperature (23 ± 2 °C). The cell voltage, the cathode potential and the anode potential were measured under (quasi-)steady state at given values of the resistance. The resistance values were decreased stepwise. The potentials were recorded about 20 s after the change of the resistance.

Figure 5, panel A shows the cell voltage, the cathode potential and the anode potential as functions of the current density, while panel B shows the current density dependence of the cell power density. The open-circuit voltage was 0.79 V. The maximum current density was 6.5 mA cm^{-2} and the maximum power density was 2.6 mW cm^{-2} at 0.46 V of the cell voltage.

As mentioned in section 3.2, the limiting current at the BOD-adsorbed BL-KB-CPE was controlled by the mass transfer of the O_2. Judging from Fig. 5, the limiting current density controlled by the O_2 transfer seems to be 6.5 mA cm^{-2}, and the rate-determining factor of this biofuel cell is still the cathode reaction. However, the maximum power density was achieved at 5.8 mA cm^{-2}, thus this biofuel cell can fully operate with minimized disadvantage of the limited O_2 supply. For further improvement, high performance gas-diffusion-type biocathode, which can passively supply increased amount of O_2, will be needed.

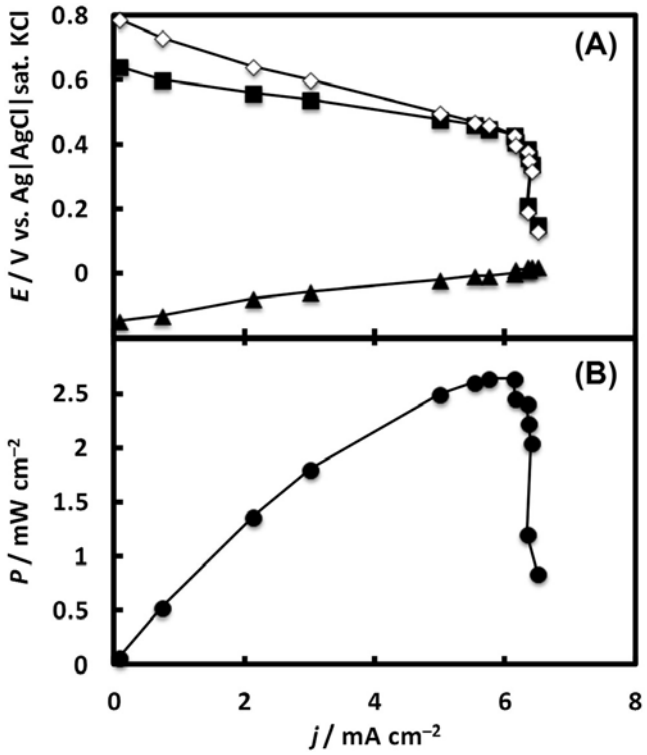

Figure 5
(A) Polarization curves of the biofuel cell. The cell voltage (◇), the cathode potential (■) and the anode potential (▲) are plotted as functions of the current density (*j*). The measurements were performed in 1 M citrate buffer (pH 5.0) containing 500 mM D-fructose under quiescent and air atmospheric conditions (in a passive mode) at room temperature (23 ± 2 °C).
(B) The power density (*P*) as a function of the current density (*j*) of the biofuel cell.

4. Conclusion

Bilirubin modification is capable of increasing the surface electron transfer rate constant and the effective amount of adsorbed BOD on the electrode. Moreover, this method is very simple and easy. The BOD-adsorbed BL-KB-CPE has been successfully constructed, which is applicable as a biocathode for DET-type biofuel cells. The author has also optimized the way of the constructing FDH-adsorbed CCG-CPE by examining the effect of pre-treatments of the electrode and shaking during adsorption. As a result, the FDH-catalyzed current density reached 38 mA cm^{-2}, which is 10 times higher compared with a previous work[13]. Finally, the author constructed the DET-type biofuel cell with BOD and FDH. The maximum power density was 2.6 mW cm^{-2}.

However, development of covalent bonding methods for the biocatalysts is urgent and important subject in this field. In this sense, covalent bonding of an enzyme to 4-aminophenyl

monolayer on an electrode is very interesting and worthy of notice[48]. Hydrogenase is linked to the amino group with *N*-hydroxysuccinimide and *N*-(3-dimethylaminopropyl)-*N*'-ethylcarbodiimide hydrochloride, and works effectively as a DET-type bioelectrocatalysis[48]. It would be necessary to evaluate the usefulness of the method for other biocatalysts.

On the other hand, the DET-type biofuel cell was operated at pH 5 in this work due to the requirement from the FDH characteristics, though the cathode performance was examined at pH 7 also. However, one of the advantages of BOD is the strong catalytic activity at neutral pH. Since the number of DET-type biocatalysts for bioanodes working at neutral pH is limited (the typical examples being hydrogenase[49] and PQQ-dependent glucose dehydrogenase[12]), MET-type biocatalysts may also be coupled with the BOD-based DET-type bioanode in future.

5. References

1 J. A. Cracknell, K. A. Vincent and F. A. Armstrong, *Chem. Rev.*, 2008, **108**, 2439–2461.

2 M. J. Moehlenbrock and S. D. Minteer, *Chem. Soc. Rev*., 2008, **37**, 1188–1196.

3 N. Mano, F. Mao and A. Heller, *ChemBioChem*, 2004, **5**, 1703–1705.

4 D. Leech, P. Kavanagha and W. Schuhmann, *Electrochim. Acta*, 2012, **84**, 223–234.

5 S. C. Barton, J. Gallaway and P. Atanassov, *Chem. Rev*., 2004, **104**, 4867–4886.

6 M. H. Osman, A. A. Shah and F. C. Walsh, *Biosens. Bioelectron*., 2011, **26**, 3087−3102.

7 M. Falk, Z. Blum and S. Shleev, *Electrochimica Acta*, 2012, **82**, 191–202.

8 M. Rasmussen, R. E. Ritzmann, I. Lee, A. J. Pollack and D. Scherson, *J. Am. Chem. Soc.*, 2012, **134**, 1458−1460.

9 A. Szczupak, J. Halámek, L. Halámková, V. Bocharova, L. Alfonta and E. Katz, *Energy Environ. Sci.*, 2012, **5**, 8891–8895.

10 A. Zebda, S. Cosnier, J.-P. Alcaraz, M. Holzinger, A. Le Goff, C. Gondran, F. Boucher, F. Giroud, K. Gorgy, H. Lamraoui and P. Cinquin, *Scientific Reports*, 2013, **3**, art. # 1516.

11 T. Miyake, K. Haneda, N. Nagai, Y. Yatagawa, H. Onami, S. Yoshino, T. Abe and M. Nishizawa, *Energy Environ. Sci.*, 2011, **4**, 5008–5012.

12 E. Katz and K. MacVittie, *Energy Environ. Sci.*, 2013, **6**, 2791–2803.

13 Y. Kamitaka, S. Tsujimura, N. Setoyama, T. Kajino and K. Kano, *Phys. Chem. Chem. Phys*., 2007, **9**, 1793–1801.

14 T. Miyake, S. Yoshino, T. Yamada, K. Hata and M. Nishizawa, *J. Am. Chem. Soc.*, 2011, **133**, 5129–5134.

15 X. Wu, F. Zhao, J. R. Varcoe, A. E. Thumser, C. Avignone-Rossa and R. C. T. Slade, *Biosens. Bioelectron.*, 2009, **25**, 326–331.

16 M. Ameyama, E. Shinagawa, K. Matsushita and O. Adachi., *J. Bacteriol*., 1981, **145**, 814–

823.

17 S. Kawai, T. Yakushi, K. Matsushita, Y. Kitazumi, O. Shirai and K. Kano, *Electrochem. Commun.*, 2014, **38**, 28–31.

18 S. Kawai, M. Tsutsumi, T. Yakushi, K. Kano and K. Matsushita, *Appl. Environm. Microbiol.*, 2013, **7**, 1654–1660.

19 E. I. Solomon, U. M. Sundaram and T. E. Machonkin, *Chem. Rev.*, 1996, **96**, 2563–2605.

20 Y. Miura, S. Tsujimura, S. Kurose, Y. Kamitaka, K. Kataoka, T. Sakurai and K. Kano, *Fuel Cells*, 2009, **9**, 70–78.

21 S. Shleev, J. Tkac, A.Christenson, T. Ruzgas, A. I. Yaropolov, J. W. Whittaker and L. Gorton. *Biosens. Bioelectron.*, 2005, **20**, 2517–2554.

22 H. Sakai, T. Nakagawa, H. Mita, H. Kumita and Y. Tokita, *217th Electrochemical Society Meet. Abstr. - Electrochem. Soc.*, 2010, **1001**, 396.

23 R. Kontani, S. Tsujimura and K. Kano, *Bioelectrochemistry*, 2009, **76**, 10–13.

24 I. Asano, Y. Hamano, S. Tsujimura, O. Shirai and K. Kano, *Electrochemistry*, 2012, **80**, 324–326.

25 C. Lau, E. R. Adkins, R. P. Ramasamy, H. R. Luckarift, G. R. Johnson and P. Atanassov, *Adv. Energy Mater*., 2012, **2**, 162–168.

26 G. P. M. K. Ciniciato, C. Lau, A. Cochrane, S. S. Sibbett, E. R. Gonzalez and P. Atanassova, *Electrochim. Acta*, 2012, **82**, 208–213.

27 S. Tsujimura, K. Kano and T. Ikeda, *J. Electroanal. Chem.*, 2005, **576**, 113–125.

28 N. Mano and L. Edembe, *Biosens. Bioelectron.*, 2013, **50**, 478–485.

29 F. Xu, W. Shin, S. H. Brown, J. A. Wahleithner, U. M. Sundaram and E. I. Solomon, *Biochim. Biophys. Acta*, 1996, **1296**, 303–311.

30 S. Tsujimura, T. Nakagawa, K. Kano and T. Ikeda, *Electrochemistry*, 2004, **72**, 437–439.

31 A. Lindgren, T. Ruzgas, L. Gorton, E. Csöregi, G. B. Ardila, I. Y. Sakharov and I. G. Gazaryan, *Biosens. Bioelectron.*, 2000, **15**, 491–497.

32 A. Prévoteau, O. Courjean and N. Mano, *Electrochem. Commun.*, 2010, **12**, 213–215.

33 C. C. Page, C. C. Moser, X. Chen and P. L. Dutton, *Nature*, 1999, **402**, 47–52.

34 K. Hernandez and R. Fernandez-Lafuente, *Enzyme Microbial. Technol*., 2011, **48**, 107–122.

35 E. Ferapontova, K. Schmengler, T. Börcher, T. Ruzgas and L. Gorton, *Biosens. Bioelectron*., 2002, **17**, 953–963.

36 D. L. Johnson and L.L. Martin, *J. Am. Chem. Soc*., 2005, **127**, 2018–2019.

37 E. E. Ferapontova, V. G. Grigorenko. A. M. Egorov, T. Börchers, T. Ruzgas and L. Gorton, *J. Electroanal. Chem.*, 2001, **509**, 19–26.

38 C. F. Blanford, C. F. Foster, R. S. Health and F. A. Armstrong, *Faraday Discuss.*, 2008, **140**, 319–335.

39 K. Murata, M. Suzuki, K. Kajiya, N. Nakamura and H. Ohno, *Electrochem. Commun.*, 2009, **11**, 668–671.

40 C. Gutiérrez-Sánchez, M. Pita, C. Vaz-Domínguez, S. Shleev and A. L. De Lacey, *J. Am. Chem. Soc.*, 2012, **134**, 17212–17220.

41 L. Halámková, J. Halámek, V. Bocharova, A. Szczupak, L. Alfonta and E. Katz, *J. Am. Chem. Soc.*, 2012, **134**, 5040–5043.

42 C. F. Blanford, R. S. Heath and F. A. Armstrong, *Chem. Commun.*, 2007, 1710–1712.

43 S. Tsujimura, A. Nishina, Y. Hamano, K. Kano and S. Shiraishi, *Electrochem. Commun.*, 2010, **12**, 446–449.

44 Y. Hamano, S. Tsujimura, O. Shirai and K.Kano, *Bioelectrochemistry*, 2012, **88**, 114–117.

45 S. Tsujimura, A. Kuriyama, N. Fujieda, K. Kano and T. Ikeda, *Anal. Biochem.*,2005, **337**, 325–331.

46 C. Léger, A. K. Jones, S. P. J. Albracht and F. A. Armstrong, *J. Phys. Chem. B*, 2002, **106**, 13058–13063.

47 N. Tanaka and S. Murao, *Agric. Biol. Chem.*, 1982, **46**, 2499–2503.

48 O. Rüdiger, J. M. Abad, E. C. Hatchikian, V. M. Fernandez and A. L. D. Lacey, *J. Am. Chem,. Soc.*, 2005, **127**, 16008–16009.

49 K. A. Vincent, A. Parkin and F. A. Armstrong, *Chem. Rev.*, 2007, **107**, 4366–4413

1-2. Significance of the Length of Carbon Nanotubes on the Bioelectrocatalytic Activity of Bilirubin Oxidase for Dioxygen Reduction

Abstract

Bilirubin oxidase (BOD) catalyzes $4e^-$-reduction of O_2 into H_2O and is one of the enzymes allowing direct electron transfer (DET)-type bioelectrocatalysis. Mesoporous carbon materials are often used for constructing BOD-modified DET-type biocathodes. The author has examined the performance of several multi-walled carbon nanotubes (MWCNTs) as cathode platforms for BOD-catalyzed bioelectrocatalytic O_2 reduction. It has been found that the length of MWCNTs is a very important factor to control the performance. The π-π conjugated system with the carboxy groups on the surface of MWCNTs plays an important role in enhancing the DET-type bioelectrocatalytic activity of BOD. Water-soluble MWCNTs with lengths of as short as 1–4 μm are most suitable materials among the MWCNTs examined, and have been used to construct a mesoporous carbon electrode without any binder. The catalytic current density has reached a diffusion-controlled level for the first time for BOD at an electrode rotating rate of 4000 rpm and at 25 °C (8 mA cm^{-2}).

1. Introduction

Carbon nanotubes (CNTs) were discovered in 1991 [1]. CNTs are nanowires constituted from one or more layers of seamlessly enrolled graphene (called single-walled (SW) or multi-walled (MW), respectively) with different diameters, length, and chirality. CNTs exhibit large specific surface area, high conductivity, high mechanical strength, and several chemical properties (e.g. π-π conjugated system and the functional groups on the CNT) [2]. The materials have two types of the chemical characteristics originating from the sidewalls and the opened ends [3]. The sidewalls are mainly constituted by the hydrophobic graphene sheets, and there are some functional groups around the hollows of the sidewalls. On the other hand, the opened ends are terminated with hydrophilic carboxy groups. In the field of bioelectrochemistry, CNTs have proven to have good biocompatibility and ability to electrically communicate with many redox enzymes [4-12]. CNTs-based electrodes are simply constructed with hydrophobic interaction (π-π stacking due to the graphene sheets) between the CNTs and electrodes [4-12]. Furthermore, it is possible to further modify the CNT surface with several techniques, such as the chemical reactions to provide functionalized groups and the physical adsorption of surfactants or small molecules [6-12].

Bioelectrocatalysis, which is a coupled reaction of the enzymatic catalytic reaction and the electrode reaction, is classified into two types according to the electric connection systems [13-18]. One is the mediated electron transfer (MET)-type, in which artificial redox mediators shuttle the electrons between electrodes and enzymes to reduce the kinetic hindrance in the interfacial electron

transfer. The other is the direct electron transfer (DET)-type, in which enzymes can directly transfer the electrons to or from electrodes. Combining with such enzyme-modified electrodes (called bioanode and biocathode), we can construct biofuel cells as electric generators that utilize redox enzymes as catalysts. The devices are very secure since they can operate under mild conditions (room temperature, atmospheric pressure, and neutral pH). Concerning the DET-type biofuel cells [19], hydrogenase [20,21], fructose dehydrogenase [22,23], glucose dehydrogenase [24], and cellobiose dehydrogenase [25,26] are mainly used as the catalysts of bioanodes, while multi-copper oxidases (MCOs) are used as those of biocathodes [27]. MCO is a family of the enzymes that include bilirubin oxidase (BOD) [28-30], laccase [31,32], and Cu efflux oxidase (CueO) [33,34], etc. They have usually four copper atoms that are classified into three types according to their spectroscopic and magnetic properties: type I (T1), type II (T2), and type III (T3) coppers. MCOs can receive electrons at the T1 copper site from electrodes [27,34,35]. The electrons are transferred to the T2-3 cluster, where dioxygen (O_2) is reduced to water in a four-electron reduction process [27,34,35].

Several researchers have utilized MCOs for constructing DET-type biocathodes [8-11,34,36-39]. Not only the CNTs but also other porous carbon materials such as carbon aerogel (CG), Ketjen Black EC300J (KB), and Au nanoparticles are used as electrode materials [8-11,34,36-39]. In addition, a gas-diffusion-type electrode that makes it possible to directly uptake gaseous substrate from the gas phase is utilized for practical application [37,40-45].

In DET-type bioelectrocatalysis of O_2 reduction, solution system is simpler than gas-diffusion-type system. Therefore, the author believes that the examination in solution is a reasonable first step to evaluate the performance of the enzyme-modified electrodes. However, the performance is still affected by many factors even in solution, such as the effective amount of the enzyme, the activity of the adsorbed enzyme, the roughness factor of the electrode, the adsorption state of the enzyme on the electrode, and the O_2 diffusion. Fortunately, we can control the O_2 diffusion by using the rotating disk electrode voltammetry to minimize the number of the factors governing the performance [46]. The voltammograms tell us the characteristics concerning the catalytic current density and the potential. In the case of biocathode, it is important to achieve high catalytic current densities at high potentials for improvement of DET-type biofuel cells. In stirred solution, CueO-adsorbed CG-modified electrode achieves a high catalytic current density (8 mA cm^{-2} at 25 °C, 4000 rpm) which is completely controlled by the O_2 diffusion [34]. The O_2 diffusion current can be expressed by Levich equation and is determined by the concentration of dissolved O_2, the diffusion coefficient of O_2, the kinematic viscosity of water (these three parameters are the function of the reaction temperature), and the electrode rotating rate [46]. However the formal potential of the T1 site of CueO is lower than those of BOD and laccase [34]. On the other hand, laccase-adsorbed CNT-modified or CG-modified electrode can catalyzes the O_2 reduction at high potentials, but the catalytic current density is not so high (2–2.5 mA cm^{-2}) [10,36]. In order to construct a DET-type biocathode

with high performance, BOD is mainly used as a catalyst, since BOD-adsorbed KB-modified and Au nanoparticles-modified electrode show high catalytic current densities (4–5 mA cm^{-2}) at relatively high potentials [37,38] and also at neutral pH.

Since the electron transfer rate constant decreases exponentially with an increase in the distance between the electrode surface and the redox site of the enzymes [47], it is very important to control the enzyme orientation on the electrode surface. In the case of BOD, modification of the electrode surface with bilirubin (the substrate of BOD) improves the enzyme orientation [9,37,48]. On the other hand, carboxylated aromatic compound-modified electrodes, which are fabricated by a diazonium coupling reaction on the carbon electrode or physical adsorption on the MWCNT-based electrode, enhance the bioelectrocatalytic activity of BOD [11,39]. Judging from these studies, the π-π conjugated system and carboxy groups on the electrode surface seem to be effective to improve the activity of BOD for DET-type bioelectrocatalysis.

In this research, the author focuses on the length of MWCNTs. For the most part, MWCNTs have two chemical properties: the π-π conjugated system on the graphene sheets of sidewalls and the carboxy groups at the opened ends. These properties seem to affect the bioelectrocatalytic activity of BOD, and the relative extents of the two factors can be considered as a function of the MWCNTs' length. The author constructed BOD-adsorbed MWCNTs-modified glassy carbon electrodes (BOD/MWCNT/GCEs) and BOD-adsorbed KB-modified GCE (BOD/KB/GCE) and evaluated their DET-type bioelectrocatalytic properties with rotating disk electrode voltammetry in solution.

2. Experimental

2.1. Materials

Four types of water-dispersed MWCNTs were obtained as follows. Water-dispersed MWCNT1 (outer diameter: 10–15 nm, length: 1–4 μm, without surfactant), water-dispersed MWCNT2 (the diameter and length are the same as those of MWCNT1, but dispersed with Triton-X® as a surfactant), and water-dispersed MWCNT3 (outer diameter: 8–10 nm, length: <1 μm, without surfactant) were kindly donated from Nitta Corp. (Japan). Powdered MWCNT4 (Flotube 9000, outer diameter: 10–15 nm, length: 10 μm) was kindly donated by CNano Technology Limited (U.S.A) and was dispersed in water (after ethanol dispersion and subsequent displacement of ethanol to water). Ketjen Black EC300J (KB) was kindly donated from Lion Co. (Japan). Bilirubin oxidase (BOD; EC 1.3.3.5) from *Myrothecium verrucaria* was donated from Amano Enzyme Inc. (Japan) and used without further purification. Bovine serum albumin (BSA) was purchased from Wako Corp. (Japan). All other chemicals used in this study were of analytical grade unless otherwise specified and all solutions were prepared with distilled water.

2.2. Preparation of electrodes

MWCNTs or KB were modified on a glassy carbon electrode (GCE for rotating electrode, 3 mm in diameter, BAS). GCE was polished with alumina slurry (Buehler, 1 mm), sonicated and washed with distilled water. Sixty μL of water-dispersed MWCNTs solution (0.1 wt%) are applied to a GCE and dried at 60 °C to prepare MWCNTs-modified GCEs (MWCNT/GCEs) (1 L = 1 dm^3). KB-modified GCE (KB:PTFE = 8:2 (w/w)) (KB/GCE) was prepared according to the literature [37]. Subsequently, BOD solution (10 mg mL^{-1}) dissolved in 10 mM phosphate buffer (pH 7) was then applied on the surface of the MWCNT/GCEs or KB/GCE, (1 M = 1 mol dm^{-3}) and they were kept in water-saturated atmosphere for 1.5 h at 4 °C to be dried slowly, washed with buffer solution, and used immediately for electrochemical measurements. BSA was added into the BOD solution in order to decrease the fraction of BOD (BSA:BOD = 8:2 (w/w)). The BSA/BOD solution (BOD 20 wt%) was then applied on the surface of the MWCNT/GCEs in the same way.

2.3. Electrochemical measurements

Linear sweep voltammetry, cyclic voltammetry, and chronoamperometry were conducted on an electrochemical analyzer BAS CV 50W. Steady-state measurements were carried out with rotating disk GCEs (RDE-2, BAS Inc.) at a rotating rate (ω) of 4000 rpm and a scan rate (v) of 5 mV s^{-1} unless otherwise stated. A platinum wire and an Ag|AgCl|sat. KCl electrode were used as a counter electrode and a reference electrode, respectively. All potentials in this work are referred to the reference electrode. The measurements were carried out in 100 mM phosphate buffer (pH 7) at 25 ± 1 °C or 4 ± 1 °C.

3. Results and Discussion

3.1 DET-type bioelectrocatalysis of BOD-adsorbed MWCNT/GCE

Fig. 1 (A) shows a linear sweep voltammogram (LSV) at a BOD-adsorbed MWCNT1/GCE (BOD/MWCNT1/GCE). A typical and sigmoidal reduction wave is observed under the rotating electrode conditions. This wave is ascribed to the DET-type bioelectrocatalysis with BOD according to the literature [28-30,37,38]. Fig. 1 (B) shows a chronoamperogram (CA) at BOD/MWCNT1/GCE at ω = 4000 rpm and at 25 °C under O_2-saturated conditions. The steady-state O_2 reduction current density reached about –8 mA cm^{-2} for 60 s. At the limiting current conditions, the bioelectrocatalysis is composed of two steps: the substrate diffusion and the enzyme reaction. As mentioned in

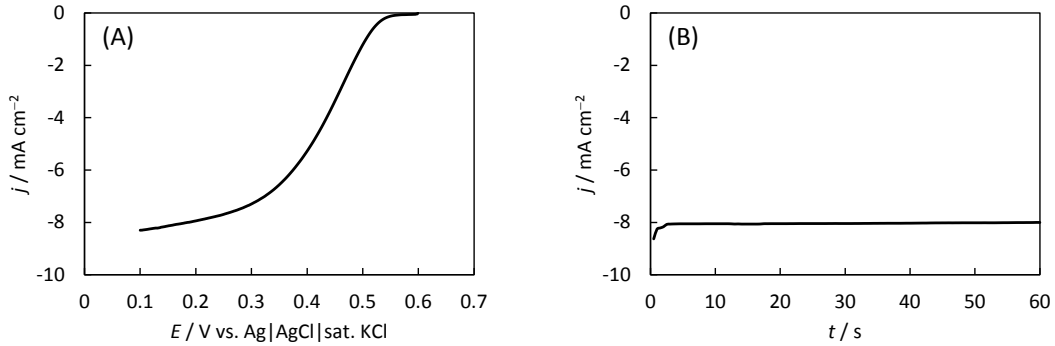

Figure 1
(A) LSV of the catalytic O_2 reduction at BOD/MWCNT1/GCE in O_2-saturated 100 mM phosphate buffer (pH 7) at 25 ± 1 °C, ω = 4000 rpm, and ν = 5 mV s^{-1}.
(B) CA at BOD/MWCNT1/GCE in the O_2-saturated buffer solution at 25 ± 1 °C and ω = 4000 rpm.

Introduction, we can estimate the O_2 diffusion current density, and the characteristics can be expressed by Koutecký-Levich equation [12,46].

$$\frac{1}{j} = \frac{1}{j_{\mathrm{dif}}} + \frac{1}{j_{\mathrm{cat}}} \tag{1}$$

Here, j, j_{dif}, and j_{cat} are, respectively, the measured current density, the diffusion-controlled current density at a rotating disk electrode, and the catalysis-kinetics-controlled current density.

$$j_{\mathrm{dif}} = -0.62nFD_{\mathrm{O_2}}^{2/3}\nu^{-1/6}c_{\mathrm{O_2}}\omega^{1/2} \tag{2}$$

$$j_{\mathrm{cat}} = -n_{\mathrm{E}}Fk_{\mathrm{cat}}\Gamma \tag{3}$$

where n, F, $D_{\mathrm{O_2}}$, ν, $c_{\mathrm{O_2}}$, n_{E}, k_{cat}, and Γ are, respectively, the number of electrons (4 in this case), the Faraday constant, the diffusion coefficient of O_2, the kinematic viscosity of water, and the concentration of dissolved O_2, the number of electrons of enzyme reaction in one catalytic turnover (= n in this case), the catalytic constant, and the surface concentration of the effective enzyme immobilized on the electrode. According to the literature [34,46], $D_{\mathrm{O_2}}$, ν and $c_{\mathrm{O_2}}$ are, respectively, 1.7×10^{-5} cm^2 s^{-1}, 0.01 cm^2 s^{-1}, and 1.2 mM at 25 °C. Therefore, the author can estimate that $j_{\mathrm{dif}} = -8.4\ \mathrm{mA\ cm^{-2}}$ at ω = 4000 rpm and at 25 °C [34,46]. The value of j at BOD/MWCNT1/GCE at ω = 4000 rpm and at 25 °C is almost identical with j_{dif}. This means that BOD/MWCNT1/GCE has realized a diffusion-controlled electrolysis at ω of as high as 4000 rpm, but also that it is difficult to get information about the bioelectrocatalytic activity. Consequently, the author tried to decrease the catalytic current by lowering the fraction of the BOD solution or by lowering the

reaction temperature.

3.2 Attempt to get the enzyme-kinetic-controlled conditions

Fig. 2 shows the results of the steady-state O_2 reduction current densities at BOD/MWCNT2/GCE (left side of each column) and BOD/MWCNT3/GCE (right side of each column). The author will define the fraction of BOD as 100 % for the BOD stock solution prepared with BOD as obtained alone. When the 100 % BOD solution was used, the reduction current densities at 25 °C were -3.8 ± 0.2 mA cm^{-2} at BOD/MWCNT2/GCE and -3.7 ± 0.4 mA cm^{-2} at BOD/MWCNT3/GCE. There is no systematic difference between the two electrodes, as judged from the Student *t*-test at 90 % confidence level. When the BOD fraction is decreased down to 20 wt% BOD by adding BSA to BOD solution, the reduction current densities decreased to -0.8 ± 0.4 mA cm^{-2} at BOD/MWCNT2/GCE and -0.27 ± 0.05 mA cm^{-2} at BOD/MWCNT3/GCE. It is found that the attempt to decrease in the fraction of BOD is effective to increase in the kinetic contribution to the observed current density (see Eq. (1)). If the co-adsorption of BSA does not affect the bioelectrocatalytic activity of BOD, the extents of the decrease in the reduction current density at BOD/MWCNT2/GCE will be the same as that at BOD/MWCNT3/GCE. However, there existed systematic difference, as judged from the Student *t*-test at 90 % confidence level. The interference by co-existing BSA against the bioelectrocatalytic activity of BOD depends on the surface conditions. Therefore, we can say that the lowering fraction of BOD is effective for achieving kinetic-controlled conditions at the BOD modified

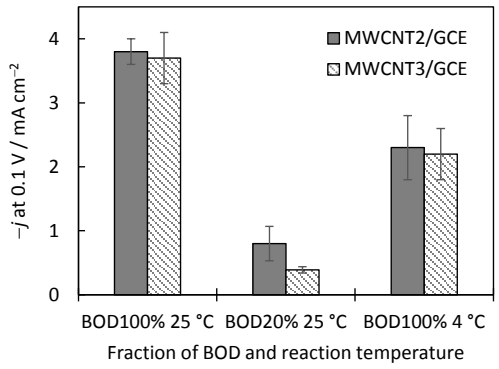

Figure 2
Steady-state O_2 reduction current densities in CA (0.1 V, taken at 60 s) at BOD/MWCNT2/GCE (left side of each column) and BOD/MWCNT3/GCE (right side of each column). The left, central, and right columns are, respectively, the results measured at 25 °C with BOD 100 % solution, measured at 25 °C with BOD 20 wt% solution, and measured at 4 °C with BOD 100 % solution. The measurements were carried out in O_2-saturated 100 mM phosphate buffer (pH 7) at ω = 4000 rpm. The error bars were evaluated by the Student *t*-distribution at 90 % confidence level.

electrodes at 25 °C, but is not suitable for evaluation of effects of the electrode surface property on the BOD activity.

On the other hand, when the author measured the catalytic current at 4 °C, the reduction current density decreased down to -2.3 ± 0.5 mA cm^{-2} at BOD/MWCNT2/GCE. The value was almost identical with that at BOD/MWCNT3/GCE (-2.2 ± 0.4 mA cm^{-2}). Consequently, the author choses the temperature control method to evaluate the kinetic factor.

3.3 Effects of surfactant and MWCNT length on the bioelectrocatalytic activity of BOD

Fig. 3 shows LSVs at BOD/MWCNT/GCEs and BOD/KB/GCE. Table 1 summarizes j at 0.1 V and at 4 °C in CA together with the relative value of the electroactive surface areas. The relative electroactive surface areas of the electrodes are evaluated from the amplitude of the non-faradic charging currents in cyclic voltammetry at a given ν under Ar-saturated conditions (data not shown). The measurements were carried out at 4 °C and at ω = 4000 rpm. Although the non-faradic charging current seems to be affected both by surface area and presence of charged species on CNTs, it is one of the effective methods for the evaluation of the relative values of the electroactive surface area, as far as we know. In this study, the relative electroactive surface area is utilized as a supplementary index to support our conclusion that the enlargement of the catalytic current at BOD/MWCNT1/GCE is not simply due to the increase of the electroactive surface area. At BOD/MWCNT1/GCE, the limiting catalytic reduction current decreased due to a decrease in the temperature (Fig. 3, black solid line), as compared with that given in Fig. 1 (A). At 4 °C, D_{O_2}, ν and c_{O_2} are, respectively, 1.2×10^{-5} cm^2 s^{-1} [49], 0.0156 cm^2 s^{-1} [50,51], and 2.0 mM [52]. According to Eq. (2), the author can estimate

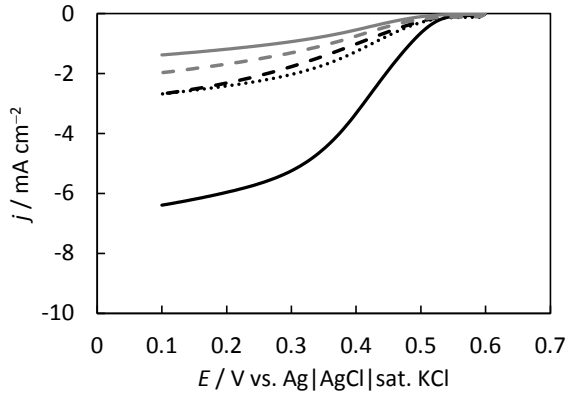

Figure 3
LSVs at BOD-adsorbed MWCNTs/GCE and BOD-adsorbed KB/GCE in O_2-saturated 100 mM phosphate buffer (pH 7) at 4 ± 1 °C, ω = 4000 rpm, and ν = 5 mV s^{-1}. MWCNTs indicate MWCNT1 (black solid line), MWCNT2 (black broken line), MWCNT3 (black dotted line) and MWCNT4 (gray solid line). KB is expressed by a gray broken line.

Table 1
Summary of information on the characteristics of MWCNTs, BOD-adsorbed MWCNTs, and BOD-adsorbed KB for the bioelectrocatalytic O_2 reduction.

BOD-adsorbed electrodes	Properties of water-dispersed MWCNTs			$-j$ (at 0.1 V, 4 °C) / mA cm^{-2} *	$-j_{cat}$ (at 0.1 V, 4 °C) / mA cm^{-2} **	Relative electroactive surface area ***
	With or without surfactant	Outer diameter / nm	Length / μm			
MWCNT1/GCE	w/o	10-15	1-4	6.1 ± 0.4	15 ± 2	1
MWCNT2/GCE	with	10-15	1-4	2.3 ± 0.5	3.0 ± 0.8	1.7
MWCNT3/GCE	w/o	8-10	<1	2.2 ± 0.4	2.8 ± 0.7	2.3
MWCNT4/GCE	w/o	10-15	10	1.2 ± 0.2	1.4 ± 0.2	0.42
KB/GCE	–	–	–	1.7 ± 0.1	2.0 ± 0.2	2

* The steady-state O_2 reduction current densities were taken at 60 s after the closed circuit in chronoamperometry. The electrode potential is 0.1 V. The measurements were carried out in O_2-saturated 100 mM phosphate buffer (pH 7) at 4 ± 1 °C at ω = 4000 rpm. The error bars were evaluated by the Student *t*-distribution at 90 % confidence level.
** The catalytic current densities (j_{cat}) were calculated from the measured current densities (j) by Eqs. (1) and (2)
*** The relative electroactive surface areas were evaluated from the amplitude of non-faradic charging current under Ar-saturated conditions in cyclic voltammetry.

$j_{dif} = -10.3\,\mathrm{mA\,cm^{-2}}$ at 4000 rpm and at 4 °C. The experimental value of j (–6.1 mA cm^{-2}) at BOD/MWCNT1/GCE is sufficiently smaller than j_{dif} in the absolute value. However, j was affected by ω at even increased ω (data not shown). Therefore, we can say that the limiting current at BOD/MWCNT1/GCE is controlled by the enzyme kinetics as well as the mass-transfer in part. Therefore, the author evaluated j_{cat} from j and j_{dif} by utilizing Eqs. (1) and (2). The evaluated values of j_{cat} are also collected in Table 1.

At first, let us consider effects of the surfactant (Triton-X®). BOD/MWCNT2/GCE (Fig. 3, black broken line) gave a small value of j in LSV compared with BOD/MWCNT1/GCE (Fig. 3, black solid line). As shown in Table 1, j_{cat} is 5-times smaller than that at BOD/MWCNT1/GCE. Consequently, the surfactant seems to interfere the DET-type bioelectrocatalysis of BOD.

Second, the author compared the three types of water-dispersed MWCNTs (MWCNT1, 3 and 4) without surfactant. Concerning the outer diameter, there are no significant differences among these threes MWCNTs. BOD/MWCNT3/GCE and BOD/MWCNT4/GCE (Fig. 3, black dotted line and gray solid line, respectively) gave low values of j compared with BOD/MWCNT1/GCE. Taking into account of the relative electroactive surface areas given in Table 1, the author can conclude that the increase in j (as the absolute value) at BOD/MWCNT1/GCE is not ascribed to the effect of the electroactive surface area, and that the improvement in the bioelectrocatalytic activity can be

reasonably ascribed to the electrode surface property suitable for the bioelectrocatalysis of BOD. As mentioned in Introduction, the π-π conjugated system and the carboxy groups on the electrode surface seem to be key factors for improving the activity of BOD for DET-type bioelectrocatalysis [11,39]. Since the opened ends of CNTs are terminated with the carboxy groups, the amount of the carboxy groups on the surface of CNTs-based electrodes seems to increase with a decrease in the length of CNTs [3]. The author can conclude that the surface of MWCNT1/GCE provides suitable extent of the π-π conjugated system and the carboxy groups.

In constructing the enzyme-modified electrodes, KB is often utilized as one of the porous carbon materials [19,28,36,37,40,44,45]. However, BOD/KB/GCE gives a relatively small value of the limiting current density in the catalytic O_2 reduction wave in LSV compared with BOD/MWCNT1/GCE (Fig. 3). As shown in Table1, the author can conclude that the BOD/MWCNT1/GCE achieves 7.5 times higher bioelectrocatalytic activity than BOD/KB/GCE in solution.

4. Conclusion

The author has examined four types of water-dispersed MWCNTs which have different length with or without surfactant, and compared the characteristics of MWCNTs-based biocathodes at low temperature (to decrease the enzyme activity for evaluation of the kinetic contribution of BOD). At first, it has been found that the surfactant interferes the DET-type bioelectrocatalysis of BOD. Second, the author concludes that the amounts of the π-π conjugated system and the carboxy groups on the electrode surface, which can be controlled by the length of MWCNT, determines the bioelectrocatalytic activity of BOD. By utilizing the MWCNT with short lengths of 1–4 μm (named MWCNT1), the author has achieved a diffusion-controlled catalytic reduction of O_2 in solution (–8 mA cm^{-2}) at 25 °C and at ω = 4000 rpm. Furthermore, the author has evaluated the kinetic-controlled current density at 4 °C and, it has been found that the electrode achieves the 7.5 times improvement in the kinetic factor compared to the KB-based electrode.

In this study, the author has improved and elucidated the performance of BOD-adsorbed biocathodes in solution by using MWCNTs with short lengths. This study will give an important knowledge to enhance performance of biocathodes and biofuels for practical use in the near future. For practical application such as gas-diffusion-type electrode, MWCNT1 can be utilized in place of KB, and it will contribute to the great advancement in constructing the O_2 reducing biocathode.

5. References

[1] S. Iijima, Helical microtubules of graphitic carbon, Nature 354 (1991) 56.

[2] A. Merkoci, M. Pumera, X. Llopis, B. Pérez, M.D. Valle, S. Alegret, New materials for electrochemical sensing VI: Carbon nanotubes, Trends in Anal. Chem. 24 (2005) 826.

[3] J. Chen, M.A. Hamon, H. Hu, Y. Chen, A.M. Rao, P.C. Eklund, R.C. Haddon, Solution properties of single-walled carbon nanotubes, Science 282 (1998) 95.

[4] R.J. Chen, Y. Zhang, D. Wang, H. Dai, Noncovalent sidewall functionalization of single-walled carbon nanotubes for protein immobilization, J. Am. Chem. Soc. 123 (2001) 3838.

[5] M. Holzinger, A.L. Goff, S. Cosnier, Carbon nanotube/enzyme biofuel cells, Electrochim. Acta 82 (2012) 179.

[6] Y. Ogawa, S. Yoshino, T. Miyake, M. Nishizawa, Surfactant-assisted direct electron transfer between multi-copper oxidases and carbon nanotube-based porous electrodes, Phys. Chem. Chem. Phys. 16 (2014) 13059.

[7] W. Zheng, Q. Li, L. Su, Y. Yan, J. Zhang, L. Mao, Direct electrochemistry of multi-copper oxidases at carbon nanotubes noncovalently functionalized with cellulose derivatives, Electroanalysis 18 (2006) 587.

[8] Y. Ulyanova, S. Babanova, E. Pinchon, I. Matanovic, S. Singhal, P. Atanassov, Effect of enzymatic orientation through the use of syringaldazine molecules on multiple multi-copper oxidase enzymes, Phys. Chem. Chem. Phys. 16 (2014) 13367.

[9] R.J. Lopez, S. Babanova, Y. Ulyanova, S. Singhal, P. Atanassov, Improved interfacial electron transfer in modified bilirubin oxidase biocathodes, ChemElectroChem 1 (2014) 241.

[10] T. Miyake, S. Yoshino, T. Yamada, K. Hata, M. Nishizawa, Self-regulating enzyme-nanotube ensemble films and their application as flexible electrodes for biofuel cells, J. Am. Chem. Soc. 133 (2011) 5129.

[11] G. Göbel, F. Lisdat, Organic interlayers for oxygen reducing electrodes based on bilirubin oxidase and MWCNT modified gold, Electrochem. Commun. 10 (2008) 1691.

[12] M. Jönsson-Niedziolka, A. Kaminska, M. Opallo, Pyrene-functionalised single walled carbon nanotubes for mediatorless dioxygen bioelectrocatalysis, Electrochimica Acta 55 (2010) 8744.

[13] J.A. Cracknell, K.A. Vincent, F.A. Armstrong, Enzymes as working inspirational

electrocatalysts for fuel cells and electrolysis, Chem. Rev. 108 (2008) 2439.

[14] M.J. Moehlenbrock, S.D. Minteer, Extended lifetime biofuel cells, Chem. Soc. Rev. 37 (2008) 1188.

[15] N. Mano, F. Mao, A. Heller, A miniature membrane-less biofuel cell operating at +0.60 V under physiological conditions, ChemBioChem 5 (2004) 1703.

[16] D. Leech, P. Kavanagh, W. Schuhmann, Enzymatic fuel cells: Recent progress, Electrochim. Acta 84 (2012) 223.

[17] S.C. Barton, J. Gallaway, P. Atanassov, Enzymatic biofuel cells for implantable and microscale devices, Chem. Rev. 104 (2004) 4867.

[18] C. Léger, P. Bertrand, Direct electrochemistry of redox enzymes as a tool for mechanistic studies, Chem. Rev. 108 (2008) 2379.

[19] M. Rasmussen, S. Abdellaoui, S.D. Minteer, Enzymatic biofuel cells: 30 years of critical advancements, Biosens. Bioelectron. in press DOI: 10.1016/j.bios.2015.06.029.

[20] K.A. Vincent, A. Parkin, F.A. Armstrong, Investigating and exploiting the electrocatalytic properties of hydrogenases, Chem. Rev. 107 (2007) 4366.

[21] H.S. Shafaat, O. Rüdiger, H. Ogata, W. Lubitz, [NiFe] hydrogenases: A common active site for hydrogen metabolism under diverse conditions, Biochimica et Biophysica Acta 1827 (2013) 986.

[22] S. Kawai, M. Goda-Tsutsumi, T. Yakushi, K. Kano, K. Matsushita, Heterologous overexpression and characterization of a Flavoprotein-cytochrome *c* complex fructose dehydrogenase of *Gluconobacter japonicus* NBRC3260, Appl. Environ. Microbiol. 7 (2013) 1564.

[23] S. Kawai, T. Yakushi, K. Matsushita, Y. Kitazumi, O. Shirai, K. Kano, The electron transfer pathway in direct electrochemical communication of fructose dehydrogenase with electrodes, Electrochem. Commun. 38 (2014) 28.

[24] V. Flexer, F. Durand, S. Tsujimura, N. Mano, Efficient direct electron transfer of PQQ-glucose dehydrogenase on carbon cryogel electrodes at neutral pH, Anal. Chem. 83 (2011) 5721.

[25] A. Lindgren, L. Gorton, T. Ruzgas, U. Baminger, D. Haltrich, M. Schülein, Direct electron transfer of cellobiose dehydrogenase from various biological origins at gold and graphite electrodes, J. Electroanal. Chem. 496 (2001) 76.

[26] V. Fridman, U. Wollenberger, V. Bogdanovskaya, F. Lisdat, T. Ruzgas, A. Lindgren, L. Gorton, F.W. Scheller, Electrochemical investigation of cellobiose oxidation by cellobiose dehydrogenase in the presence of cytochrome c as mediator, Biochem. Soc. Trans. 28 (2000) 63.

[27] E.I. Solomon, U.M. Sundaram, T.E. Machonkin, Multicopper oxidases and oxygenases, Chem. Rev. 96 (1996) 2563.

[28] N. Mano, L. Edembe, Bilirubin oxidases in bioelectrochemistry: Features and recent findings, Biosens. Bioelectron. 50 (2013) 478.

[29] S. Murao, N. Tanaka, A new enzyme “bilirubin oxidase” produced by *Myrothecium verrucaria* MT-1, Agric. Biol. Chem. 45 (1981) 2383.

[30] S. Tsujimura, T. Nakagawa, K. Kano, T. Ikeda, Kinetic study of direct bioelectrocatalysis of dioxygen reduction with bilirubin oxidase at carbon electrodes, Electrochemistry 72 (2004) 437.

[31] M.R. Tarasevich, A.I. Yaropolov, V.A. Bogdanovskaya, S.D. Varfolomeev, 293 - Electrocatalysis of a cathodic oxygen reduction by laccase, Bioelectrochem. Bioenerg. 6 (1979) 393.

[32] S. Shleev, A. Jarosz-Wilkolazka, A. Khalunina, O. Morozova, A. Yaropolov, T. Ruzgas, L. Gorton, Direct electron transfer reactions of laccases from different origins on carbon electrodes, Bioelectrochemistry 67 (2005) 115.

[33] K. Kataoka, H. Komori, Y. Ueki, Y. Konno, Y. Kamitaka, S. Kurose, S. Tsujimura, Y. Higuchi, K. Kano, D. Seo, T. Sakurai, Structure and fuction of the engineered multicopper oxidase CueO from *Escherichia coli* – Deletion of the methionine-rich helical region covering the substrate-binding site, J. Mol. Biol. 373 (2007) 141.

[34] Y. Miura, S. Tsujimura, S. Kurose, K. Kataoka, T. Sakurai, K. Kano, Direct electrochemistry of CueO and its mutants at residues to and near type I Cu for oxygen-reducing biocathode, Fuel Cells 9 (2009) 70.

[35] S. Shleev, J. Tkac, A. Christenson, T. Ruzgas, A.I. Yaropolov, J.W. Whittaker, L. Gorton, Direct electron transfer between copper-containing proteins and electrodes, Biosens. Bioelectron. 20 (2005) 2517.

[36] Y. Kamitaka, S. Tsujimura, N. Setoyama, T. Kajino, K. Kano, Fructose/dioxygen biofuel cell based on direct electron transfer-type bioelectrocatalysis, Phys. Chem. Chem. Phys. 9 (2007) 1793.

[37] K. So, S. Kawai, Y. Hamano, Y. Kitazumi, O. Shirai, M. Hibi, J. Ogawa, K. Kano, Improvement of a direct electron transfer-type fructose/dioxygen biofuel cell with a substrate-modified biocathode, Phys. Chem. Chem. Phys. 16 (2014) 4823.

[38] K. Murata, K. Kajiya, N. Nakamura, H. Ohno, Direct electrochemistry of bilirubin oxidase on three-dimensional gold nanoparticle electrodes and its application in a biofuel cell, Energy Environ. Sci. 2 (2009) 1280.

[39] L.D. Santos, V. Climent, C.F. Blanford, F.A. Armstrong, Mechanistic studies of the 'blue' Cu enzyme, bilirubin oxidase, as a highly efficient electrocatalyst for the oxygen reduction reaction, Phys. Chem. Chem. Phys. 12 (2010) 13962.

[40] R. Kontani, S. Tsujimura, K. Kano, Air diffusion biocathode with CueO as electrocatalyst adsorbed on carbon particle-modified electrodes, Bioelectrochemistry 76 (2009) 10.

[41] G. Gupta, C. Lau, V. Rajendran, F. Colon, B. Branch, D. Ivnitski, P. Atanassov, Direct electron transfer catalyzed by bilirubin oxidase for air breathing gas-diffusion electrodes, Electrochem. Commun. 13 (2011) 247.

[42] T. Miyake, K. Haneda, S. Yoshino, M. Nishizawa, Flexible, layered biofuel cells, Biosens. Bioelectron. 40 (2013) 45.

[43] N. Lalaoui, A.D. Poulpiquet, R. Haddad, A.L. Goff, M. Holzinger, S. Gounel, M. Mermoux, P. Infossi, N. Mano, E. Lojou, S. Cosnier, A membraneless air-breathing hydrogen biofuel cell based on direct wiring of thermostable enzymes on carbon nanotube electrodes, Chem. Commun. 51 (2015) 7447.

[44] K. So, Y. Kitazumi, O. Shirai, K. Kurita, H. Nishihara, Y. Higuchi, K. Kano, Kinetic analysis of inactivation and enzyme reaction of oxygen-tolerant [NiFe]-hydrogenase at direct electron-transfer bioanode, Bull. Chem. Soc. Jpn. 87 (2014) 1177.

[45] K. So Y. Kitazumi, O. Shirai, K. Kurita, H. Nishihara, Y. Higuchi, K. Kano, Gas-diffusion and Direct-electron-transfer-type bioanode for hydrogen oxidation with oxygen-tolerant [NiFe]-hydrogenase as an electrocatalyst, Chem. Lett. 43 (2014) 1575.

[46] A.J. Bard, L. R. Faulkner, Electrochemical methods: fundamentals and applications 2nd ed., Wiley, New York 335.

[47] C.C. Page, C.C. Moser, X. Chen, P.L. Dutton, Natural engineering principles of electron tunneling in biological oxidation-reduction, Nature 402 (1999) 47.

[48] J.A. Cracknell, T.P. Mcnamara, E.D. Lowe, C.F. Blanford, Bilirubin oxidase form *Myrothecium verrucaria*: X-ray determination of the complete crystal structure and a rational surface modification for enhanced electrocatalytic O_2 reduction, Dalton Trans. 40 (2011) 6668.

[49] D.M. Himmelblau, Diffusion of dissolved gases in liquids, Chem. Rev. 64 (1964) 527.

[50] A. Nagashima, Viscosity of water substance – new international formulation and its background, J. Phys. Chem. Ref. Data 6 (1977) 1133.

[51] D. R. Lide, Ed., CRC Handbook of Chemistry and Physics, 90th ed., CRC Press, New York (2009)

[52] R. Battino, Ed., IUPAC Solubility Data Series, Vol. 7, Oxygen and Ozone, Pergamon Press, Oxford (1981)

1-3. Analysis of factors governing direct electron transfer-type bioelectrocatalysis of bilirubin oxidase at modified electrodes

Abstract

Direct electron transfer (DET)-type bioelectrocatalysis is an essential technique for constructing simple bioelectrochemical devices such as biosensors, bioreactors, and biofuel cells. Bilirubin oxidase (BOD), a biocatalyst for the four-electron reduction of dioxygen (O_2) into water, is a promising enzyme for powerful DET-type biocathodes. Mesoporous carbon materials are often used in BOD-modified biocathodes. However, the supply of O_2 becomes a key factor governing BOD-catalyzed current densities owing to its low solubility. In this study, the author analyzed steady-state rotating disk voltammograms of a BOD-catalyzed reaction in a rigid manner by taking into account the mass-transport as well as the enzymatic and the interfacial electron transfer kinetics. Non-catalytic redox signals of adsorbed BOD were also analyzed to obtain the surface redox properties of BOD. The analysis revealed that modification of electrodes with bilirubin and/or negatively charged carbon nanotubes to improve the DET-type catalytic performance increased the amount of BOD molecules with the proper orientation for bioelectrocatalysis. The interfacial electron transfer kinetic characteristics remained almost unchanged.

1. Introduction

Bioelectrocatalysis, a coupled process involving enzymatic and electrode reactions, is a subject of interest for practical applications of bioelectrochemical devices such as biosensors, bioreactors, and biofuel cells [1–7]. The reactions are classified into two types according to the difference in the electric connection systems between the enzyme and the electrode [1–7]. The first type is mediated electron transfer (MET) in which an artificial redox mediator shuttles electrons to reduce the kinetic hindrance of the interfacial electron transfer. The second type is direct electron transfer (DET) in which an enzyme can directly communicate with an electrode without a mediator. DET-type bioelectrocatalysis is expected to be utilized for advanced applications since it only requires an enzyme and an electrode as structural components [1–7].

In DET-type bioelectrocatalysis, an enzyme is adsorbed on an electrode to catalyze the electron transfer between the enzyme substrate and the electrode [1–7]. In this sense, it is very important to control the orientation of the enzyme on the electrode surface because the interfacial electron transfer rate constant increases exponentially upon decreasing the distance between the electrode surface and the redox site of the enzyme [8–10]. There are two major models for enzyme orientation namely, “simple orientation” [11–13] and “random orientation” (or dispersion model) [4,14,15]. The former model assumes the existence of two types of adsorbed enzymes (i.e.,

electroactive and inactive) with the electroactive enzyme facing its the redox site toward the electrode surface with a uniform orientation [11–13]. On the other hand, the latter model assumes spherical enzymes and considers uniform dispersion of the adsorbed enzymes [4,14,15]. In both cases, favorite (i.e., productive) orientation for DET may result in increasing amounts of electroactive enzymes and higher interfacial electron transfer rate constants. Detailed and rigid analysis of catalytic DET-type voltammograms of enzyme-modified electrodes was shown to provide valuable information on the kinetics and orientation of the enzyme [4,11–15]. Under the limited conditions by which the rate of substrate supply is sufficiently fast compared to that of the catalytic reaction, the increase in the limiting catalytic current density was ascribed to the higher amounts of electroactive enzymes, while the shift of the midpoint potential or the change in the catalytic wave shape reflected a change in the interfacial electron transfer kinetics [4,11–15].

There are several DET-type enzymes including hydrogenases [16–18], glucose oxidase [19], glucose dehydrogenase [20], fructose dehydrogenase [21,22], cellobiose dehydrogenase [23,24], and multi-copper oxidases (MCOs) [25–28]. Among them, hydrogenases and MCOs react with gaseous substrates (i.e., dihydrogen (H_2) and dioxygen (O_2), respectively), and the solubility of the gaseous substrates is very low (i.e., less than sub-mM at atmospheric pressure (1 M = 1 mol dm^{-3})) [16–18,25–28]. MCOs are enzymes that catalyze the four-electron reduction of O_2 into water and are utilized as biocatalysts for biocathodes of DET-type biofuel cells using glucose, fructose, or hydrogen as fuels [29–36]. For practical use, mesoporous materials with high specific surface areas are used as electrode material components.

Among MCOs, bilirubin oxidase (BOD) is a promising enzyme for DET-type biocathodes. BOD has a high bioelectrocatalytic activity under mild conditions, and its formal potential is close to that of the H_2O/O_2 redox couple [26,31,35–38]. These features allow high DET-type catalytic current densities with minimum overpotentials. BOD is frequently supported on carbon electrodes to examine its DET-type properties [31,35,39–47]. BOD (and generally MCOs) has four copper atoms that constitute its active site. The copper atoms are classified into three types according to their spectroscopic and magnetic properties namely, type I (T1), type II (T2), and type III (T3) coppers [25,26]. BOD can receive electrons at the T1 copper site from the electrode, and the electrons are transferred to the T2–T3 copper cluster to carry out the reduction of O_2. [25,26] Thus, it is important to control the orientation of adsorbed BOD with the aim to shorten the distance between the T1 copper site and the electrode.

In order to achieve favorite orientation of BOD onto the electrode surface, several approaches have been proposed [31,35,39–47]. Improved DET-type bioelectrocatalysis has been accomplished at negatively charged electrodes constructed by modification with diazonium coupling [39] or amine oxidation [40] reactions. In addition, physical adsorption of bilirubin [31,35,41,42] or other aromatic compounds [43] and utilization of functionalized carbon nanotubes (CNTs) [44,45]

have been also shown to be effective for enhancing DET-type bioelectrocatalysis of BOD especially from *Myrothecium verrucaria*. CNTs have been widely used as electrode platforms to achieve favorable orientation of enzymes [48]. Furthermore, the amounts of π-π conjugated systems and carboxy groups on the electrode surface, which can be controlled by the length of the multi-walled CNTs, are considered to be the factors governing the bioelectrocatalytic activity of BOD [46]. It is noted here, however, that not all BODs have similar surface characteristics. For example, for BOD from *Bacillus pumilus*, the above mentioned procedures were not effective to improve the orientation [47].

Enzyme orientation can affect either the amount of effective enzymes or the interfacial electron transfer rate constant, or both [4,11–15]. The detailed reasons of the effectiveness of these modification approaches should be evaluated from robust analysis of catalytic DET-type voltammograms. In this sense, it is noted that catalytic voltammograms have to be carefully analyzed by considering the mass-transport of substrates [4]. In the case of BOD, owing to the low solubility of O_2 and the enlargement of the specific surface areas upon deposition on porous materials, the DET-type bioelectrocatalytic current is likely to be governed by the mass-transport. The diffusion current density in a rotating disk electrode system is ca. −8–12 mA cm^{-2} at 4–25 °C and 4000 rpm [27,46].

In this study, the author elucidated the DET-type bioelectrocatalytic properties of BOD by considering the effect of the mass-transport. Ketjen black (KB) and water-dispersed multi-walled CNTs with lengths of 1–4 μm were used as carbon materials to construct the electrodes. Furthermore, bilirubin, a natural substrate of BOD, was supported onto these electrodes. These methods are known to achieve high current densities of the DET-type bioelectrocatalysis (i.e., close to the diffusion current density of O_2) under rotating disk conditions at neutral pH and room temperature [31,41,42,46]. DET-type bioelectrocatalysis consists of three processes namely, heterogeneous electron transfer, enzymatic catalytic reaction, and mass-transport [4]. Under diffusion-controlled conditions, it is impossible (or difficult) to extract the kinetic factors concerning the heterogeneous electron transfer and the enzymatic reaction from the voltammetric characteristics. For the sake of accurate analysis, conditions at which the DET-type bioelectrocatalysis is predominantly governed by the reaction kinetics should be preferably selected. Thus, the author carried out measurements at low temperature and high pH conditions at which the activity of BOD decreases while the stability remains unaffected [38]. Under the conditions, the author analyzed steady-state rotating disk voltammograms of BOD based on a robust electrochemical model by taking into account of the contribution of the mass-transport. In addition, the author evaluated the surface redox properties of adsorbed BOD from non-catalytic Faradaic signals. Combining these data, the author discussed the orientation of BOD on the surface of the mesoporous carbon electrodes prepared by the aforementioned methods (utilization of water-dispersed multi-walled CNT with lengths of 1–4 μm and bilirubin modification). The detailed effects of the methods on controlling the enzyme orientation were still unclear [31,35,41,42,46], however the

analysis in this study revealed that both methods increased the surface concentration of the effective enzyme, while the interfacial electron transfer kinetics remained almost unchanged.

2. Experimental

2.1. Materials

KB (EC300J) was kindly donated from Lion Co. (Japan). Poly(1,1,2,2-tetrafluoroethylene) (PTFE, 6-J) fine powder was purchased from DuPont-Mitsui Fluorochemicals Co., Ltd., (Japan). Bilirubin was purchased from Wako Pure Chemical (Japan) and dissolved in a 30 mM NaOH aqueous solution. Water-dispersed multi-walled carbon nanotubes (MWCNTs) (outer diameter: 10–15 nm, length: 1–4 μm, without surfactant) were kindly donated from Nitta Co. (Japan). Bilirubin oxidase (BOD; EC 1.3.3.5) from *Myrothecium verrucaria* was donated from Amano Enzyme Inc. (Japan) and used without further purification. The rest of chemicals used in this study were of analytical grade unless otherwise specified, and all aqueous solutions were prepared with distilled water.

2.2. Preparation of the electrodes

KB or MWCNTs were supported on a glassy carbon electrode (GCE for rotating electrode, 3 mm in diameter, BAS). GCE was polished with alumina slurry (Buehler, 1 mm), sonicated, and finally washed with distilled water. KB-modified GCE (KB:PTFE = 8:2 (w/w)) (KB/GCE) and MWCNT-modified GCE (MWCNT/GCE) were prepared according to protocols reported in the literature [31,46]. Note that the author sonicated the MWCNT-dispersed solution in an ultrasonic bath for 3 min to completely disperse MWCNT before use. Besides, 10 μL (1 L = 1 dm^3) of a bilirubin solution (3 mM) was applied onto KB/GCE or MWCNT/GCE, dried at room temperature, and subsequently washed with distilled water [31]. The as-prepared electrodes were denoted as BL/KB/GCE and BL/MWCNT/GCE, respectively. Subsequently, 30 μL of a BOD solution (10 mg mL^{-1}) dissolved in a 10 mM phosphate buffer (pH = 7.0) was then applied onto the surface of the prepared electrodes (KB/GCE, BL/KB/GCE, MWCNT/GCE, and BL/MWCNT/GCE), and they were subsequently kept in a water-saturated atmosphere for 1.5 h at 4 °C for slow drying, washed with a buffer solution, and used immediately for electrochemical measurements. In the case of the control experiments carried out to confirm the non-catalytic redox signals of adsorbed BOD, 30 μL of a 10 mM phosphate buffer (pH = 7.0) without BOD were applied onto the surface of the prepared electrodes, and the author followed the same procedure as in the case of the BOD-modified electrodes.

2.3 Electrochemical measurements

Linear sweep voltammetry, cyclic voltammetry, and chronoamperometry were conducted on BAS CV50W and ALS 714C electrochemical analyzers. Steady-state measurements were carried out with a rotating disk GCE (RDE-2, BAS Inc.) at 4000 rpm and a scan rate of 5 mV s^{-1} unless otherwise stated. Anaerobic measurements were conducted in a nitrogen (N_2) chamber filled with a mixture of 96% N_2 and 4% H_2. A platinum wire and an Ag|AgCl|sat KCl electrode were used as counter and reference electrodes, respectively. All potentials in this work were referred to the reference electrode. The measurements were carried out in 100 mM phosphate (pH = 7.0) or 100 mM Tris-HCl (pH = 8.5 or 9.4) buffers at 25 ± 1 or 4 ± 1 °C.

3. Results and discussion

3.1 Effects of the mass-transport on the DET-type bioelectrocatalysis

Fig. 1(A) shows the background-subtracted rotating disk linear sweep voltammograms (LSVs) of BOD-adsorbed KB/GCE (BOD/KB/GCE), BL/KB/GCE (BOD/BL/KB/GCE), and MWCNT/GCE (BOD/MWCNT/GCE) under O_2-saturated conditions at a pH of 7.0, 25 °C, and an electrode rotating speed (ω) of 4000 rpm. A typical and sigmoidal reduction wave was observed under the rotating electrode conditions. According to the literature, this wave was ascribed to DET-type bioelectrocatalysis on BOD [31,35,39–47]. Modification with bilirubin and utilization of MWCNTs

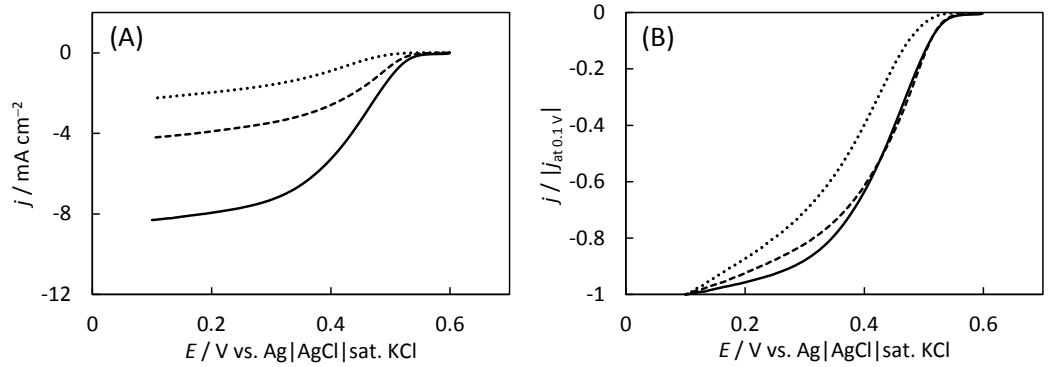

Figure 1
(A) Background-subtracted LSVs of the catalytic O_2 reduction for BOD/KB/GCE (dotted line), BOD/BL/KB/GCE (broken line), and BOD/MWCNT/GCE (solid line) in a O_2-saturated 100 mM phosphate buffer (pH = 7.0) at 25 ± 1 °C, ω = 4000 rpm, and ν = 5 mV s^{-1}.
(B) Normalized LSV for each limiting catalytic current at 0.1 V shown in Fig. 1(A). Dotted, broken, and solid lines correspond to the results of BOD/KB/GCE, BOD/BL/KB/GCE, and BOD/MWCNT/GCE, respectively.

are known to be effective methods to enhance the bioelectrocatalytic current density of BOD by achieving selective orientation for DET [31,35,41,42,45–47]. In fact, these methods achieved higher reduction current densities as compared to BOD/KB/GCE. Although an slight increase in the reduction current may be observed at sufficiently negative potential regions owing to unfavorable orientation of adsorbed enzymes (called as "residual slope" in a random orientation model) [4,14,15], the author considered that the current nearly reached the limiting value at an overpotential of 0.1 V. The increase in the limiting reduction current revealed the presence of larger amounts of electrochemically active (or effective) BOD. In addition, the normalization of LSVs with the limiting reduction current at 0.1 V (Fig. 1(B)) showed an apparent shift of the half-wave potential to the positive direction upon electrode modifications (i.e., a decrease in the overpotential for O_2 reduction). Based on these results and discussion, the effectiveness of the electrode modifications were considered to be ascribed to larger amounts of effectively adsorbed BOD molecules and higher interfacial electron transfer rate constants.

However, the limiting reduction current density was strongly controlled by the mass-transport, as judged from the observed limiting reduction current density of −8 mA cm^{-2} of BOD/MWCNT/GCE, which is very close to the diffusion current density (−8.4 mA cm^{-2}) in an O_2-saturated phosphate buffer (pH = 7.0) at 25 ± 1 °C and 4000 rpm [46]. Consequently, we should take into account the effects of the mass-transport and therefore carefully analyze the voltammograms. As mentioned in the Introduction, DET-type bioelectrocatalysis is composed of three successive steps in series (i.e., interfacial electron transfer, catalytic reaction, and mass-transport) [4]. By setting the current density determined by the individual rate-determining step, the observable current density (j) can be expressed by Eq. (1) and rewritten as expressed by Eq. (2):

$$\frac{1}{j} = \frac{1}{j_{et}} + \frac{1}{j_{cat}} + \frac{1}{j_{mt}}, \tag{1}$$

$$j = \frac{j_{cat}}{1 + j_{cat}/j_{et} + j_{cat}/j_{mt}}, \tag{2}$$

where, j_{et}, j_{cat}, and j_{mt} are the forward electron transfer current density, the catalytic reaction-controlled current density, and the mass-transport-controlled current density in a rotating disk electrode system, respectively [49,50]:

$$j_{et} = -n_s F k^\circ \exp\left\{\frac{-\alpha n_{enz} F}{RT}\left(E - E^{\circ\prime}_{enz}\right)\right\}\Gamma_{enz,eff}, \tag{3}$$

$$j_{cat} = -n_s F k_{cat} \Gamma_{enz,eff}, \tag{4}$$

$$j_{mt} = -0.62 n_s F D_O^{2/3} \nu^{-1/6} \omega^{1/2} c_O, \tag{5}$$

where n_s, n_{enz}, F, k°, α, R, T, E, $E^{\circ\prime}_{enz}$, $\Gamma_{enz,eff}$, k_{cat}, D_O, ν, and c_O are the number of electrons involved

in the redox reaction of the substrate (4 in the case of O_2 reduction), the number of electrons of the enzyme (1 in the case of the T1 Cu electron accepting active site in BOD), the Faraday constant, the standard electron transfer rate constant, the transfer coefficient, the gas constant, the temperature, the electrode potential, the formal potential of the enzyme, the surface concentration of the effective enzyme, the catalytic constant for one enzymatic turnover, the diffusion coefficient of O_2, the kinematic viscosity of water, and the concentration of dissolved O_2, respectively. In this study, the author assumed that the electroactive enzymes were adsorbed with a uniform orientation [11–13]. The author also rules out backward electron transfer phenomena for simplification, since the standard interfacial electron transfer rate constant of BOD is low and the backward reaction is therefore negligible at the potentials at which the catalytic current is observed [31,35,39–47].

Theoretically, we may extract information on j_{et} and j_{cat} of BOD even under conditions at which the DET-type bioelectrocatalysis is affected by the mass-transport on the basis of the equations described above. However, for the sake of accurate analysis, we preferably selected the conditions at which j_{et} and j_{cat} are significantly lower than j_{mt}. With this aim, the author focused on the properties of BOD by which the enzyme activity decreases at low temperature and high pH conditions [38].

3.2 Attempt to achieve the catalytic kinetic-controlled conditions

Fig. 2(A) shows the LSVs of BOD/MWCNT/GCE at varying pH values, 4 °C, and 4000 rpm under O_2-saturated conditions. Compared to Fig. 1(A), lowering the temperature from 25 to 4 °C was effective in decreasing j_{cat}. Moreover, the reduction current density decreased down to −2.3 mA cm^{-2} at pH = 9.4. These results are coincident with the catalytic properties of BOD in solution [38].

Fig. 2(B) shows the chronoamperograms (CA) of BOD/MWCNT/GCE at several electrode rotating rates under O_2-saturated conditions (pH = 9.4, 4 °C). The electrode potential was set to −0.1 V to achieve limiting reduction currents while varying ω (= 4000, 3000, 2000, 1000, 500, and 300 rpm) at the regions indicated by double-headed arrows (from left to right). The steady-state limiting reduction current density (j_{lim}) at a rotating disk electrode can be given by the Koutecký–Levich equation as [49,50]:

$$\frac{1}{j_{lim}} = \frac{1}{j_{cat}} + \frac{1}{j_{mt}}, \tag{6}$$

Note that Eq. (6) is obtained from Eq. (1) by assuming that j_{et} is significantly larger than j_{cat} and j_{mt}. The Levich plot is shown in the inset of Fig. 2(B) [49,50]. The data were analyzed by Gnuplot© based on Eq. (6). The regression yielded j_{cat} = −2.75 ± 0.02 mA cm^{-2} and j_{mt} = (−0.54 ± 0.01) × $\omega^{1/2}$ mA cm^{-2}. At ω = 4000 rpm ($\omega^{1/2}$ = 20.4 $s^{-1/2}$), j_{mt} was estimated to be −11.0 ± 0.2 mA cm^{-2}. This value was similar to that measured under a different buffer solution (−10.3 mA cm^{-2} in an O_2-saturated phosphate buffer (pH = 7.0) at 4 °C and 4000 rpm) [46]. Since j_{mt} is ca. four times larger than j_{cat}, the

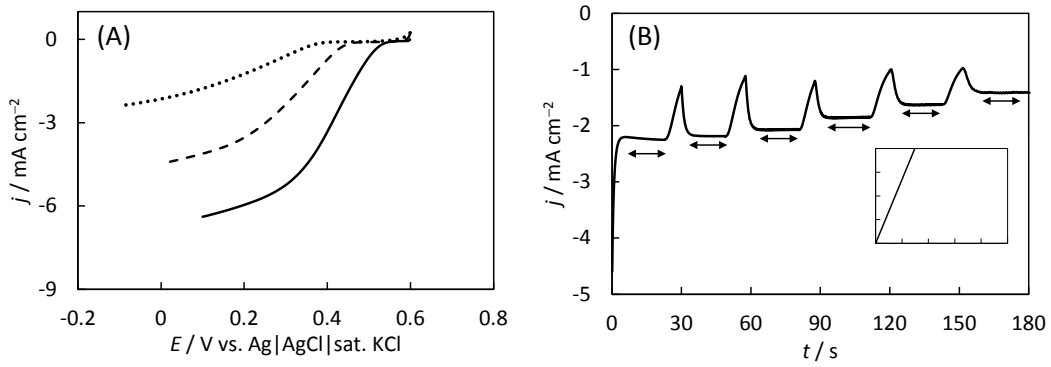

Figure 2
(A) LSVs of the catalytic O_2 reduction for BOD/MWCNT/GCE in a 100 mM phosphate buffer (pH = 7.0) (solid line), 100 mM tris-HCl buffer (pH = 8.5) (broken line), and 100 mM tris-HCl buffer (pH = 9.4) (dotted line) under O_2-saturated conditions at 4 ± 1 °C, ω = 4000 rpm, and ν = 5 mV s^{-1}.
(B) CA of BOD/MWCNT/GCE at -0.1 V. Measurements were carried out in a O_2-saturated 100 mM tris-HCl buffer (pH = 9.4) at 4 ± 1 °C. The electrode rotating rates were set as 4000, 3000, 2000, 1000, 500, and 300 rpm at the regions indicated by double head arrows from left to right. The inset shows the Levich plot (filled circles) of BOD/MWCNT/GCE based on the result shown in Fig. 2(A). j and j_{mt} estimated according to Eq. (6) are represented by dotted and solid lines, respectively.

limiting reduction current at pH = 9.4 and 4 °C was predominantly controlled by the enzyme kinetics and partially by the mass-transport. Therefore, the author decided to measure four types of BOD-adsorbed electrodes (i.e., BOD/KB/GCE, BOD/BL/KB/GCE, BOD/MWCNT/GCE, and BOD/BL/MWCNT/GCE) at pH = 9.4 and 4 °C and analyzed the voltammograms by taking j_{mt} into account.

3.3 Non-catalytic redox signals of BOD-adsorbed electrodes

Upon analyzing voltammograms of DET-type bioelectrocatalysis with Eqs. (1)–(5), five parameters (i.e., $k°$, α, $E°'_{enz}$, $\Gamma_{enz,eff}$, and k_{cat}) should be considered (as mentioned in Sec. 3.2, j_{mt} has been already estimated). Among them, $k°$, α, and j_{cat} (proportional to $\Gamma_{enz,eff}$ and k_{cat} as expressed in Eq. (4)) are the main factors to consider when discussing the orientation of DET-type enzymes [11–13]. The author may obtain some other parameters by analyzing non-catalytic voltammograms. Although the detection of non-catalytic redox signals of adsorbed enzymes is not typically easy because the redox sites are buried inside the enzymes and only a limited number of electroactive enzymes can communicate with electrodes, once clear redox signals are observed, important parameters such as $E°'_{enz}$, $\Gamma_{enz,eff}$, $k°$, and α can be evaluated, and the situation is beneficial for more fruitful discussion on the catalytic characteristics of adsorbed enzymes [16,20,27,51–53]. The author can evaluate k_{cat} in DET-type bioelectrocatalytic devices by determining $\Gamma_{enz,eff}$ in Eq. (4). Note that

k_{cat} is different from (although it may be proportional to) the catalytic constant k_c that depends on the electron acceptor or donor species in solution. For example, k_{cat} of hydrogenases measured from DET-type bioelectrocatalytic waves (1500–9000 s^{-1}) was significantly greater than k_c evaluated in solution assays with several artificial mediators (300 or 650–900 s^{-1}) [14,54].

Fig. 3(A) shows the cyclic voltammograms (CVs) of BOD/MWCNT/GCE and MWCNT/GCE under anaerobic conditions (pH = 9.4, 4 °C). Fig. 3(B) represents the enlarged CVs focusing on the cathodic waves. Cathodic and anodic peaks were observed at ca. 0.35 and 0.45 V, respectively. The redox peaks can be considered to be produced by non-catalytic Faradaic signals of DET between the T1 Cu active site in BOD and the electrode. The author examined the dependence of the peak potentials with the scan rate (v) (data not shown). The midpoint potentials were nearly independent of v up to 10 mV s^{-1} (data not shown). Thus, the author estimated $E^{\circ\prime}_{enz}$ and $\Gamma_{enz,eff}$ from the non-catalytic redox peaks of the CVs. Unfortunately, clear redox peaks were only observable up to v = 20 mV s^{-1}. The difference between the anodic and cathodic peak potentials (ΔE_p) was ca. 170 mV at v = 20 mV s^{-1} and lower than $200/n_{et}$ mV (n_{et} = 1). This means that the voltammograms were not irreversible (i.e., quasi-reversible) at v values lower than 20 mV s^{-1} [53]. Therefore, the author did not determine k° and α from the result since it is not appropriate to carry out such a kinetic analysis under quasi-reversible conditions. However, the author utilized these results as supporting data to discuss the k° and α values obtained in Section 3.4.

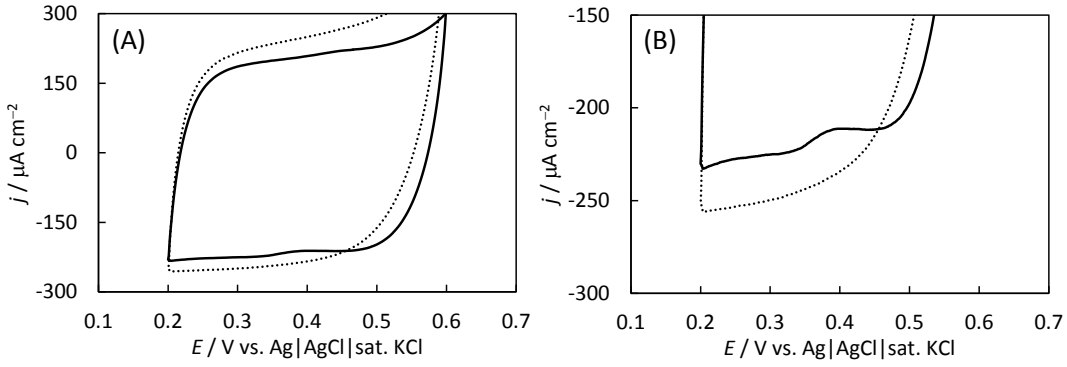

Figure 3
(A) CVs of BOD/MWCNT/GCE (solid line) and MWCNT/GCE (dotted line) in a 100 mM tris-HCl buffer (pH = 9.4) under anaerobic conditions (N_2-chamber) at 4 ± 1 °C and v = 10 mV s^{-1}.
(B) Enlargement of Fig. 3(A) focusing on the cathodic waves.

CVs of the other three types of electrodes (i.e., KB/GCE, BL/KB/GCE, and BL/MWCNT/GCE) under the same conditions of Fig. 3 (in the absence of O_2) were also measured (data not shown). Similar clear non-catalytic redox peaks were observed for BOD/BL/MWCNT/GCE, whereas no redox peaks were detected in the case of BOD/KB/GCE. Although there seem to be very small cathodic and anodic peaks at ca. 0.35 and 0.45 V, respectively in the case of BOD/BL/KB/GCE, the signals were too low to be properly analyzed. These results are summarized in Table 1. Based on these data, the author sets $E^{\circ\prime}_{enz}$ to be 0.395 V at pH = 9.4 and 4 °C, and concluded that $E^{\circ\prime}_{enz}$ was nearly independent of the types of electrodes studied herein. On the other hand, the relative values of the electroactive surface area of the electrodes were evaluated from the amplitude of the non-Faradic charging currents in the CVs at a given v (Figs. 3 and S2). Although the non-Faradic charging current was affected by both the surface areas and the presence of charged species on the electrodes, the author believes that this is one of the effective methods to evaluate the relative values of the electroactive surface area. The author confirmed that the electroactive surface areas were nearly identical among the electrodes prepared, and these results are also summarized in Table 1.

Similar experiments were conducted at pH = 7.0. CVs of BOD/MWCNT/GCE and MWCNT/GCE under anaerobic conditions (pH = 7.0, 4 °C) were measured (data not shown). While the amount of electricity of the corresponding non-catalytic redox peak was nearly identical than that obtained at pH = 9.4, the midpoint potential shifted toward the positive direction upon the change in pH to reach 0.53 ± 0.01 V (Table 1). A previous spectroelectrochemical study of our group showed that $E^{\circ\prime}_{enz}$ value for the T1 copper of BOD from *Myrothecium verrucaria* was 0.460 ± 0.008 V in solution at pH = 7.0 [55]. This difference in $E^{\circ\prime}_{enz}$ might be produced by the different environments of BOD. $E^{\circ\prime}_{enz}$ of the T1 site in MCO is known to be affected by the axial ligand [12,56,57]. In fact, $E^{\circ\prime}_{enz}$ of BOD from *Myrothecium verrucaria* with methionine (Met) moiety as the T1 axial ligand was more negative (> 0.4 V vs. Ag|AgCl) than that from *Trachyderma tsunodae* (ca. 0.5 V vs. Ag|AgCl) with a

Table 1
Properties of the adsorbed BOD and electrodes

Electrode	pH	$E^{\circ\prime}_{enz}$ / V vs. Ag|AgCl|sat. KCl	$\Gamma_{enz,\,eff}$ / 10^{-10} mol cm^{-2}	Relative electroactive surface area*
KB	9.4	undetectable	undetectable	1.1 ± 0.2
BL/KB	9.4	hard to estimate	hard to estimate	0.8 ± 0.5
MWCNT	9.4	0.39 ± 0.01	7 ± 2	1.0 ± 0.2
BL/MWCNT	9.4	0.40 ± 0.01	8 ± 3	1.0 ± 0.2
MWCNT	7.0	0.53 ± 0.01	6 ± 2	N.A.

N.A. = Not Applicable
The error bars were evaluated by the Student *t*-distribution at a 90% confidence level.
* The relative electroactive surface areas were evaluated from the amplitude of the non-Faradic charging current in cyclic voltammetry.

phenylalanine (Phe) moiety as the T1 axial ligand [26]. This difference can be ascribed to the electron donating properties of the Met moiety compared with the Phe moiety. In the case of DET-type bioelectrocatalysis, $E^{\circ\prime}_{enz}$ may be affected by both the adsorption on charged electrode surfaces and possible slight conformational changes [58–63]. The author considers that these factors are responsible for the positive shift of $E^{\circ\prime}_{enz}$ of BOD upon adsorption.

3.4 Electrochemical analysis on DET-type bioelectrocatalysis with BOD-adsorbed electrodes

Fig. 4 shows the steady-state voltammograms of BOD/KB/GCE, BOD/BL/KB/GCE, BOD/MWCNT/GCE, and BOD/BL/MWCNT/GCE under O_2-saturated conditions (pH = 9.4, 4 °C, and 4000 rpm). The error bars were evaluated with a Student *t*-distribution at a 90% confidence level. The author sets the parameters as follows: $j_{mt} = -11.0$ mA cm^{-2} and $E^{\circ\prime}_{enz} = 0.395$ V, and Eqs. (1)–(5) were fitted to the data with j_{cat}, k_{cat}/k°, and α as the adjustable parameters by using the non-linear regression program Gnuplot©. The regression results are summarized in Table 2, and the regression curves are given in Fig. 4 as dotted lines.

At first, let us compare and discuss the obtained parameters for the four types of electrodes examined. Bilirubin modification and utilization of MWCNTs increased j_{cat} by three and eight times, respectively, as compared to the untreated KB electrode. Since k_{cat} was identical among the electrodes used, the increase in j_{cat} was ascribed to larger $\Gamma_{enz,eff}$ based on Eq. (4). The j_{cat} values of BOD/MWCNT/GCE and BOD/BL/MWCNT/GCE revealed that bilirubin modification was not synergistically effective in the case of MWCNT/GCEs. In the case of k°, the value slightly increased (less than 1.7 times) upon bilirubin modification and utilization of MWCNTs, assuming that k_{cat} was

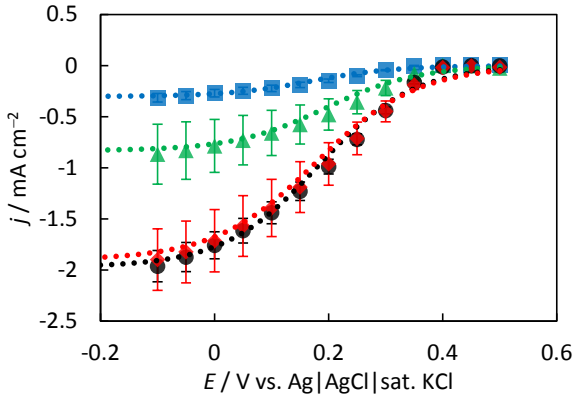

Figure 4
Steady-state voltammograms of BOD/KB/GCE (squares), BOD/BL/KB/GCE (triangles), BOD/MWCNT/GCE (circles), and BOD/BL/MWCNT/GCE (diamonds) in an O_2-saturated 100 mM tris-HCl buffer (pH = 9.4) at 4 ± 1 °C and ω = 4000 rpm. The error bars were evaluated by the Student *t*-distribution at a 90% confidence level. Each dotted line shows the regression result estimated according to Eqs. (1)–(5).

Table 2
Regression results in DET-type bioelectrocatalysis with BOD and the estimated properties of BOD

Electrode	pH	Obtained parameters			Estimated properties	
		j_{cat} / mA cm^{-2}	k_{cat} / $k°$	α	k_{cat} / s^{-1}	$k°$ / s^{-1}
KB	9.4	–0.31 ± 0.08	22 ± 6	0.35 ± 0.03	N.A.	N.A.
BL/KB	9.4	–0.9 ± 0.6	13 ± 3	0.32 ± 0.05	N.A.	N.A.
MWCNT	9.4	–2.4 ± 0.4	16 ± 1	0.31 ± 0.01	9 ± 3	0.6 ± 0.2
BL/MWCNT	9.4	–2.3 ± 0.7	14 ± 2	0.29 ± 0.03	7 ± 4	0.5 ± 0.3
MWCNT	7.0	–15.3 ± 0.7	27 ± 5	0.46 ± 0.04	70 ± 20	2.6 ± 0.9

N.A. = Not Applicable
The error bars were evaluated by the Student *t*-distribution at a 90% confidence level.

not affected by the electrodes. As mentioned in the Introduction, the electron transfer rate constant increased exponentially upon lowering the distance between the electrode surface and the redox site of the enzyme and is simply described as [8–10]:

$$k°_1 = k°_2 \exp\{-\beta(d_1 - d_2)\}, \quad (7)$$

where $k°_1$ and $k°_2$ are the interfacial electron transfer rate constants at distances (d_1 and d_2) between the redox cofactor and the electrode, respectively, while β is the decay constant (1.4 Å^{-1} for proteins [8–10]). For example, based on Eq. (7), the 1.7 times increase in $k°$ corresponds to a distance decrease of only 0.38 Å. Considering that the diameter of BOD ranges from 5 to 6 nm based on crystallographic data [64], almost all electroactive enzymes adsorb in a proper orientation on the modified electrode surfaces (e.g., to control the orientation of BOD), and the contribution to the current from enzymes in other orientations is little or none.

In the case of α, there were no clear differences, and the values (ca. 0.3) were in good agreement with previous studies [11–13]. Considering these results, the author can state that the electrode modifications employed here mainly improved the BOD orientation by increasing $\Gamma_{enz,eff}$ (and not by increasing $k°$). This consideration shed light on the confusing effect of the mass-transport of the DET-type voltammogram analysis, as discussed in Section 3.1. From the viewpoint of the properties on the electrode surface, the four types of electrodes showed negative and hydrophobic surface properties because of the presence of carboxyl groups and π-π conjugated systems, which favor the preferential orientation of BOD upon adsorption in DET-type bioelectrocatalysis devices. This discussion agreed well with previous studies reporting improved BOD orientations [31,35,39–47]. Thus, the mechanism of improvement by both methods (i.e., bilirubin modification and utilization of MWCNTs) is possibly the same, with the main factor being the enlargement of the surface area of platforms suitable for preferential orientation of BOD. Therefore, since there is no synergetic effect between the methods, MWCNT/GCE was more convenient and effective to achieve preferential

orientation of BOD.

Second, the author discussed the correlation between $\Gamma_{enz,eff}$ evaluated in Section 3.3 and the regression results of j_{cat}. Since DET takes place at the interface of the electrode, the non-catalytic redox signals were inherently low [16,20,27,51,52]. Accordingly, $\Gamma_{enz,eff}$ is a key factor for detection. In fact, in the cases of BOD/MWCNT/GCE and BOD/BL/MWCNT/GCE, the author was able to obtain clear redox signals. However, in the case of BOD/KB/GCE, the author did not obtain clear redox signals. Only slight redox signals were detectable in the case of BOD/BL/KB/GCE. Considering that $\Gamma_{enz,eff}$ is proportional to j_{cat} based on Eq. (4), these results support the regression results of j_{cat} summarized in Table 2.

Third, the author discussed $k°$ of the adsorbed BOD by using $\Gamma_{enz,eff}$ evaluated in Section 3.3. The k_{cat} value was estimated based on Eq. (4), and $k°$ was estimated by assigning the obtained k_{cat} value into the regression results shown in Table 2. These results were also listed in Table 2. The estimated values of $k°$ (0.6 ± 0.2 and 0.5 ± 0.3 s^{-1}) were significantly lower than those (45–240 s^{-1}) reported in the literature [11,13,31]. However, the value of $k°$ estimated herein upon the wave analysis is acceptable to explain the result of the non-catalytic voltammograms (Fig. 3). The theoretical slopes for the anodic and cathodic peak potentials at $\alpha = 0.5$ and $\alpha = 0.3$ under irreversible conditions were depicted as solid and dotted lines, respectively [53]. Since the electron transfer was not completely irreversible as mentioned in Section 3.3, the author roughly calculated $k°$, and the value was ca. 0.07 s^{-1} at $\alpha = 0.5$ or $\alpha = 0.3$. Although there is a minor difference between the $k°$ values estimated by the independent methods, the author can safely conclude that the obtained $k°$ values (0.6 ± 0.2 and 0.5 ± 0.3 s^{-1}) can explain the slow interfacial electron transfer properties of BOD in DET-type bioelectrocatalysis. The author considers that the difference between the $k°$ values obtained herein and those reported in the literature can be ascribed to the k_{cat} value used. In other words, previous studies utilized the catalytic constant measured in solution as k_{cat}.

Finally, a regression was conducted over the data of BOD/MWCNT/GCE at pH = 7.0 (Fig. 5) in the same manner as at pH = 9.4. Note that the author sets the parameters as $j_{mt} = -10.3$ mA cm^{-2} according to previous studies [46] while $E°'_{enz} = 0.53$ V estimated in Section 3.3. The regression curve is given in Fig. 5 as a dotted line. The regression results and the estimation of $k°$ and k_{cat} (using $\Gamma_{enz,eff} = 6 \times 10^{-10}$ mol cm^{-2}) are summarized in Table 2. The high k_{cat} value obtained at pH = 7.0 was in good agreement with the pH dependence of BOD [38], although the $k°$ values differed in some aspects. As mentioned in Section 3.1, for accurate analysis on DET-type bioelectrocatalysis, it is desirable to carry out the measurements under catalytic kinetics-controlled conditions. Conclusively, the author is sure that the discussions and the estimations at pH = 9.4 are more reliable for explaining the properties of BOD. The robust analysis of the steady-state catalytic voltammograms under decreased contribution of the mass-transport allowed us to more accurately understand the factors governing DET-type bioelectrocatalysis of BOD.

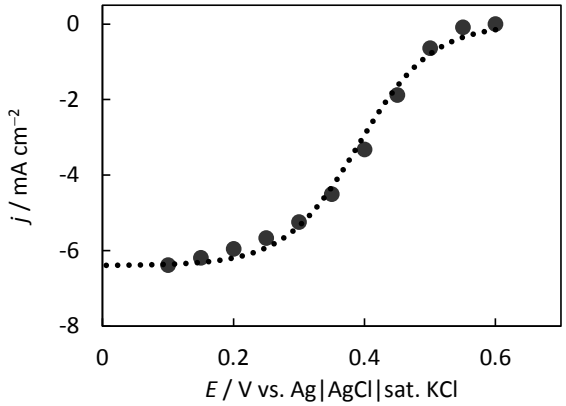

Figure 5
Steady-state voltammograms of BOD/MWCNT/GCE (circles) in an O_2-saturated 100 mM phosphate buffer (pH = 7.0) at 4 ± 1 °C and ω = 4000 rpm. Dotted line shows the regression result estimated according to Eqs. (1)–(5).

4. Conclusions

The author examined and compared the characteristics of four types of BOD-adsorbed electrodes (BOD/KB/GCE, BOD/BL/KB/GCE, BOD/MWCNT/GCE, and BOD/BL/MWCNT/GCE) in a DET-type bioelectrocatalysis device for O_2 reduction. The effect of the mass-transport on the catalytic current was minimized by decreasing the BOD activity at low temperature and high pH. This operation was carried out to more accurately extract the kinetic parameters of the enzyme reaction and interfacial electron transfer steps from the voltammetric data. Taking into account the contribution of the mass-transport, the author accurately analyzed the effects of bilirubin modification and utilization of MWCNTs by using direct electrochemistry. The electrochemical analysis revealed that the improvement obtained upon application of both methods was predominantly ascribed to an increased amount of effective enzymes (i.e., enzymes with productive orientation). The interfacial electron transfer remained nearly unchanged. Furthermore, both bilirubin modification and utilization of MWCNTs affected the BOD orientation in a similar way. Since there was no synergetic effect between both methods, MWCNT/GCE seemed to provide a convenient and effective platform for BOD preferential orientation. These conclusions offer new insights in the field of DET-type bioelectrocatalysis.

In addition, the author successfully detected clear non-catalytic redox signals of adsorbed BOD in BOD/MWCNT/GCE and BOD/BL/MWCNT/GCE samples owing to their high $\Gamma_{enz,eff}$ values. This finding provided information concerning $E^{\circ\prime}_{enz}$ and $\Gamma_{enz,eff}$ of the adsorbed BOD. Consequently, the author separately evaluated k_{cat} and k° of adsorbed BOD in DET-type bioelectrocatalysis devices from the steady-state catalytic voltammograms. The obtained kinetic parameters (k° and α) corresponding to the interfacial electron transfer step were acceptable for explaining the properties of the non-catalytic Faradaic responses.

5. References

[1] S.C. Barton, J. Gallaway, P. Atanassov, Enzymatic biofuel cells for implantable and microscale devices, Chem. Rev. 104 (2004) 4867–4886.

[2] A.D. Poulpiquet, D. Ranava, K. Monsalve, M.T. Giudici-Orticoni, E. Lojou, Biohydrogen for a new generation of H_2/O_2 biofuel cells: A sustainable energy perspectives, ChemElectroChem 1 (2014) 1724–1750.

[3] D. Leech, P. Kavanagh, W. Schuhmann, Enzymatic fuel cells: Recent progress, Electrochim. Acta 84 (2012) 223–234.

[4] C. Léger, P. Bertrand, Direct electrochemistry of redox enzymes as a tool for mechanistic studies, Chem. Rev. 108 (2008) 2379–2438.

[5] N. Mano, F. Mao, A. Heller, A miniature membrane-less biofuel cell operating at +0.60 V under physiological conditions, ChemBioChem 5 (2004) 1703–1705.

[6] M. Rasmussen, S. Abdellaoui, S.D. Minteer, Enzymatic biofuel cells: 30 years of critical advancements, Biosens. Bioelectron. 76 (2016) 91–102.

[7] J.A. Cracknell, K.A. Vincent, F.A. Armstrong, Enzymes as working or inspirational electrocatalysts for fuel cells and electrolysis, Chem. Rev. 108 (2008) 2439–2461.

[8] C.C. Moser, J.M. Keske, K. Warncke, R.S. Farid, P.L. Dutton, Nature of biological electron transfer, Nature 355 (1992) 796–802.

[9] C.C. Page, C.C. Moser, X. Chen, P.L. Dutton, Natural engineering principles of electron tunneling in biological oxidation-reduction, Nature 402 (1999) 47–52.

[10] R.A. Marcus, Electron transfer reactions in chemistry: Theory and experiment, Angew. Chem. Int. Ed. 32 (1993) 1111–1121.

[11] S. Tsujimura, T. Nakagawa, K. Kano, T. Ikeda, Kinetic study of direct bioelectrocatalysis of dioxygen reduction with bilirubin oxidase at carbon electrodes, Electrochemistry 72 (2004) 437–439.

[12] Y. Kamitaka, S. Tsujimura, K. Kataoka, T. Sakurai, T. Ikeda, K. Kano, Effects of axial ligand mutation of the type I copper site in bilirubin oxidase on direct electron transfer-type bioelectrocatalytic reduction of dioxygen, J. Electroanal. Chem. 601 (2007) 119–124.

[13] J. Lim, N. Cirigliano, J. Wang, B. Dunn, Direct electron transfer in nanostructured sol-gel electrodes containing bilirubin oxidase, Phys. Chem. Chem. Phys. 9 (2007) 1809–1814.

[14] C. Léger, A.K. Jones, S.P.J. Albracht, F.A. Armstrong, Effect of a dispersion of interfacial electron transfer tates on steady state catalytic electron transport in [NiFe]-hydrogenase and other enzymes, J. Phys. Chem. B 106 (2002) 13058–13063.

[15] V. Fourmond, C. Baffert, K. Sybirna, T. Lautier, A.A. Hamdan, S. Dementin, P. Soucaille, I. Meynial-Salles, H. Bottin, C. Léger, Steady-state catalytic wave-shapes for 2-electron reversible electrocatalysts and enzymes, J. Am. Chem. Soc. 135 (2013) 3926–3938.

[16] K.A. Vincent, A. Parkin, F.A. Armstrong, Investigating and exploiting the electrocatalytic properties of hydrogenases, Chem. Rev. 107 (2007) 4366–4413.

[17] H.S. Shafaat, O. Rüdiger, H. Ogata, W. Lubitz, [NiFe] hydrogenases: A common active site for hydrogen metabolism under diverse conditions, Biochim. Biophys. Acta 1827 (2013) 986–1002.

[18] T. Yagi, Y. Higuchi, Studies on hydrogenase, Proc. Jpn. Acad. Ser. B 89 (2013) 16–33.

[19] J.T. Holland, C. Lau, S. Brozik, P. Atanassov, S. Banta, Engineering of glucose oxidase for direct electron transfer via site-specific gold nanoparticle conjugation, J. Am. Chem. Soc. 133 (2011) 19262–19265.

[20] V. Flexer, F. Durand, S. Tsujimura, N. Mano, Efficient direct electron rransfer of PQQ-glucose dehydrogenase on carbon cryogel electrodes at neutral pH, Anal. Chem. 83 (2011) 5721–5727.

[21] S. Kawai, M. Goda-Tsutsumi, T. Yakushi, K. Kano, K. Matsushita, Heterologous overexpression and characterization of a flavoprotein-cytochrome *c* complex fructose dehydrogenase of *Gluconobacter japonicus* NBRC3260, Appl. Environ. Microbiol. 79 (2013) 1654–1660.

[22] S. Kawai, T. Yakushi, K. Matsushita, Y. Kitazumi, O. Shirai, K. Kano, The electron transfer pathway in direct electrochemical communication of fructose dehydrogenase with electrodes, Electrochem. Commun. 38 (2014) 28-31.

[23] A. Lindgren, L. Gorton, T. Ruzgas, U. Baminger, D. Haltrich, M. Schülein, Direct electron transfer of cellobiose dehydrogenase from various biological origins at gold and graphite electrodes, J. Electroanal. Chem. 496 (2001) 76–81.

[24] V. Fridman, U. Wollenberger, V. Bogdanovskaya, F. Lisdat, T. Ruzgas, A. Lindgren, L. Gorton, F.W. Scheller, Biosensors and novel bioanalytical methods, Biochem. Soc. 28 (2000) 63–70.

[25] E.I. Solomon, U.M. Sundaram, T.E. Machonkin, Multicopper oxidases and oxygenases, Chem. Rev. 96 (1996) 2563–2605.

[26] N. Mano, L. Edembe, Bilirubin oxidases in bioelectrochemistry: Features and recent findings, Biosens. Bioelectron. 50 (2013) 478–485.

[27] Y. Miura, S. Tsujimura, S. Kurose, Y. Kamitaka, K. Kataoka, T. Sakurai, K. Kano, Direct electrochemistry of CueO and its mutants at residues to and near type I Cu for oxygen-reducing biocathode, Fuel Cells 9 (2009) 70–78.

[28] S. Shleev, A. Jarosz-Wilkolazka, A. Khalunina, O. Morozova, A. Yaropolov, T. Ruzgas, L.

Gorton, Direct electron transfer reactions of laccases from different origins on carbon electrodes, Bioelectrochemistry 67 (2005) 115–124.

[29] A. Zebda, C. Gondran, A.L. Goff, M. Holzinger, P. Cinquin, S. Cosnier, Mediatorless high-power glucose biofuel cells based on compressed carbon nanotube-enzyme electrodes, Nat. Commun. 2 (2011) 1–6.

[30] T. Miyake, K. Haneda, S. Yoshino, M. Nishizawa, Flexible, layered biofuel cells, Biosens. Bioelectron. 40 (2013) 45–49.

[31] K. So, S. Kawai, Y. Hamano, Y. Kitazumi, O. Shirai, M. Hibi, J. Ogawa, K. Kano, Improvement of a direct electron transfer-type fructose/dioxygen biofuel cell with a substrate-modified biocathode, Phys. Chem. Chem. Phys. 16 (2014) 4823–4829.

[32] N. Lalaoui, A.D. Poulpiquet, R. Haddad, A.L. Goff, M. Holzinger, S. Gounel, M. Mermoux, P. Infossi, N. Mano, E. Lojou, S. Cosnier, A membraneless air-breathing hydrogen biofuel cell based on direct wiring of thermostable enzymes on carbon nanotube electrodes, Chem. Commun. 51 (2015) 7447–7450.

[33] A.D. Poulpiquet, A. Ciaccafava, R. Gadiou, S. Gounel, M.T. Giudici-Orticoni, N. Mano, E. Lojou, Design of a H_2/O_2 biofuel cell based on thermostable enzymes, Electrochem. Commun. 42 (2014) 72–74.

[34] L. Xu, F.A. Armstrong, Optimizing the power of enzyme-based membrane-less hydrogen fuel cells for hydrogen-rich H_2–air mixtures, Energy Environ. Sci. 6 (2013) 2166–2171.

[35] K. So, Y. Kitazumi, O. Shirai, K. Nishikawa, Y. Higuchi, K. Kano, Direct electron transfer-type dual gas diffusion H_2/O_2 biofuel cells, J. Mater. Chem. A 4 (2016) 8742–8749.

[36] H. Xia, K. So, Y. Kitazumi, O. Shirai, K. Nishikawa, Y. Higuchi, K. Kano, Dual gas-diffusion membrane- and mediatorless dihydrogen/air breathing biofuel cell operating at room temperature, J. Power Sources, 335 (2016) 105–112.

[37] S. Murao, N. Tanaka, A new enzyme “Bilirubin oxidase” produced by *Myrothecium verrucaria* MT-1, Agric. Biol. Chem. 45 (1981) 2383–2384.

[38] N. Tanaka, S. Murao, Purification and Some Properties of Bilirubin Oxidase of *Myrothecium verrucaria* MT-1, Agric. Biol. Chem. 46 (1982) 2499–2503.

[39] L.D. Santos, V. Climent, C.F. Blanford, F.A. Armstrong, Mechanistic studies of the “blue” Cu enzyme, bilirubin oxidase, as a highly efficient electrocatalyst for the oxygen reduction reaction, Phys. Chem. Chem. Phys. 12 (2010) 13962–13974.

[40] H. Xia, Y. Kitazumi, O. Shirai, K. Kano, Enhanced direct electron transfer-type bioelectrocatalysis of bilirubin oxidase on negatively charged aromatic compound-modified carbon electrode, J. Electroanal. Chem. 763 (2016) 104–109.

[41] J.A Cracknell, T.P. McNamara, E.D. Lowe, C.F. Blanford, Bilirubin oxidase from *Myrothecium verrucaria*: X-ray determination of the complete crystal structure and a rational surface modification for enhanced electrocatalytic O_2 reduction, Dalton Trans. 40 (2011) 6668-6675.

[42] R.J. Lopez, S. Babanova, Y. Ulyanova, S. Singhal, P. Atanassov, Improved interfacial electron transfer in modified bilirubin oxidase biocathodes, ChemElectroChem 1 (2014) 241–248.

[43] G. Göbel, F. Lisdat, Organic interlayers for oxygen reducing electrodes based on bilirubin oxidase and MWCNT modified gold, Electrochem. Commun. 10 (2008) 1691–1694.

[44] M. Jönsson-Niedziolka, A. Kaminska, M. Opallo, Pyrene-functionalised single-walled carbon nanotubes for mediatorless dioxygen bioelectrocatalysis, Electrochim. Acta 55 (2010) 8744–8750.

[45] N. Lalaoui, M. Holzinger, A.L. Goff, S. Cosnier, Diazonium functionalization of carbon nanotubes for specific orientation of multicopper oxidases: controlling electron entry points and oxygen diffusion to the enzyme, Chem. Eur. J. 22 (2016) 10494–10500.

[46] K. So, M. Onizuka, T. Komukai, Y. Kitazumi, O. Shirai, K. Kano, Significance of the length of carbon nanotubes on the bioelectrocatalytic activity of bilirubin oxidase for dioxygen reduction, Electrochim. Acta 192 (2016) 133–138.

[47] I. Mazurenko, K. Monsalve, J. Rouhana, P. Parent, C. Laffon, A.L. Goff, S. Szunerits, R. Boukherroub, M.T. Giudici-Orticoni, N. Mano, E. Lojou, How the intricate interactions between carbon nanotubes and two bilirubin oxidases control direct and mediated O_2 reduction, ACS Appl. Mater. Interfaces 8 (2016) 23074–23085

[48] K. Monsalve, I. Mazurenko, C. Gutierrez-Sanchez, M. Ilbert, P. Infossi, S. Frielingsdorf, M.T. Giudici-Orticoni, O. Lenz, E. Lojou, Impact of carbon nanotube surface chemistry on hydrogen oxidation by membrane-bound oxygen-tolerant hydrogenases, ChemElectroChem DOI: 10.1002/celc.201600460

[49] A.J. Bird, L.R. Faulkner, Electrochemical methods: fundamentals and applications, 2nd ed., Wiley, New York, 2016, p. 335.

[50] J.A. Koutecký, B.G. Levich, The application of the rotating disc electrode to studies of kinetic and catalytic processes, Zh. Fiz. Khim. USSR 32 (1958) 1565−1575.

[51] D. Ivnitski, K. Artyushkova, P. Atanassov, Surface characterization and direct electrochemistry of redox copper centers of bilirubin oxidase from fungi *Myrothecium verrucaria*, Bioelectrochemistry 74 (2008) 101−110.

[52] P. Ramírez, N. Mano, R. Andreu, T. Ruzgas, A. Heller, L. Gorton, S. Shleev, Direct electron transfer from graphite and functionalized gold electrodes to T1 and T2/T3 copper centers of bilirubin oxidase, Biochim. Biophys. Acta 1777 (2008) 1364−1369.

[53] E. Laviron, General expression of the linear potential sweep voltammogram in the case of diffusionless electrochemical systems, J. Electroanal. Chem. 101 (1979) 19–28.

[54] H.R. Pershad, J.L.C. Duff, H.A. Heering, E.C. Duin, S.P.J. Albracht, F.A. Armstrong, Catalytic electron transport in *Chromatium vinosum* [NiFe]-hydrogenase: Application of voltammetry in detecting redox-active centers and establishing that hydrogen oxidation is very fast even at potentials close to the reversible H^+/H_2 value, Biochemistry 38 (1999) 8992–8999.

[55] S. Tsujimura, A. Kuriyama, N. Fujieda, K. Kano, T. Ikeda, Mediated spectroelectrochemical titration of proteins for redox potential measurements by a separator-less one-compartment bulk electrolysis method, Anal. Biochem. 337 (2005) 325–331.

[56] G. Battistuzzi, M. Borsari, J.A. Cowan, A. Ranieri, M. Sola, Control of cytochrome *c* redox potential: Axial ligation and protein environment effects, J. Am. Chem. Soc. 124 (2002) 5315–5324.

[57] Y. Hibino, S. Kawai, Y. Kitazumi, O. Shirai, K. Kano, Mutation of heme *c* axial ligands in D-fructose dehydrogenase for investigation of electron transfer pathways and reduction of overpotential in direct electron transfer-type bioelectrocatalysis, Electrochem. Commun. 67 (2016) 43−46.

[58] D. Pankratov, J. Sotres, A. Barrantes, T. Arnebrant, S. Shleev, Interfacial behavior and activity of laccase and bilirubin oxidase on bare gold surfaces, Langmuir 30 (2014) 2943−2951.

[59] K.A. Wilson, C.A. Finch, P. Anderson, F. Vollmer, J.J. Hickman, Combining an optical resonance biosensor with enzyme activity kinetics to understand protein adsorption and denaturation, Biomaterials 38 (2015) 86–96.

[60] Q. Chi, J. Zhang, S. Dong, E. Wang, Direct electrochemistry and surface characterization of

glucose oxidase adsorbed on anodized carbon electrodes, Electrochim. Acta 39 (1994) 2431–2438.

[61] F.A. Armstrong, Probing metalloproteins by voltammetry, Struct. Bond. 72 (1990) 137–221.

[62] Y. Sugimoto, Y. Kitazumi, S. Tsujimura, O. Shirai, M. Yamamoto, K. Kano, Electrostatic interaction between an enzyme and electrodes in the electric double layer examined in a view of direct electron transfer-type bioelectrocatalysis, Biosens. Bioelectron. 63 (2015) 138–144.

[63] Y. Sugimoto, Y. Kitazumi, O. Shirai, M. Yamamoto, K. Kano, Role of 2-mercaptoethanol in direct electron transfer-type bioelectrocatalysis of fructose dehydrogenase at Au electrodes, Electrochim. Acta 170 (2015) 242–247.

[64] K. Mizutani, M. Toyoda, K. Sagara, N. Takahashi, A. Sato, Y. Kamitaka, S. Tsujimura, Y. Nakanishi, T. Sugiura, S. Yamaguchi, K. Kano, B. Mikami, X-ray analysis of bilirubin oxidase from *Myrothecium verrucaria* at 2.3 Å resolution using a twinned crystal, Acta Cryst. F66 (2010) 765–770.

Chapter 2
Construction of Gas Diffusion-Type Biocathode and Bioanode

2-1. Binder/surfactant-free biocathode with bilirubin oxidase for gas-diffusion-type system

Abstract

Direct electron transfer (DET)-type bioelectrocatalysis of dioxygen (O_2) reduction is an essential process for constructing a biocathode for use in an enzymatic biofuel cell. In this study, a gas-diffusion-type electrode without any binders or surfactants, which are both known to interfere with DET-type bioelectrocatalysis, was constructed. Bilirubin oxidase (BOD), a promising catalyst for DET-type O_2 reduction, and water-dispersed multiwalled carbon nanotubes compatible with BOD were used. The electrode displayed high kinetic performance in the DET reaction and large steady-state current density under quiescent conditions. In addition, the electrode provided a platform that was eight times more suitable for BOD than a traditional electrode.

1. Introduction

Enzymatic biofuel cell is an energy conversion system in which enzymes oxidize a substrate or reduce dioxygen (O_2) at the bioanode or biocathode, respectively [1-3]. Owing to the properties of enzymes, the device can operate under very mild and safe conditions such as neutral pH, room temperature, and atmospheric pressure [1-3]. Furthermore, biofuel cells can be used in micropower devices to extract energy from biological sources and are expected to find applications in implantable biomedical power devices [4-7]. Multicopper oxidases (MCOs) catalyze four-electron reduction of O_2 into H_2O and are utilized as biocatalysts [8,9]. In addition, several MCOs are classified as direct electron transfer (DET)-type enzymes that can shuttle electrons to or from an electrode without any redox mediators [9-12]. Therefore, DET-type enzymatic biofuel cells are suitable for realizing efficient and compact energy conversion systems [13,14].

The low solubility and low diffusion coefficient of O_2 cause limitations in the catalytic current and result in a decrease in power in O_2 reduction with MCOs in solution. A gas-diffusion-type electrode, which can supply a gaseous substrate from the gas phase, has been utilized to solve this problem [15-22]. A simple numerical simulation has predicted that the limiting catalytic current continues to increase with the thickness of the gas-diffusion-type electrode up to millimeter thickness [22]. Accordingly, it is invaluable for the achievement of efficient DET-type bioelectrocatalysis with MCOs in the limited layer of the gas-diffusion-type electrode.

Hydrophobized carbon materials such as Ketjen black (KB), carbon black with Teflon®, and carbon nanotubes (CNTs) [23] are often utilized for constructing gas-diffusion-type electrodes [15-22]. Teflon® is frequently used as a binder between carbon particles and as a hydrophobic material; however, Teflon® is known to act as an insulator. Therefore, enzymes adsorbed onto the Teflon® cannot directly communicate with the electrode. On the other hand, most CNT suspensions contain surfactants for dispersion. Surfactants are considered to strongly adsorb onto the CNT surface and interfere with the DET reaction between an enzyme and the electrode [24,25]. To enhance the performance and efficiency of DET- and gas-diffusion-type electrodes, it is necessary to avoid using these additives.

Among MCOs, bilirubin oxidase (BOD) is a promising enzyme for DET-type bioelectrocatalysis [26] because it has a high bioelectrocatalytic activity in DET-type O_2 reduction. The type I Cu site acts as the electron accepting site, and its formal potential of BOD is relatively close to that of the H_2O/O_2 redox pair [26]. Because the rate constant of the DET reaction decreases exponentially with the tunneling distance between the electrode and the active site of an enzyme [27], a suitable orientation of the adsorbed enzyme is essential for fast electron transfer [28,29]. Focusing on the type I Cu active site of BOD to communicate with an electrode, several approaches have been reported to realize efficient DET-type bioelectrocatalysis with BOD [21,25,30-35]. Premodification of the electrode with negatively charged chemical compounds has been reported as an effective method. This includes covalent modification by diazonium coupling [30] or by oxidation of amines [31], physical adsorption of bilirubin [21,32,33] or other aromatic compounds [34], and the utilization of functionalized CNT such as pyrene-functionalized CNTs [35] or water-soluble CNTs of length 1–4 μm [25].

In this study, the author aimed to construct a gas-diffusion-type electrode that meets the aforementioned requirements. Binder/surfactant-free CNTs, which are highly compatible with BOD [25], were deposited on a water-proof carbon cloth (WPCC) base to construct a gas-diffusion-type biocathode with BOD. The author characterized the biocathodes via microscopic and bioelectrochemical analysis.

2. Experimental

2.1. Materials

Water-dispersed multiwalled CNTs (MWCNTs; outer diameter: 10–15 nm, length: 1–4 μm without surfactant) were kindly donated by Nitta Corp. (Japan). WPCC (EC-CC1-060T) was purchased from Toyo Corp., (Japan), and carbon paper (CP, TGP-H-120) was purchased from Toray Industries, Inc., (Japan). KB EC300J was kindly donated by Lion Corp., (Japan). Poly(1,1,2,2-tetrafluoroethylene) (PTFE, 6-J) fine powder was purchased from DuPont-Mitsui Fluorochemicals

Co., Ltd., (Japan). PTFE sheets (EN0701405) were obtained from Nippon Donaldson, Ltd. (Japan). BOD (EC 1.3.3.5) from *Myrothecium verrucaria* was donated by Amano Enzyme Inc. (Japan) and used without further purification. All other chemicals used in this study were of analytical grade unless otherwise specified and all solutions were prepared with distilled water.

2.2. Electrode preparation

The MWCNT suspension was applied to one-side of WPCC sheets and dried at 55 °C to prepare MWCNT-modified WPCC electrodes (labeled CNT1–CNT5 depending on the amount of MWCNTs on the WPCC electrode, as characterized in Table 1). The KB-modified CP electrode (KB/PTFE) was prepared at KB:PTFE = 6:4 (w/w) according to the literature [21]. The PTFE sheet was attached to the opposite side (without MWCNT) of the WPCC electrodes by pressure bonding to completely hold electrolysis solutions. Subsequently, 300 μL (1 L = 1 dm^3) BOD solution (20 mg mL^{-1}) dissolved in 10 mM (1 M = 1 mol dm^{-3}) phosphate buffer (pH 7) was applied to the MWCNT-mounted electrode surfaces (CNT1–CNT5 and KB/PTFE), which were dried for 2 h under reduced pressure at room temperature.

2.3. Microscopic and electrochemical measurements

Scanning electron microscopy (SEM) was performed on a Hitachi S-4300. Cyclic voltammetry and chronoamperometry were carried out on an electrochemical analyzer BAS CV 50W and ALS 714C. A handmade gas-diffusion-type electrolysis cell identical to that reported in a previous paper [21] was used for the measurements. The projected surface area of the working electrode was set to 1.0 cm^2. The electrode was set as the PTFE sheet-attached side facing to gas phase. A Ti mesh served as a current collector, and was attached to the MWCNT-mounted and BOD-adsorbed side of the working electrode. A Pt mesh and an Ag|AgCl|sat. KCl electrode were used as counter and reference electrodes, respectively. All potentials in this study are in reference to the reference electrode. The measurements were performed in 1.5 M citrate buffer (pH 5) at 40 °C under quiescent and O_2 atmospheric conditions.

3. Results and Discussion

3.1 Characterization of the MWCNT-based gas-diffusion-type electrodes

Fig. 1A shows photographs of the BOD solution on the WPCC and CNT1–CNT5. Since the surface of WPCC is very hydrophobic, the BOD solution on the WPCC and CNT1 was strongly

repelled. The electrode surface became more hydrophilic with an increasing amount of MWCNTs on the WPCC (CNT1–CNT5), at which point the BOD solution soaked more easily on the inside of the electrodes.

SEM was conducted to BOD-adsorbed CNT5 from the top and vertical views (Figs. 1B and C, respectively). Fig. 1B shows that the WPCC surface of CNT5 (the BOD/MWCNT deposited side) was homogeneously covered with MWCNTs. Compared to the control electrode without BOD (Fig. 1B inset), the fuzzy films observed on MWCNTs are attributed to the adsorbed BOD. Fig. 1C indicates that the deposited MWCNT accumulated on the WPCC in a layer-by-layer fashion.

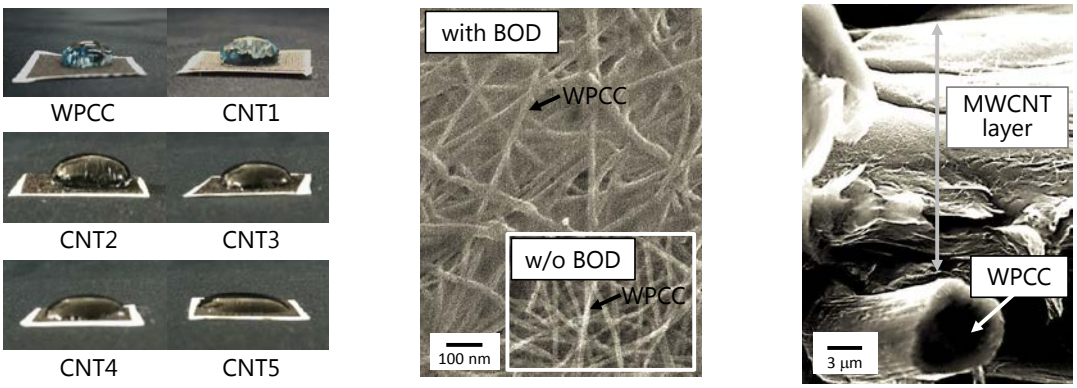

Figure 1
(A) Photographs of BOD solution deposited on the WPCC and MWCNT-based WPCC electrodes (CNT1–CNT5). Before BOD deposition, the PTFE sheet is attached to the opposite side of each electrode.
(B) SEM of BOD-adsorbed CNT5 from the top view. The inset shows the SEM of CNT5 without BOD. The black arrows indicate the MWCNT.
(C) SEM of BOD-adsorbed CNT5 from the vertical view. The white arrow indicates a fiber of the WPCC. The accumulated MWCNT layer is indicated by the bidirectional arrow.

3.2 DET-type bioelectrocatalysis at BOD-adsorbed electrodes

Fig. 2A shows cyclic voltammograms (CVs) at BOD-adsorbed CNT1–CNT5 (gray to black solid lines) and KB/PTFE (black dotted line) under quiescent and O_2 atmospheric conditions. The faradic waves are ascribed to the O_2 reduction due to DET-type bioelectrocatalysis with BOD, as described in the literature [10,21,25,30-35]. Judging from the shapes of the voltammograms, BOD-adsorbed MWCNT-based electrodes (solid lines) show clearer sigmoidal shapes compared to KB/PTFE (dotted line). These characteristics indicate that the interfacial electron transfer between BOD and the MWCNT-based electrode is faster than that between BOD and KB/PTFE [27-29]. Accordingly, the author can conclude that the MWCNT-based electrodes are able to achieve a more favorable orientation of adsorbed BOD. This enables efficient utilization of BOD within the limited area of the gas-diffusion-type electrode. The reduction current density at 0 V (close to the limiting value) increased with an increasing amount of MWCNTs and reached 15 mA cm^{-2}. This value is slightly smaller than that of BOD-adsorbed KB/PTFE utilized for construction of a powerful DET-type biofuel cell. Note that due to the difference in measuring conditions, the characteristic of BOD-adsorbed KB/PTFE is slightly different to that in a previous study [21]. However, because of the sigmoidal shape of the CVs at BOD-adsorbed MWCNT-based electrodes, the current density at positive potential was much larger than that of BOD-adsorbed KB/PTFE. For example, the current density of CNT5 is twice that of KB/PTFE at 0.5 V, and the potential to reach 10 mA cm^{-2} of CNT5

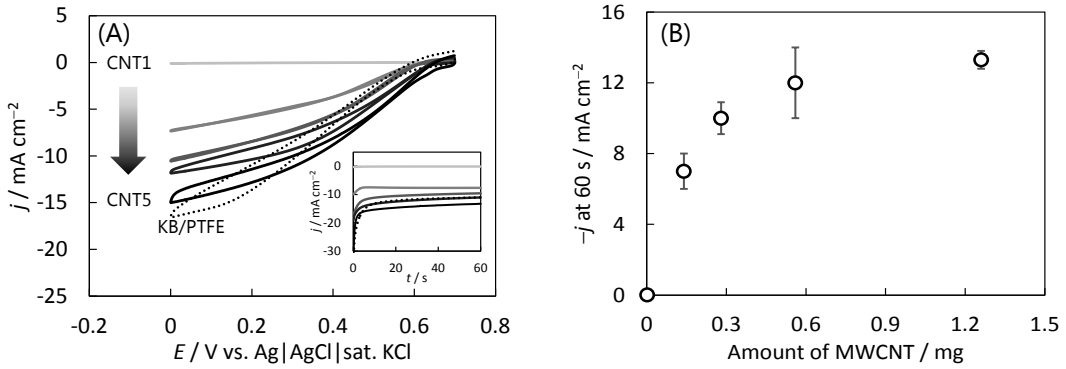

Figure 2
(A) CVs at BOD-adsorbed MWCNT-based WPCC electrodes (CNT1–CNT5, gray to black solid lines) and KB/PTFE (black dotted line). The scan rate was 10 mV s^{-1}. The inset shows CAs (at 0 V) at BOD-adsorbed MWCNT-based WPCC electrodes (CNT1–CNT5, gray to black solid lines) and KB/PTFE (black dotted line). Measurements were carried out in 1.5 M citrate buffer (pH 5) at 40 °C under quiescent and O_2 atmospheric conditions.
(B) Effects of the amount of MWCNTs on the steady-state catalytic reduction current densities after 60 s in CAs. The error bars were evaluated by the Student *t*-distribution at 90 %-confidence level.

was 0.07 V more positive than that of KB/PTFE. These characteristics are very important for improving the performance of biofuel cells.

On the other hand, chronoamperograms (CAs) at 0 V of the aforementioned electrodes are shown in the inset of Fig. 2A. Steady-state reduction waves were obtained for 60 s. After the current drop due to a rapid decrease in the non-faradic charging current, the rate-determining step of the O_2 reduction is the steady-state O_2 supply from the gas phase. In contrast to the CV results, the current densities of the BOD-adsorbed CNT4 and CNT5 were larger than that of KB/PTFE. This indicates that an improvement in the steady-state O_2 supply for DET-type bioelectrocatalysis with BOD has been realized by utilizing the MWCNT-based WPCC electrode. Fig. 2B shows the effects of the amount of MWCNTs on the steady-state catalytic reduction current densities after 60 s in CAs (Fig. 2A inset). The saturating characteristics indicate that the amount of MWCNTs is sufficient in the case of CNT5 for constructing the MWCNT-based WPCC electrode. As already shown in Fig. 1C, the excess MWCNTs accumulate on the surface of the WPCC, and the O_2 supply is hindered.

Table 1 also summarizes several properties of BOD-adsorbed electrodes with additional information on the relative electroactive surface area. The relative electroactive surface areas were evaluated from the amplitude of the non-faradic charging current under Ar-saturated conditions in CVs (data not shown). Since the charging current is affected by both the surface area and the presence of charged species, the author cannot exactly compare the electroactive surface areas of the MWCNT-based WPCC electrodes (CNT1–CNT5) and KB/PTFE. However, to the best of our knowledge, it is one of the most effective methods for evaluating the relative values of the electroactive surface area. As judged from Table 1, the relative values of the electroactive surface area increased linearly with the amount of MWCNTs. Therefore, it can be considered that all parts of the MWCNTs work as

Table 1
Characteristics of BOD-adsorbed electrodes*

BOD-adsorbed electrodes	Amount of MWCNT/mg	$-j$ (at 0 V, 60 s) /mA cm^{-2}	Relative electroactive surface area (A)**	Efficiency ($-j/A$)
CNT1	1.4×10^{-3}	0.0007	0.03	0.023
CNT2	0.14	7 ± 1	0.12 ± 0.02	58 ± 13
CNT3	0.28	10 ± 0.9	0.25 ± 0.02	40 ± 5
CNT4	0.56	12 ± 2	0.42 ± 0.01	28 ± 5
CNT5	1.26	13.3 ± 0.5	1	13.3 ± 0.5
KB/PTFE	N/A	11.4 ± 0.6	1.5 ± 0.1	7.6 ± 0.6

* The errors were evaluated by the Student t-distribution at 90 %-confidence level.
** The relative electroactive surface areas were evaluated from the amplitude of non-faradic charging current on CVs under Ar-saturated conditions.

electroactive electrodes in aqueous solution.

Let us consider the current density of DET-type bioelectrocatalysis per electroactive surface area in the gas-diffusion-type electrode. The reduction current densities after 60 s in CAs (Fig. 2A inset) are divided by the corresponding relative electroactive surface area in this study and the values are summarized as “efficiency” in Table 1. In terms of efficiency, CNT2 provides a platform that is eight times more effective for BOD than KB/PTFE. In addition, CNT4 shows approximately four times greater efficiency in O_2 reduction ability. At electrodes with increased amounts of MWCNTs, the O_2 supply seems to be partially inhibited. However, the data clearly show the significance of water-dispersed MWCNT as the platform for BOD in the gas-diffusion biocathode for O_2 reduction.

4. Conclusion

To achieve powerful and efficient DET-type bioelectrocatalysis of O_2 reduction with BOD, MWCNT-based WPCC electrodes (CNT1–CNT5) were successfully constructed for use as gas-diffusion-type electrodes. Compared to the BOD-adsorbed KB/PTFE, BOD-adsorbed CNT5 not only achieves fast interfacial electron transfer with BOD but also has a larger steady-state catalytic reduction current density. Furthermore, MWCNT-based WPCC electrodes (CNT2–CNT5) provide highly efficient platforms for BOD in DET-type bioelectrocatalysis. Consequently, the good compatibility of MWCNT with BOD is useful and effective for constructing high-performance and efficient gas-diffusion-type biocathodes in DET-type bioelectrocatalysis. Thus, this study will significantly contribute to the development of a powerful and practical enzymatic biofuel cell.

5. References

[1] D. Leech, P. Kavanagh, W. Schuhmann, Enzymatic fuel cells: Recent progress, Electrochim. Acta 84 (2012) 223-234.

[2] S.C. Barton, J. Gallaway, P. Atanassov, Enzymatic biofuel cells for implantable and microscale devices, Chem. Rev. 104 (2004) 4867-4886.

[3] M. Rasmussen, S. Abdellaoui, S.D. Minteer, Enzymatic biofuel cells: 30 years of critical advancements, Biosens. Bioelectron. 76 (2016) 91-102.

[4] M. Rasmussen, R.E. Ritzmann, I. Lee, A.J. Pollack, D. Scherson, An Implantable Biofuel Cell for a Live Insect, J. Am. Chem. Soc. 134 (2012) 1458-1460.

[5] A. Szczupak, J. Halámek, L. Halámková, V. Bocharova, L. Alfonta, E. Katz, Living battery

– biofuel cells operating in vivo in clams, Energy Environ. Sci. 5 (2012) 8891-8895.

[6] A. Zebda, S. Cosnier, J.-P. Alcaraz, M. Holzinger, A. Le Goff, C. Gondran, F. Boucher, F. Giroud, K. Gorgy, H. Lamraoui, P. Cinquin, Single Glucose Biofuel Cells Implanted in Rats Power Electronic Devices, Sci. Rep. 3 (2013) 1516.

[7] E. Katz, K. MacVittie, Implanted biofuel cells operating in vivo – methods, applications and perspectives – feature article, Energy Environ. Sci. 6 (2013) 2791-2803.

[8] E.I. Solomon, U.M. Sundaram, T.E. Machonkin, Multicopper oxidases and oxygenases, Chem. Rev. 96 (1996) 2563-2605.

[9] S. Shleev, J. Tkac, A. Christenson, T. Ruzgas, A.I. Yaropolov, J.W. Whittaker, L. Gorton, Direct electron transfer between copper-containing proteins and electrodes, Biosens. Bioelectron. 20 (2005) 2517-2554.

[10] S. Tsujimura, T. Nakagawa, K. Kano, T. Ikeda, Kinetic study of direct bioelectrocatalysis of dioxygen reduction with bilirubin oxidase at carbon electrodes, Electrochemistry 72 (2004) 437-439.

[11] S. Shleev, A. Jarosz-Wilkolazka, A. Khalunina, O. Morozova, A. Yaropolov, T. Ruzgas, L. Gorton, Direct electron transfer reactions of laccases from different origins on carbon electrodes, Bioelectrochemistry 67 (2005) 115-124.

[12] Y. Miura, S. Tsujimura, S. Kurose, K. Kataoka, T. Sakurai, K. Kano, Direct electrochemistry of CueO and its mutants at residues to and near type I Cu for oxygen-reducing biocathode, Fuel Cells 9 (2009) 70-78.

[13] J.A. Cracknell, K.A. Vincent, F.A. Armstrong, Enzymes as working inspirational electrocatalysts for fuel cells and electrolysis, Chem. Rev. 108 (2008) 2439-2461.

[14] C. Léger, P. Bertrand, Direct electrochemistry of redox enzymes as a tool for mechanistic studies, Chem. Rev. 108 (2008) 2379-2438.

[15] G. Gupta, C. Lau, V. Rajendran, F. Colon, B. Branch, D. Ivnitski, P. Atanassov, Direct electron transfer catalyzed by bilirubin oxidase for air breathing gas-diffusion electrodes, Electrochem. Commun. 13 (2011) 247-249.

[16] T. Miyake, K. Haneda, S. Yoshino, M. Nishizawa, Flexible, layered biofuel cells, Biosens.

Bioelectron. 40 (2013) 45-49.

[17] N. Lalaoui, A.D. Poulpiquet, R. Haddad, A.L. Goff, M. Holzinger, S. Gounel, M. Mermoux, P. Infossi, N. Mano, E. Lojou, S. Cosnier, A membraneless air-breathing hydrogen biofuel cell based on direct wiring of thermostable enzymes on carbon nanotube electrodes, Chem. Commun. 51 (2015) 7447-7450.

[18] R. Kontani, S. Tsujimura, K. Kano, Air diffusion biocathode with CueO as electrocatalyst adsorbed on carbon particle-modified electrodes, Bioelectrochemistry 76 (2009) 10-13.

[19] K. So, Y. Kitazumi, O. Shirai, K. Kurita, H. Nishihara, Y. Higuchi, K. Kano, Kinetic analysis of inactivation and enzyme reaction of oxygen-tolerant [NiFe]-hydrogenase at direct electron-transfer bioanode, Bull. Chem. Soc. Jpn. 87 (2014) 1177-1185.

[20] K. So Y. Kitazumi, O. Shirai, K. Kurita, H. Nishihara, Y. Higuchi, K. Kano, Gas-diffusion and Direct-electron-transfer-type bioanode for hydrogen oxidation with oxygen-tolerant [NiFe]-hydrogenase as an electrocatalyst, Chem. Lett. 43 (2014) 1575-1577.

[21] K. So, S. Kawai, Y. Hamano, Y. Kitazumi, O. Shirai, M. Hibi, J. Ogawa, K. Kano, Improvement of a direct electron transfer-type fructose/dioxygen biofuel cell with a substrate-modified biocathode, Phys. Chem. Chem. Phys. 16 (2014) 4823-4829.

[22] S.C. Barton, Oxygen transport in composite mediated biocathodes, Electrochim. Acta 50 (2005) 2145-2153.

[23] S. Iijima, Herical microtubules of graphitic carbon, Nature 354 (1991) 56-58.

[24] S. Kawai, T. Yakushi, K. Matsushita, Y. Kitazumi, O. Shirai, K. Kano, Role of a non-ionic surfactant in direct electron transfer-type bioelectrocatalysis by fructose dehydrogenase, Electrochimi. Acta 152 (2015) 19-24.

[25] K. So, M. Onizuka, T. Komukai, Y. Kitazumi, O. Shirai, K. Kano, Significance of the Length of Carbon Nanotubes on the Bioelectrocatalytic Activity of Bilirubin Oxidase for Dioxygen Reduction, Electrochim. Acta 192 (2016) 133-138.

[26] N. Mano, L. Edembe, Bilirubin oxidases in bioelectrochemistry: Features and recent findings, Biosens. Bioelectron. 50 (2013) 478-485.

[27] C.C. Page, C.C. Moser, X. Chen, P.L. Dutton, Natural engineering principles of electron

tunneling in biological oxidation-reduction, Nature 402 (1999) 47-52.

[28] C. Léger, A.K. Jones, S.P.J. Albracht, F.A. Armstrong, Effect of a Dispersion of Interfacial Electron Transfer Rates on Steady State Catalytic Electron Transport in [NiFe]-hydrogenase and Other Enzymes, J. Phys. Chem. B 106 (2002) 13058-13063.

[29] C. Léger, A.K. Jones, W. Roseboom, S.P.J. Albracht, F.A. Armstrong, Enzyme Electrokinetics: Hydrogen Evolution and Oxidation by Allochromatium vinosum [NiFe]-Hydrogenase, Biochemistry 41 (2002) 15736-15746.

[30] L.D. Santos, V. Climent, C.F. Blanford, F.A. Armstrong, Mechanistic studies of the 'blue' Cu enzyme, bilirubin oxidase, as a highly efficient electrocatalyst for the oxygen reduction reaction, Phys. Chem. Chem. Phys. 12 (2010) 13962-13974.

[31] H. Xia, Y. Kitazumi, O. Shirai, K. Kano, Enhanced direct electron transfer-type bioelectrocatalysis of bilirubin oxidase on negatively charged aromatic compound-modified carbon electrode, J. Electroanal. Chem. 763 (2016) 104-109.

[32] R.J. Lopez, S. Babanova, Y. Ulyanova, S. Singhal, P. Atanassov, Improved interfacial electron transfer in modified bilirubin oxidase biocathodes, ChemElectroChem 1 (2014) 241-248.

[33] J.A. Cracknell, T.P. Mcnamara, E.D. Lowe, C.F. Blanford, Bilirubin oxidase form Myrothecium verrucaria: X-ray determination of the complete crystal structure and a rational surface modification for enhanced electrocatalytic O_2 reduction, Dalton Trans. 40 (2011) 6668-6675.

[34] G. Göbel, F. Lisdat, Organic interlayers for oxygen reducing electrodes based on bilirubin oxidase and MWCNT modified gold, Electrochem. Commun. 10 (2008) 1691-1694.

[35] M. Jönsson-Niedziolka, A. Kaminska, M. Opallo, Pyrene-functionalised single walled carbon nanotubes for mediatorless dioxygen bioelectrocatalysis, Electrochim. Acta 55 (2010) 8744-8750.

2-2. Gas-diffusion and Direct-electron-transfer-type Bioanode for Hydrogen Oxidation with Oxygen-tolerant [NiFe]-hydrogenase as an Electrocatalyst

Abstract

A membrane-bound [NiFe]-hydrogenase (MBH) from Hydrogenovibrio marinus allows a direct electron transfer (DET)-type bioelectrocatalysis for the H_2 oxidation and is an O_2-tolerant promising enzyme for the construction of enzymatic H_2/O_2 biofuel cells. However, the oxidative and reversible inactivation called "anaerobic inactivation" limits the H_2-oxidation at high potentials. For avoiding the inhibition, the author has constructed an MBH-adsorbed gas-diffusion-type electrode, in which H_2 is spontaneously supplied to the electrode from the gas phase.

1. Introduction

In order to realize the promising hydrogen energy conversion system that is expected to smooth out the temporal fluctuations of solar power, wind power and so on, a superior catalyst to oxidize hydrogen is needed.[1] Nowadays, the power devices such as an H_2/O_2 fuel cell rely on platinum as a catalyst, which is a rare metal and thus too expensive. Many researchers have explored alternative catalysts.[2] From the aspect of bioelectrochemistry, hydrogenases that catalyze the inter-conversion between hydrogen and proton have received a lot of attention, and the bioelectrocatalytic properties has extensively been characterized all over the world.[3-8]

Enzymatic biofuel cells are electric generators that utilize redox enzymes as catalysts, and are classified into two types: mediated electron transfer (MET)-type and direct electron transfer (DET)-type.[9-12] MET-type cell utilizes artificial mediators to shuttle the electron between the enzyme and the electrode to reduce the kinetic hindrance in the interfacial electron transfer. On the other hand, DET-type cell does not require, in principle, any separator or membrane between the electrodes due to the mediator-less configuration.

To construct the high-performance bioelectrochemical power device, DET-type enzymes to be utilized should have some bioelectrocatalytic abilities to oxidize (or reduce) the substrate at high catalytic current density with minimum overpotential. Among the DET-type enzymes for bioanodes, one of promising enzymes is [NiFe]-hydrogenase for 2-electron oxidation of H_2.[3,4,13] Moreover, non-Pt H_2/O_2 enzymatic biofuel cells can be constructed by combining the bioanode with biocathode modified with multi-copper oxidase as an electrocatalyst for O_2-reduction.[14,15]

The discovery of O_2- and CO-tolerant [NiFe]-hydrogenase is one of the breakthroughs essential for the construction of the aforementioned biofuel cell, and the unique properties have been investigated from several viewpoints.[16-19] In this research, the author purified a membrane-bound

[NiFe]-hydrogenase (MBH) from *Hydrogenovibrio marinus*, an O_2-tolerant hydrogenase, according to the previous work[20] and used for electrochemical measurements.

2. Experimental

The author first measured the H_2 oxidaiton current catalyzed by MBH adsorbed on electrode in immersion system. Ketjen Black EC300J (KB; kindly donated from Lion Co., Japan) was used for electrode material and prepared according to the literature.[14] KB was mixed with polytetrafluoroethylene fine powder (PTFE 6-J; obtained from DuPont Mitsui Fluorochemicals, Japan) and homogenized in 2-propanol. The slurry was applied to glassy carbon electrode (GCE) to prepare KB-modified glassy carbon electrode (KB-GCE; KB:PTFE = 8:2(w/w)), in which a GCE for rotating disk voltammetry (RDE-2, BAS, Inc) was used. When MBH was adsorbed on the KB-GCE, a 15-μL aliquot of an MBH solution (7 μM dissolved in 10 mM phosphate buffer of pH 6) was applied on the KB-GCEs and the electrodes were kept in water-saturated atmosphere for 2 h at room temperature to slowly dry the solvent. Rotating disk electrode voltammetry was performed on electrochemical analyzer (BAS CV-50W). An Ag|AgCl|sat. KCl electrode and a Pt wire were used as the reference electrode and the counter electrode, respectively. Measurements were carried out in 100 mM phosphate buffer (pH 6) at 40 ± 2 °C.

3. Results and Discussion

Rotating disk electrode voltammograms (RDVs) at an MBH-adsorbed KB-GCE are shown in Fig. 1. At 2500 rpm and under H_2-saturated conditions, a typical oxidation wave (Fig.1 (a)) was

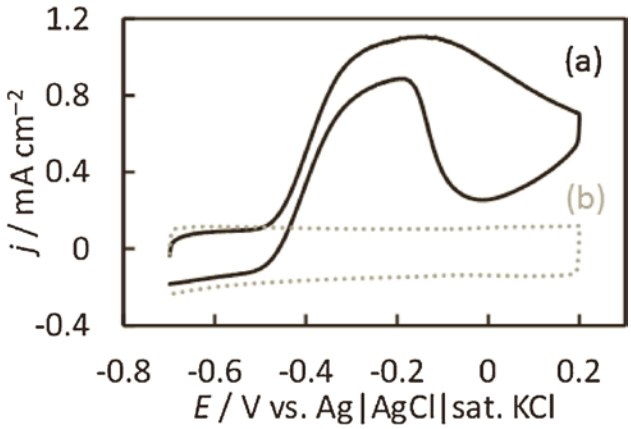

Figure 1
RDVs of MBH-adsorbed KB-GCE in (a) H_2- and (b) Ar-saturated 100 mM phosphate buffer (pH 6) at 40 ± 2 °C. The electrode was rotated at 2500 rpm. The scan rate was 20 mV s^{-1}.

observed in the electrode potential region from –0.5 V to –0.2 V. The faradaic current is ascribed to the MBH- catalyzed H_2 oxidation, as judged from the comparison with a wave under Ar-saturated conditions (Fig.1 (b)).

The current-potential curve in the potential region from –0.5 V to –0.3 V was practically independent of the scan rate at least in the range from 5 to 40 mV s^{-1} (data not shown). This indicates that the reaction is not controlled by any kinetics including the mass transfer of the substrate, the enzyme reaction and the interfacial electron transfer. Therefore, the author can safely conclude that this characteristics reflect the Nernstian response of the interfacial electron transfer of the MBH adsorbed on the electrodes. An apparent number of the electron in this process analyzed by the Nernst analysis was close to unity. However, the total number of the electron in the H_2-reduced MBH should be two. Therefore, the process can be considered as a two-step one-electron process.

Several spectroscopic studies have revealed that the catalytic cycle proceeds in three states: Ni-SI (active silent form), Ni-R (H_2-reduced form), Ni-C (one-electron oxidized form of Ni-R) (Sheme 1). [3,17,21] Therefore, the reversible two-step process reflects the catalytic process from NiR to Ni-SI via Ni-C.

However, the catalytic current decreased in the forward scan from –0.2 V to 0.2 V and was almost fully recovered in the reverse scan. The current-potential curve of the reverse scan in the potential region from –0.1 V to –0.2 V was practically independent of the scan rate at least in the range from 5 to 30 mV s^{-1} (data not shown). The Nernst analysis of the curve indicated the number of the electron is unity.

Such inactivation of MBH was observed in anaerobic solution by addition of an oxidant such as $K_3[Fe(CN)_6]$ ($E^{\circ\prime}$ = 0.18 V) and methylene blue ($E^{\circ\prime}$ = –0.21 V), and the inactivated MBH

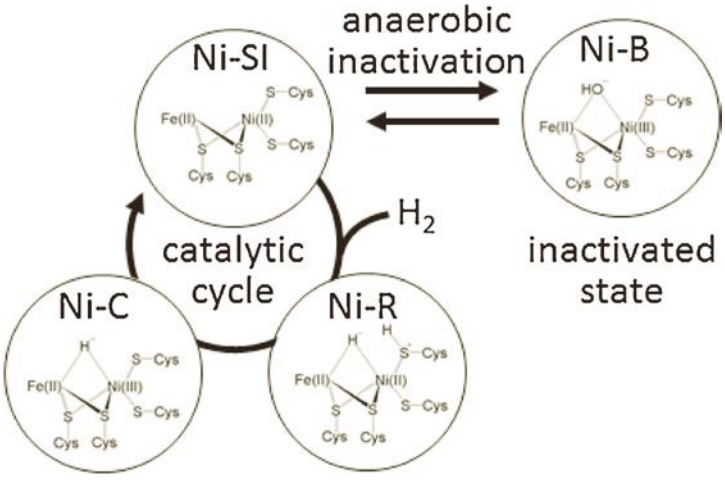

Scheme 1
Mechanism of the catalytic cycle and the anaerobic inactivation of [NiFe]-hydrogenase.

was reactivated by reduced benzyl viologen ($E^{\circ\prime}$ = –0.53 V). Similar phenomena were reported for O_2-sensitive standard hydrogenase.[22] The phenomenon is ascribed to the reversible and oxidative inactivation (called as anaerobic inactivation).[3,17,21,22] The inactivation generates a Ni(III) state form known as Ni-B by one-electron oxidation of Ni-SI, in which a hydroxide ligand is coordinated to the Ni atom in a bridging position with respect to the Fe(II) (Scheme 1).[3,17,21]

The anaerobic inactivation is one critical problem in utilization of O_2-tolelant or standard hydrogenases toward the H_2/O_2 biofuel cell. Taking into account of this mechanism, the author proposes here that the inactivation can be considered as a competitive inhibition-like reaction, and expect that the inactivation can be avoided by increasing the concentration of H_2 over the saturated level in immersion system (0.74 mM at 40 °C).[23] To achieve the high-speed H_2 supply to MBH, the author attempted to construct an MBH-modified gas-diffusion-type electrode, which is often utilized for air-breathing biocathodes to increase the O_2-uptake.[14,24-26] The electrode makes it possible to directly uptake the gaseous substrate from the gas phase.

The gas-diffusion-type electrode was prepared mainly according the literature.[14] KB was mixed with PTFE and homogenized in 2-propanol. The slurry was applied to a carbon paper (CP; purchased from Toray Co., Japan) and dried to prepare a KB-modified CP electrode (KB-CPE; KB:PTFE = 6:4(w/w), the ratio being partially optimized for gas-diffusion system). A 10-μL aliquot of an MBH solution (10 μM dissolved in 10 mM phosphate buffer of pH 6) was applied on the KB-CPEs, which was kept in water-saturated atmosphere for 6 h at 4 °C to slowly dry the solvent.

Cyclic voltammograms (CVs) of the MBH-adsorbed KB-CPEs were recorded under "quiescent (passive)" and H_2 atmospheric conditions (250 mL min^{-1}) and are depicted in Fig. 2 (a). The current density reached about 6 mA cm^{-2} at 0 V, which is much larger than that of MBH-adsorbed

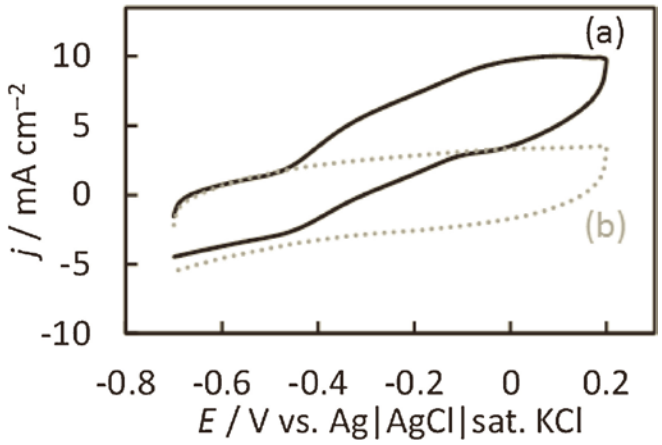

Figure 2
CVs of catalytic H_2 oxidation at MBH-adsorbed KB-CPE under (a) H_2 and (b) Ar flow in the gas phase. The measurements were carried out in 100 mM phosphate buffer (pH 6) at 40 ± 2 °C and under quiescent conditions. The scan rate was 20 mV s^{-1}.

KB-GCE at 2500 rpm. This means the successful H_2-supply from the gas phase. Moreover, the shape of the CV with sigmoidal characteristics (Fig. 2 (a)) is different from that of KB-GCE in H_2-saturated solution (Fig. 1 (a); note here that the scan rates are identical with each other). This supports the idea that the fast H_2-supply can avoid anaerobic inactivation as the competitive inhibition-like reaction. However, it seems that the current is limited not by the gas flow rate but by the gas diffusion rate in the electrode. Some improvement in the gas-diffusion system will increase the current density.

4. References

1. L. Goff, V. Artero, B. Jousselme, P. D. Tran, N. Guillet, R. Métayé, A. Fihri, S. Palacin, M. Fontecave, *Science*, 2009, **326**, 1384.R. Bashyam, P. Zelenay, *Nature*, 2006, **443**, 63.
2. F. A. Armstrong, N. A. Belsey, J. A. Cracknell, G. Goldet, A. Parkin, E. Reisner, K. A. Vincent, A. F. Wait, *Chem. Soc. Rev.*, 2009, **38**, 36.
3. M. Guiral, L. Prunetti, C. Aussignargues, A. Ciaccafava, P. Infossi, M. Ilbert, E. Lojou, M Giudici-Orticoni, *Adv. Microb. Physiol.*, 2012, **61**, 125.
4. T. Yagi, Y. Higuchi, *Proc. Jpn. Acad. Ser. B*, 2013, **89**, 16.
5. H. S. Shafaat, O. Rüdiger, H. Ogata, W. Lubitz, *Biochimca et Biophysica Acta*, 2013, **1827**, 986.
6. A. A. Karyakin, *Bioelectrochemistry*, 2012, **88**, 70.
7. T. Matsumoto, S. Eguchi, H. Nakai, T. Hibino, K. S. Yoon, S. Ogo, *Angew. Chem. Int. Ed.*, 2014, **53**, 1.
8. M. J. Moehlenbrock, S. D. Minteer, *Chem. Soc. Rev*., 2008, **37**, 1188.
9. N. Mano, F. Mao, A. Heller, *ChemBioChem*, 2004, **5**, 1703.
10. D. Leech, P. Kavanagha, W. Schuhmann, *Electrochim. Acta*, 2012, **84**, 223.
11. S. C. Barton, J. Gallaway, P. Atanassov, *Chem. Rev.*, 2004, **104**, 4867.
12. A. K. Jones, E. Sillery, S. P. J. Albracht, F. A. Armstrong, *Chem. Commun.*, 2002, 866.
13. K. So, S. Kawai, Y. Hamano, Y. Kitazumi, O. Shirai, M. Hibi, J. Ogawa, K. Kano, *Phys. Chem. Chem. Phys.*, 2014, **16**, 4823.
14. E. I. Solomon, U. M. Sundaram, T. E. Machonkin, *Chem. Rev.*, 1996, **96**, 2563.
15. R. M. Evans, A. Parkin, M. M. Roessler, B. J. Murphy, H. Adamson, M. J. Lukey, F. Sargent, A. Volbeda, J. C. Fontecilla-Camps, F. A. Armstrong, *J. Am. Chem. Soc.*, 2013, **135** 2694.
16. M. Pandelia, W. Nitschke, P. Infossi, M. Giudici-Orticoni, E. Bill, W. Lubitz, *Proc. Natl. Acad. Sci. USA*, 2011, **108**, 6097.
17. M. Ludwig, J. A. Cracknell, K. A. Vincent, F. A. Armstrong, O. Lenz, *J. Biol. Chem.*, 2009, **284**, 465.
18. Y. Shomura, K. S. Yoon, H. Nishihara, Y. Higuchi, *Nature*, 2011, **479**, 253.

19. K. S. Yoon, K. Fukuda, K. Fujisawa, H. Nishihara, *Int. J. Hydrogen Energy*, 2011, **36**, 7081.
20. A. K. Jones, S. E. Lamle, H. R. Pershad, K. A. Vincent, S. P. J. Albracht, F. A. Armstrong, *J. Am. Chem. Soc.*, 2003, **125**, 8505.
21. A. A. Hamdan, B. Burlat, O. Gutiérrez-Sanz, P. Liebgott, C. Baffert, A. L. D. Lacay, M. Rousset, B. Guigliarelli, C. Léger, S. Dementin, *Nat. Chem. Biol.*, 2013, **9**, 15.
22. C. L. Young, Ed., *IUPAC Solubility Data Series*, Vol. 5/6, Pergamon Press, Oxford, 1981.
23. C. Lau, E. R. Adkins, R. P. Ramasamy, H. R. Luckarift, G. R. Johnson, P. Atanassov, *Adv. Energy Mater.*, 2012, **2**, 162.
24. G. P. M. K. Ciniciato, C. Lau, A. Cochrane, S. S. Sibbett, E. R. Gonzalez, P. Atanassov, *Electrochim. Acta*, 2012, **82**, 208.
25. T. Nakagawa, H. Mita, H. Kumita, H. Sakai, Y. Tokita, S. Tsujimura, *Electrochem. Commun.*, 2013, **36**, 46.

2-3. Kinetic Analysis of Inactivation and Enzyme Reaction of Oxygen-Tolerant [NiFe]-Hydrogenase at Direct Electron-Transfer Bioanode

Abstract

Membrane-bound [NiFe]-hydrogenase (MBH) from *Hydrogenovibrio marinus* is an O_2-tolerant enzyme and allows a direct electron transfer (DET)-type bioelectrocatalysis for the H_2-oxidation. MBH is a promising bioelectrocatalyst for bioanode of enzymatic H_2/O_2 biofuel cells. From the practical viewpoint of the electricity production, the H_2-depletion near the electrode surface and the oxidative and reversible inactivation called "anaerobic inactivation" of [NiFe]-hydrogenases limit the H_2-oxidation at high potentials. The author has already proposed a gas-diffusion system to avoid the inactivation in our previous study. In this research, the author has analyzed the kinetics of the electrochemically induced anaerobic inactivation and the DET-type bioelectrocatalytic reaction of MBH on electrodes. When the inactivation is considered as a competitive inhibition-like reaction, the maximum value of the apparent Michaelis constant reaches 6.5 mM (at Ketjen Black-modified electrode) as analyzed on our kinetic model. Since the value is larger than the saturated H_2-concentration in solution (0.74 mM), the author concludes that high-speed H_2-supply realized by a gas-diffusion-type electrode is essential to compete the inactivation. Furthermore, the gas-diffusion-type bioanode with MBH can get rid of the H_2-depletion near the electrode surface and has reached about 10 mA cm^{-2} at 0 V (vs. Ag|AgCl|sat. KCl electrode) under quiescent (passive) and H_2-atmospheric conditions.

1. Introduction

Hydrogenases are enzymes which catalyze the inter-conversion between hydrogen and proton.[1] The two major classes of hydrogenases are known as [FeFe] or [NiFe] according to the metals in their buried active sites.[1,2] Since hydrogenases are highly active, with turnover frequencies for H_2-oxidation in excess of thousands of molecules of H_2 per second at 30 °C,[3] they can be alternative catalysts instead of platinum as an H_2/O_2 fuel cell.[4] From the aspect of bioelectrochemistry, hydrogenases have received a lot of attention, and the bioelectrocatalytic properties have extensively been characterized all over the world.[1,2,5-8]

Enzymatic biofuel cells, which are electric generators that utilize redox enzymes as catalysts, can generally operate under mild conditions (neutral pH, atmospheric pressure and room temperature). They are classified into two types: mediated electron transfer (MET)-type and direct electron transfer (DET)-type.[9-12] MET-type cell utilizes artificial mediators to shuttle the electron between the enzyme and the electrode to reduce the kinetic hindrance in the interfacial electron transfer. On the other hand, DET-type cell does not require, in principle, any separator or membrane between the electrodes due

to the mediator-less configuration. In addition, the DET-type one can reduce the possible health hazard problems caused by artificial mediators and the thermodynamic loss ascribed to the difference in the redox potentials between the mediator and the active site of the enzyme. Furthermore, the DET-type system enables us to construct a very simple and compact enzymatic biofuel cell.

Unfortunately, the number of the enzymes capable of DET-type bioelectrocatalysis is limited.[2,11,12] Fructose dehydrogenase[13] and hydrogenase[2] are often used for DET-type bioelectrocatalyst to oxidize fructose and hydrogen, respectively, as fuels and multi-copper oxidases (MCO), such as laccase, bilirubin oxidase (BOD) and Cu efflux oxidase, are utilized for DET-type bioelectrocatalyst for O_2-reduction.[14-17] However the power density of high-performance DET-type biofuel cell (a few mW cm^{-2})[14,18,19] is much lower than that of MET-type with the best performance (10 mW cm^{-2}).[20] Among the DET-type enzymes for bioanodes, one of promising enzymes is [NiFe]-hydrogenase due to their special bioelectrocatalytic ability to catalyze the 2-electron oxidation of H_2 at high catalytic current density with minimum overpotential.[2,3,5] Moreover, non-Pt H_2/O_2 enzymatic biofuel cells can be constructed by combining the bioanode with the biocathode modified with MCO.[14,15]

The discovery of O_2- and CO-tolerant [NiFe]-hydrogenase is one of the breakthroughs essential for the construction of the aforementioned biofuel cell, and the unique properties have been investigated from several viewpoints.[21-24] DET-type H_2/O_2 biofuel cell with tolerant [NiFe]-hydrogenase has already been constructed.[18,19] Lojou's group achieved the highest power density (1.5 mW cm^{-2} at pH 6 and 60 °C) with [NiFe]-hydrogenase from *A. aerolicus* and BOD from *B. pumilus*.[18] They recorded high H_2-oxidation current (4 mA cm^{-2} at pH 7 and 70 °C) under bubbling the gas into the electrolyte solution to minimize substrate depletion.[18]

One critical problem in utilization of [NiFe]-hydrogenase is the anaerobic inactivation which is a reversible inactivation caused by the anaerobic oxidation at high electrode potentials or high solution potentials.[2,25] Several spectroscopic studies have revealed that the catalytic cycle proceeds in three state forms: Ni-SI (active silent form), Ni-R (H_2-reduced form), Ni-C (one-electron oxidized form of Ni-R), and that the inactivation generates a Ni(III) state form known as Ni-B by one-electron oxidation of Ni-SI, in which a hydroxide ligand is coordinated to the Ni atom in a bridging position with respect to the Fe(II).[2,22,26]

Taking into account of this mechanism, the author has proposed that the inactivation can be considered as a competitive inhibition-like reaction.[27] The author utilized a membrane-bound O_2-tolerant [NiFe]-hydrogenase from *Hydrogenovibrio marinus* (MBH) and succeeded in avoiding the inactivation by increasing the concentration of H_2 over the saturated level in immersion system. For this purpose, the author constructed an MBH-modified gas-diffusion-type electrode, which was often utilized for air-breathing biocathodes to increase the O_2-uptake.[14,28-30] The electrode makes it possible to directly uptake the gaseous substrate from the gas phase, and this attempt was the first case for H_2-

oxidizing bioanodes, as far as we know.[27] For discussing the effect in detail, it is very important to evaluate the thermodynamic and kinetic parameters of MBH

In this research, the author investigates the bioelectrochemical properties of MBH from the viewpoint of the anaerobic inactivation. The inactivation kinetics is studied by analyzing time and potential dependence of the DET-type catalytic current of MBH adsorbed on electrodes, while the enzyme kinetics of MBH on electrodes is evaluated from rotating rate dependence of the steady-state catalytic current using rotating disk electrode method. Moreover, the Michaelis constant for H_2 is estimated by analyzing the H_2-concentration dependence of the catalytic current of MBH. Finally, the author has proposed an analytical model for the anaerobic inactivation and evaluated the inhibition constant and the apparent Michaelis constant. The results show that an MBH-modified gas-diffusion-type electrode is very effective and necessary for avoiding the inactivation.

2. Experimental

2.1. Materials

Ketjen Black EC300J (KB) was kindly donated from Lion Co. (Japan). Carbon paper (CP, TGP-H-120) was purchased from Toray Co. (Japan). Polytetrafluoroethylene fine powder (PTFE, 6-J) was obtained from DuPont Mitsui Fluorochemicals (Japan). 4-Nitrobenzenediazonium tetrafluoroborate and *N*-hydroxy-succinimide (98%, NHS) were purchased from Sigma-Aldrich Co. (USA). 1-Ethyl-3-(3-dimethylaminopropyl)-carbodiimide, hydrochloride (EDC) was purchased from Dojindo Laboratory (Japan). MBH was purified according to the literature.[31] All other chemicals used in this study were of analytical grade and all solutions were prepared with distilled water.

2.2. Preparation of MBH-adsorbed electrode

Au electrode (3 mm in diameter, BAS) was polished with alumina slurry (Buehler, 1 μm), sonicated and washed with distilled water. A 15-μL aliquot of an MBH solution (7 μM dissolved in 10 mM phosphate buffer of pH 6) was applied on the Au electrodes and the electrodes were kept in water-saturated atmosphere for 2 h at room temperature to slowly dry the solvent.

KB-modified glassy carbon electrode (KB:PTFE = 8:2 (w/w)) (KB-GCE) was prepared according to the literature,[14] in which a GCE for rotating disk voltammetry (RDE-2, BAS, Inc.) was used. The projective surface area of the GCE was 0.071 cm^2. When MBH was adsorbed on the KB-GCE, a 15-μL aliquot of an MBH solution (7 μM dissolved in 10 mM phosphate buffer of pH 6) was applied on the KB-GCEs and the electrodes were kept in water-saturated atmosphere for 2 h at room temperature to slowly dry the solvent.

2.3 Immobilization of MBH on KB-GCE

MBH was chemically immobilized on the KB-GCE through the amide-linkage[32,33] to avoid the desorption of MBH under strongly convective conditions. The bare KB-GCE was electrochemically pre-treated to generate 4-aminophenyl layer on the surface according to the literature with minor modification.[34] In brief, 4-nitrophenyl layer was produced on the electrode surface by the potential sweep method from 0.8 V to −0.4 V at 200 mV s^{-1} for 4 cycles in an acetonitrile solution containing 2 mM 4-nitrobenzenediazonium tetrafluoroborate and 50 mM tetrabutylammonium tetrakis(4-fluorophenyl)borate, and then reduced to 4-aminophenyl layer by the potential sweep method from −0.3 V to −1.6 V at 200 mV s^{-1} for 4 cycles in a water/ethanol mixed solution (9 : 1 in volume) containing 100 mM NaCl. The electrode is called NH_2-KB-GCE. A 15-μL aliquot of an MBH/reagent solution (7 μM MBH, 12 mM EDC, and 6 mM NHS dissolved in 10 mM phosphate buffer of pH 6) was applied on the NH_2-KB-GCEs to immobilize MBH on the electrode through the amide-linkage.[35] The electrodes were kept in water-saturated atmosphere for 2 h at room temperature to slowly dry the solvent.

2.4 Preparation of KB-modified carbon paper electrode

A gas-diffusion-type carbon paper electrode (KB-CPE; KB:PTFE = 6:4 (w/w)) was prepared according to the literature.[14,27] The active and projected surface area of the CPE was 0.03 cm^2. A 10-μL aliquot of an MBH solution (10 μM dissolved in 10 mM phosphate buffer of pH 6) was applied on the KB-CPE, which was kept in water-saturated atmosphere for 6 h at 4 °C to slowly dry the solvent.

2.5 Electrochemical measurements

Cyclic voltammetry and chronoamperometry were performed on electrochemical analyzers BAS CV-50W and ALS 714C. Steady-state chronoamperometry was carried out with the rotating disk KB-GCE. An Ag|AgCl|sat. KCl electrode and a Pt wire were used as the reference electrode and the counter electrode, respectively. Measurements were carried out in 100 mM phosphate buffer (pH 6) at 40 ± 2 °C. The partial pressure of H_2 (p_{H_2}) is adjusted by mixing the Ar and H_2 gas by using flowmeters with flowcontrollers (PK2504FR, KOFLOC Co., Japan). A handmade gas-diffusion-type electrolysis cell, which is similar to that reported in a previous paper for O_2-reducing biocathode,[14,27] was used for measurements with the KB-CPE.

3. Results and discussion

3.1 DET-type bioelectrocatalysis on MBH-modified electrodes in immersion system

Cyclic voltammograms (CVs) at an MBH-adsorbed Au electrode are shown in Fig. 1(A). In quiescent but H_2-saturated buffer solution, a typical oxidation wave (solid line) was observed in the electrode potential region from –0.5 V to –0.2 V. The wave is ascribed to the MBH-catalyzed H_2-oxidation, as judged from the comparison with a wave under Ar-atmospheric conditions (Fig. 1(A), broken line). Since the H_2-oxidation current was practically independent of the scan rate (v) in the potential region from –0.5 V to –0.2 V (data not shown), the catalytic current is controlled by the enzyme kinetics.

However, the catalytic current decreased in the forward scan from –0.2 V to 0.2 V and was almost fully recovered in the reverse scan. The phenomenon is ascribed to the reversible and oxidative

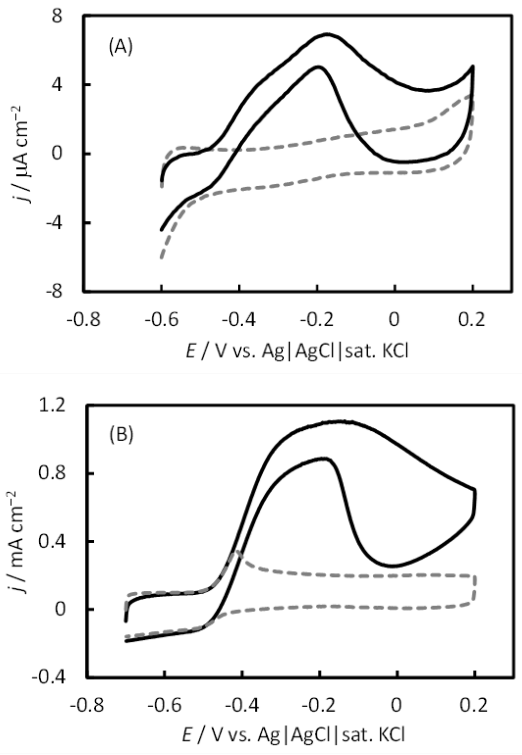

Figure 1
(A) CVs of the MBH-adsorbed Au electrode in H_2-(solid line) and Ar-(broken line) saturated buffer solution under quiescent conditions.
(B) CVs of the MBH-adsorbed KB-GCE at ω = 2500 rpm (solid line) and 0 rpm (broken line) under H_2-atmospheric conditions. (The solid line is identical with curve (a) of Fig. 1 in Ref. 27.)
The measurements were carried out in 100 mM phosphate buffer (pH 6) at 40 ± 2 °C. The scan rate was 20 mV s^{-1}.

inactivation (called as anaerobic inactivation) to generate Ni-B. The anodic wave shape due to the inactivation depended on *v* (data not shown), indicating relatively slow inactivation. On the other hand, the reverse scan wave corresponds to the reactivation was almost independent of *v*, indicating fast reactivation.

When an MBH-adsorbed KB-GCE was rotated in the H_2-saturated solution (at a rotating rate (ω) of 2500 rpm (262 s^{-1})), a similar shape of the catalytic wave was observed (Fig. 1(B), solid line). The oxidation current density became much larger than that at MBH-adsorbed Au electrode. This effect is predominantly due to an increase in the electro-active surface area of the electrode by use of KB-GCE. However, under the quiescent conditions (0 rpm), the voltammogram showed only a small catalytic anodic peak around –0.45 V (Fig. 1(B), broken line). The H_2-depletion near the electrode surface causes the drastic decrease in the current. Similar phenomena were observed and studied with carbon nanotube (CNT) electrodes.[36] The *v* dependence of the wave at the KB-GCE was very similar to that at Au electrodes (data not shown) except the fact that the decrease in the catalytic wave due to the inactivation at the KB-GCEs is slow compared with that at the Au electrode.

3.2 Kinetic analysis of reversible anaerobic inactivation

For studying the anaerobic inactivation and reactivation process, the author assumes a reversible first-order reaction scheme which connects the active (E_A) and inactive (E_I) forms of the enzyme according to the previous study.[37]

$$E_A \underset{k_A}{\overset{k_I}{\rightleftharpoons}} E_I \qquad (1)$$

where k_I and k_A are the apparent inactivation and reactivation rate constants, respectively. The author conducted the potential-step chronoamperometric method to follow the inactivation and reactivation processes. In the beginning, the electrode potential (E_1) was set at –0.2 V, where the anaerobic inactivation does not occur and the maximum catalytic current density is observed (Fig. 1, solid line). After then the potential was stepped at $t = 0$ to a given potential (E_2), at which the anaerobic inactivation occurs. The open circles in Fig. 2(A) indicate chronoamperogram (CA) of the H_2-oxidation current at the MBH-adsorbed Au electrode at $E_2 = -0.02$ V. The data just after the potential step ($t < 3$ s) involved the charging current and were eliminated for the present analysis. Since the catalytic current at the Au electrode is controlled by the enzyme kinetics as mentioned in section 3.1, the current decay reflects the reversible first-order inactivation as expressed by eqn. (2).

$$I_{cat}(t) = I_0 \left\{ \frac{k_I}{k_I + k_A} \exp\left[-(k_I + k_A)t\right] + \frac{k_A}{k_I + k_A} \right\} \qquad (2)$$

where I_0 is the fully activated catalytic current. Equation (2) was fitted to the date in Fig. 2(A) in the time region from 3 to 30 s with I_0, k_I and k_A as the adjustable parameters using a non-linear regression analysis by Gnuplot®. The regression curve is shown in Fig. 2(A) as a solid line. The experimental data are well reproduced by the model. The author will discuss the evaluated values of the rate constants in section 3.3.

In the case of MBH-adsorbed KB-GCE, however, the potential-step chronoamperometric method cannot be simply applied to the kinetic analysis of the inactivation and reactivation, since outstanding depression of H_2 occurs near the KB-GCE due to large surface area as mentioned in section 3.1. In order to eliminate the H_2-depression effect, the author attempted to utilize rotating disk electrode method. In addition, the author immobilized MBH chemically on the NH_2-KB-GCE through the amide-linkage between the carboxyl group and amino group by using EDC and NHS as the coupling reagents. The resultant electrode is called MBH-immobilized KB-GCE. The CV at MBH-

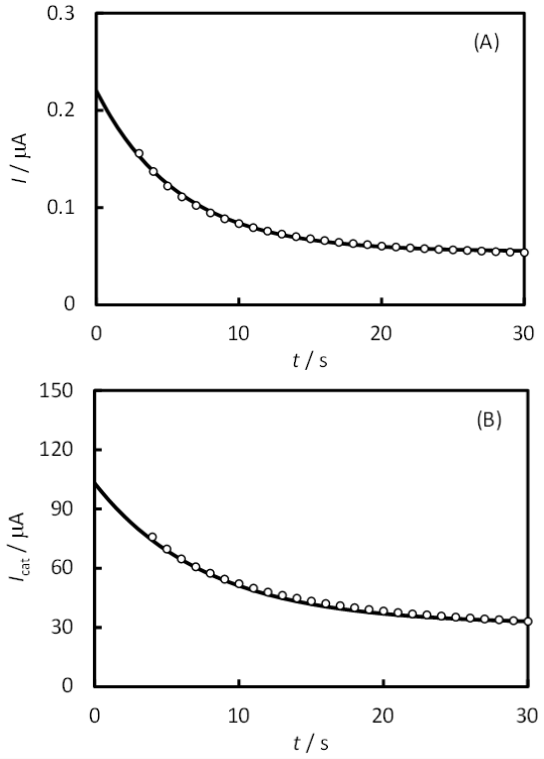

Figure 2
(A) CA of the MBH-adsorbed Au electrode (open circles) at –0.02 V under H_2-atmospheric conditions. The solid curve was evaluated by a non-linear regression analysis based on eqn. (2). The best fit was obtained with the parameters: I_0 = 0.22 μA, k_I = 0.13 s^{-1}, k_A = 0.043 s^{-1}. The measurements were carried out in 100 mM phosphate buffer (pH 6) at 40 ± 2 °C.
(B) The time dependence of I_cat (open circles) estimated from CA of MBH-adsorbed KB-GCE on the basis of eqns. (3) and (4). The solid curve was evaluated by a non-linear regression analysis based on eqn. (2). The best fit was obtained with the parameters: I_0 = 103 μA, k_I = 0.09 s^{-1}, k_A = 0.040 s^{-1}.

immobilized KB-GCE in H_2-saturated solution (data not shown) shows a steady-state catalytic wave of H_2-oxidation (in the potential range from –0.35 to –0.2 V) at ω = 2500 rpm. The immobilization stabilized MBH on the electrode (see the next paragraph also), but led to a decrease in the current density. The reason is not clear at the present moment, since the evaluation of the surface concentration is very difficult. The appearance of the steady-state current indicates that any time-dependent change in the enzyme activity due for example to local pH change, if any, is negligible during the measurements. However, a couple of large redox waves were also observed. The waves are originated from the surface modifier (most probably hydorxylamine intermediate).

Figure 3(A) shows the CA under H_2-saturated conditions at various values of ω and at E_1 (–0.2 V). The steady-state H_2-oxidation current (I_s) was first measured at 2500 rpm, and the ω value was stepwise changed from 50 to 2500 rpm. The I_s value at 2500 rpm (t > 350 s) was recovered up to the initial value at 0 < t < 50 s at 2500 rpm, indicating the stable immobilization of MBH on the KB-GCE. The $\sqrt{\omega}$ dependence of I_s under H_2-saturated conditions shows curved characteristics (Fig. 3(B)).

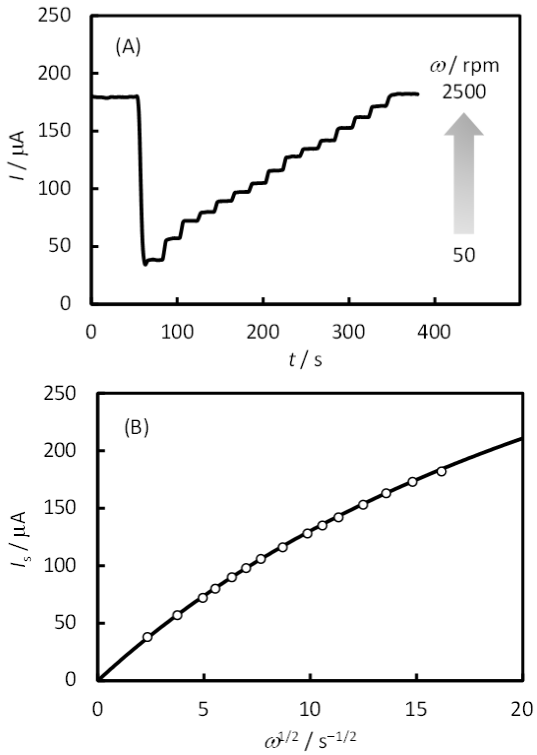

Figure 3
(A) CA of the MBH-immobilized KB-GCE at –0.2 V under H_2-atmospheric conditions (p_{H_2} = 1 atm). I_s was first measured at ω = 2500 rpm and the ω value was stepwise changed from 50 to 2500 rpm. The measurements were carried out in 100 mM phosphate buffer (pH 6) at 40 ± 2 °C.
(B) ω dependence of the steady-state H_2-oxidation current (open circles) at the MBH-immobilized KB-GCE. The current was measured as shown in panel A. The solid curve was evaluated by a non-linear regression analysis based on eqns. (3) and (4).

The result indicates that I_s is governed by both the H_2-diffusion and the enzymatic kinetics. The characteristics can be as expressed by Koutecky–Levich equation.[38]

$$\frac{1}{I_s} = \frac{1}{I_D} + \frac{1}{I_{cat}} \quad (3)$$

Here, I_D is the diffusion-controlled current at a rotating disk electrode:

$$I_D = 0.62nFAD_{H_2}^{2/3}\upsilon^{-1/6}c_{H_2}\omega^{1/2} \quad (4)$$

where n, F, A, D_{H_2}, υ, and c_{H_2} are, respectively, the number of electrons (2 in this case), the Faraday constant, the projected electrode surface area, the diffusion coefficient of H_2, the kinematic viscosity of water (0.0066 $cm^2\ s^{-1}$ at 40 °C),[39,40] and the concentration of dissolved H_2. The saturated concentration of dissolved H_2 was set to be 0.74 mM at 40 °C and p_{H_2} = 1 atm.[41] Equations (3) and (4) were fitted to the data in Fig. 3(B) (open circles) with I_{cat} and D_{H_2} as the adjustable parameters using a non-linear regression analysis by Gnuplot®, and the regression curve is shown in Fig. 3(B) as a solid line. The refined values of I_{cat} and D_{H_2} were 543 ± 8 μA and (4.01 ± 0.03) × 10^{-5} $cm^2\ s^{-1}$, respectively. The error is given as the asymptotic standard error. Consequently, the author can now extract the true contribution of the enzyme kinetic-controlled catalytic current (i.e. I_{cat}) from the total steady-state current I_s with eqns. (3) and (4). However, the current in the beginning of the potential step would be disturbed by the redox reaction of the surface modifier at the MBH-immobilized KB-GCE (data not shown). Thus MBH was simply adsorbed on the KB-GCE and the time dependence of I_s (at ω = 2500 rpm) due to the inactivation of MBH on the KB-GCE was measured by potential-step chronoamperometry (data not shown), and the I_{cat} contribution was extracted from the observed I_s by using the evaluated I_D. The extracted values of I_{cat} are plotted as a function of the time in Fig. 2(B) as open circles. The author analyzed the decay characteristics of I_{cat} (from 4 to 30 s) with eqn. (2) in the same manner as that used for the data obtained at the Au electrode. The regression curve is shown in Fig.2 (B) as a solid line. The decay characteristics are well explained by eqn. (2).

3.3 Potential dependence of the apparent inactivation and reactivation rate constants

Figure 4 shows the potential dependence of k_I and k_A at MBH-adsorbed Au electrode (open circles) and MBH-adsorbed KB-GCE (open triangles). Since the magnitude of the inactivation (the catalytic current decay) is very small in the low potential region (from –0.2 to –0.15 V), the evaluation of the rate constants were very difficult in the region. The evaluated values of k_I at least in the potential range from –0.1 to 0.1 V seems to be independent of the potential (Fig. 4 (A)). In contrast, the logarithmic values of k_A decrease linearly with the electrode potential and reach a limiting value at high potentials (E > 0.05 V) (Fig. 4 (B)). These characters are coincident with those described in a previous study using tolerant *A. aeolicus* [NiFe]-hydrogenase.[37] The inactivation

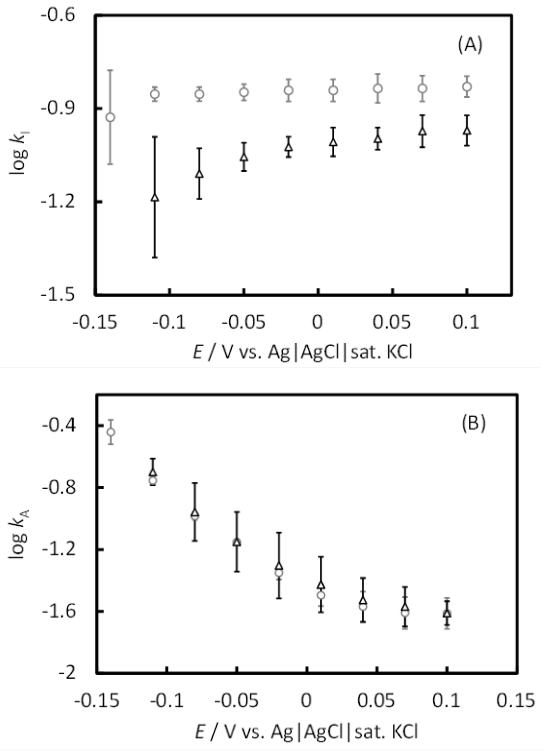

Figure 4
(A) The potential dependence of the apparent rate constants of the inactivation
(B) The open circles and triangles correspond to the results obtained at Au electrode and KB-GCE, respectively. The error bars were evaluated by the Student *t*-distribution at 90% confidence level.

process involves the one-electron oxidation of the Ni(II) in the [NiFe] catalytic center and the hydroxide ligand coordination to the Ni(III).[2,22,26] The fact that k_I is independent of the electrode potential means that the rate of the hydroxide ligand coordination to the Ni(III) (the coordination of water on the [NiFe]-active site and the succeeding deprotonation) is the rate-determining step of the inactivation. Some conformational change around the [NiFe]-active might also be involved. The k_I values evaluated for the MBH adsorbed on the KB-GCE is smaller than those for the MBH adsorbed on the Au electrode (Fig. 4 (A)). Some restriction in the movement of MBH adsorbed in the mesopore of the KB-BCE seems to decelerate the hydroxide ligand coordination to the Ni(III). Actually, the chemical immobilization of MBH on an Au electrode caused a decrease in the k_I value (data not shown).

On the other hand, the potential dependence of k_A (Fig. 4 (B)) indicates that the rate-determining process of the reactivation process is one-electron reduction of the Ni(III) atom in the Ni-B state. The electrode materials do not affect the reduction rate of the Ni(III), since the k_A values at the MBH-adsorbed KB-GCE is identical with those at the MBH-adsorbed Au electrode (Fig. 4 (B)).

3.4 Competitive inhibition-like model for the anaerobic inactivation

As to the anaerobic inactivation, the generation of Ni-B (the inactive state form) from Ni-SI seems to compete with the catalytic reduction of Ni-SI to Ni-R by H_2 as described in the previous studies.[2,22,26] Thus, the reaction scheme can be simply represented in Fig. 5. In the case of the competitive inhibition-like catalytic reaction, I_{cat} can be expressed by eqns. (5) and (6) using steady-state approximation.

$$I_{\mathrm{cat}} = nFA\frac{k_{\mathrm{cat}}\Gamma_{\mathrm{enz,eff}}}{1+\dfrac{K_{\mathrm{M}}^{'}}{c_{\mathrm{H_2}}}} = \frac{I_{\max}}{1+\dfrac{K_{\mathrm{M}}^{'}}{c_{\mathrm{H_2}}}} \tag{5}$$

while K_{M}' is the apparent Michaelis constant given by

$$K_{\mathrm{M}}^{'} = \left(1+\frac{k_2}{k_{-2}}\right)K_{\mathrm{M}} = (1+K_{\mathrm{I}})K_{\mathrm{M}} \tag{6}$$

where k_{cat}, $\Gamma_{\mathrm{enz,eff}}$, K_{M}, k_2 and k_{-2} are, respectively, the catalytic constant and the total effective surface concentration of MBH, the Michaelis constant, the inactivation rate constant and the reactivation rate constant. Since it is difficult to evaluate $\Gamma_{\mathrm{enz,eff}}$ at the present moment, the author will not discuss the independent evaluation of k_{cat} in this work.

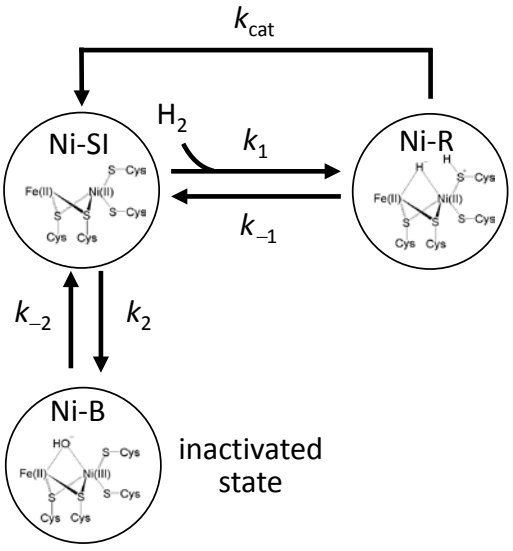

Figure 5
The reaction scheme of the anaerobic inactivation. Ni-SI, Ni-R and Ni-B are, respectively, the active silent form of MBH, H_2-reduced form of Ni-SI and one-electron oxidized form of Ni-SI caused by the anaerobic inactivation. k_1, k_{-1}, k_2, k_{-2} and k_{cat} are, respectively, the forward and backward rate constants of H_2-binding reaction, the inactivation and reactivation rate constant and the catalytic constant.

The author has already evaluated and discussed the apparent inactivation rate constant (k_{I}) and reactivation rate constant (k_{A}) in section 3.2 and 3.3, respectively. However, the physical meaning of the rate constants are not necessarily identical with the enzyme kinetic parameters. Therefore, let us here consider the relation between the apparent rate constant (k_{I}, k_{A}) and the true value (k_2, k_{-2}) based on the Fig. 5. The author assumes that the H_2-binding reaction to the Ni-SI state form is at rapid equilibrium ($k_{-1} >> k_{\mathrm{cat}}$). The K_{M} is defined as

$$K_{\mathrm{M}} = \frac{k_{-1}}{k_1} = \frac{\Gamma_{\mathrm{Ni-SI}} c_{\mathrm{H_2}}}{\Gamma_{\mathrm{Ni-R}}} \tag{7}$$

where k_1, k_{-1}, $\Gamma_{\mathrm{Ni-SI}}$ and $\Gamma_{\mathrm{Ni-R}}$ are, respectively, the forward and backward rate constants of the H_2-binding reaction to the Ni-SI state form, the effective surface concentrations of Ni-SI and Ni-R state forms. Under the conditions, I_{cat} can be expressed by eqn. (8).

$$I_{\mathrm{cat}} = nFAk_{\mathrm{cat}}\Gamma_{\mathrm{Ni-R}} = nFAk_{\mathrm{cat}} \frac{c_{\mathrm{H_2}}}{K_{\mathrm{M}}} \Gamma_{\mathrm{Ni-SI}} \tag{8}$$

The time dependence of $\Gamma_{\mathrm{Ni-SI},t}$ during inactivation and activation in the presence of H_2 is described as follows.

$$\frac{\mathrm{d}\Gamma_{\mathrm{Ni-SI},t}}{\mathrm{d}t} = k_{-2}\Gamma_{\mathrm{Ni-B},t} + \left(k_{-1} + k_{\mathrm{cat}}\right)\Gamma_{\mathrm{Ni-R},t} - \left(k_1 c_{\mathrm{H_2}} + k_2\right)\Gamma_{\mathrm{Ni-SI},t} \tag{9}$$

where $\Gamma_{\mathrm{Ni-B},t}$ is the effective surface concentration of the Ni-B state form at *t*. Considering the mass balance of the surface concentration of MBH and the fully-activated conditions for MBH, the author can obtain eqns. (10)

$$\Gamma_{\mathrm{enz,eff}} = \Gamma_{\mathrm{Ni-SI},t} + \Gamma_{\mathrm{Ni-R},t} + \Gamma_{\mathrm{Ni-B},t} \tag{10}$$

with the initial condition (at $t = 0$ at $E_1 = -0.2$ V)

$$\Gamma_{\mathrm{enz,eff}} = \Gamma_{\mathrm{Ni-SI},0} + \Gamma_{\mathrm{Ni-R},0} \tag{11}$$

Solving eqn. (9) with eqns. (7), (10) and (11), $\Gamma_{\mathrm{Ni-SI},t}$ is expressed by eqn. (12)

$$\Gamma_{\mathrm{Ni-SI},t} = \Gamma_{\mathrm{Ni-SI},0}\left[\frac{k_2}{k_2 + k'_{-2}} \exp\left\{-\left(k_2 + k'_{-2}\right)t\right\} + \frac{k'_{-2}}{k_2 + k'_{-2}}\right] \tag{12}$$

while k'_{-2} is given by

$$k'_{-2} = \left(1 + \frac{c_{\mathrm{H_2}}}{K_{\mathrm{M}}}\right)k_{-2} \tag{13}$$

Thus, the decay of the catalytic current is given by

$$I_{\mathrm{cat}}(t) = I_0\left[\frac{k_2}{k_2 + k'_{-2}}\exp\{-(k_2 + k'_{-2})t\} + \frac{k'_{-2}}{k_2 + k'_{-2}}\right] \quad (14)$$

Compering the eqns. (2) and (14), the author can conclude that $k_{\mathrm{I}} = k_2$, and that $k_{\mathrm{A}} = k'_{-2} = \left(1 + \frac{c_{\mathrm{H_2}}}{K_{\mathrm{M}}}\right)k_{-2}$. Consequently, the inhibition constant can be given as

$$K_{\mathrm{I}} = \frac{k_2}{k_{-2}} = \frac{k_{\mathrm{I}}}{k_{\mathrm{A}}}\left(1 + \frac{c_{\mathrm{H_2}}}{K_{\mathrm{M}}}\right) \quad (15)$$

Therefore, it is important to evaluate K_{M} for DET-type H_2-oxidation of MBH on the electrode. A simple and easy electrochemical method for determining K_{M} of adsorbed [NiFe]-hydrogenase was reported by Léger *et al.*[42] The time dependence of the catalytic current during the convective H_2-gas removal was analyzed under the assumption that the removal of the gas from solution on flushing with an inert gas follows the simple exponential kinetics and that the H_2-concentration is homogeneous in solution during the inert gas flushing and the enzyme reaction near the electrode surface. However, in order to evaluate an accurate value of K_{M} of the adsorbed MBH, it will be recommended to analyze H_2-concentration dependence of the steady-state catalytic current (I_{cat}) at rotating disk electrodes with a constant amount of adsorbed MBH.

Figure 6(A) shows the CA at the MBH-immobilized KB-GCE and at several $p_{\mathrm{H_2}}$ (0.05–1 atm). The measurement potential was set at −0.2 V, where the anaerobic inactivation does not occur. First, in the light zone ($p_{\mathrm{H_2}}$ = 1 atm), I_{s} was measured at ω = 2500 rpm (as indicated by the arrow). Next, the ω value was stepwise changed from 50 to 2500 rpm. The time dependence of the I_{s} during the ω change (the left side light zone in Fig. 6(A)) is magnified and depicted in Fig. 3(A). Quick response to ω was obtained. Subsequently, in the shaded zone, $p_{\mathrm{H_2}}$ was changed from 0.9 to 0.05 atm step by step. When $p_{\mathrm{H_2}}$ was changed, ω was hold at 2500 rpm until the I_{s} value reached a constant value (at which the H_2-concentration reached a constant value). After then, the ω value was stepwise changed from 50 to 2500 rpm. As judged from I_{s} at ω = 2500 rpm and $p_{\mathrm{H_2}}$ = 1 atm (as indicated by the arrows in light zone), the MBH-immobilized KB-GCE shows almost the identical value of the steady-state H_2-oxidation current. The result verifies the relatively high stability of the MBH-immobilized KB-GCE over the 2-h continuous measurements under strong convection.

In the case at $p_{\mathrm{H_2}}$ = 1 atm, I_{cat} has already been evaluated in section 3.2. The ω dependence of I_{s} at several $p_{\mathrm{H_2}}$ (0.05–0.9 atm) also shows curved characteristics (Fig. 6(B)). Equations (3) and (4) were fitted to the data taken at $p_{\mathrm{H_2}}$ = 0.05–0.9 atm in Fig. 6(B) with I_{cat} and $c_{\mathrm{H_2}}$ as the adjustable parameters using a non-linear regression analysis by Gnuplot®. The analytical

results are collected in Fig. 6(C). The error bar is given as the asymptotic standard error. Under the conditions where the anaerobic inactivation does not occur, I_{cat} is given by an equation similar to Michaelis-Menten equation[43]

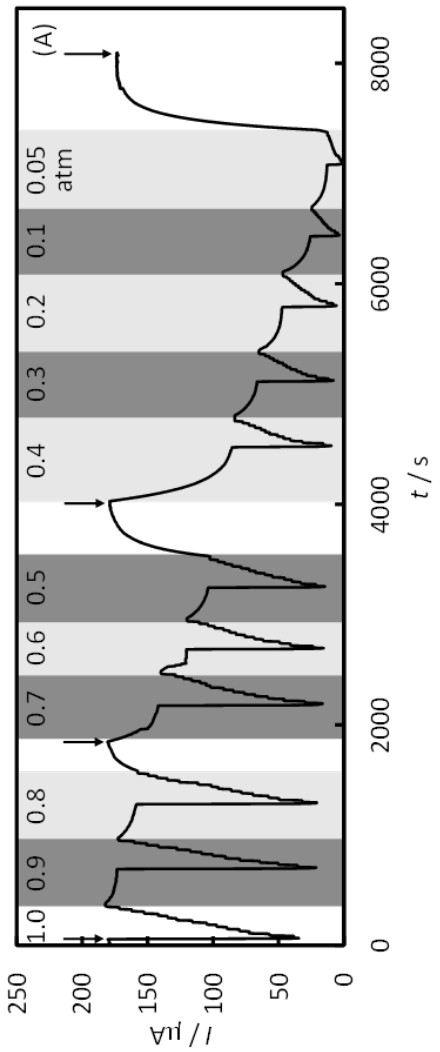

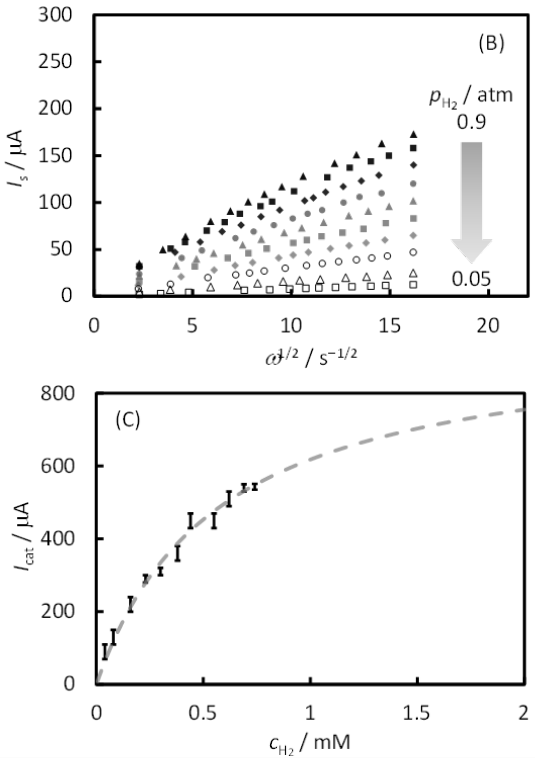

Figure 6
(A) CA of the MBH-immobilized KB-GCE at –0.2 V and at several p_{H_2} (0.05–1 atm). In the light zone, p_{H_2} was set to be 1 atm. First, I_s at p_{H_2} = 1 atm was measured at ω = 2500 rpm (as indicated by an arrow). Next, the ω value was stepwise changed from 50 to 2500 rpm. p_{H_2} was set to be 1 atm at the position indicated by the arrows to check the stability of MBH on the electrode surface. In the shaded zone, p_{H_2} was changed from 0.9 to 0.05 atm. After the current reaches to the constant at ω = 2500 rpm, the ω value was stepwise changed from 50 to 2500 rpm. The CA profile in the left side light zone is identical with that given in Fig, 3 (A).
(B) ω dependence of I_s at the MBH-immobilized KB-GCE at p_{H_2} = 0.05-0.9. The current was measured as shown in panel A.
(C) I_{cat} contribution as a function of c_{H_2} for the MBH-catalyzed H_2-oxidation. The broken curve was evaluated by a non-linear regression analysis based on eqn. (16).

$$I_{\mathrm{cat}} = nFA\frac{I_{\max}}{1+\dfrac{K_{\mathrm{M}}}{c_{\mathrm{H_2}}}} \tag{16}$$

Equation (16) was fitted to the $c_{\mathrm{H_2}}$ dependence of I_{cat} depicted in Fig. 6(C) with $I_{\max}$ and K_{M} as the adjustable parameters using a non-linear regression analysis by Gnuplot®. The regression shows that $I_{\max}$ = 970 ± 70 μA and that K_{M} = 0.57 ± 0.08 mM. The K_{M} value of the immobilized MBH is rather large compared with that of MBH in solution measured by an activity assay (12 μM).[31] The result might be due to the effect of MBH-immobilization or the differences in the reaction character between the interfacial reaction (DET-type bioelectrocatalysis) and the solution reaction (activity assay using mediators as an electron accepter).

The $k_{\mathrm{I}}/k_{\mathrm{A}}$ value increases with the electrode potential and reaches an almost constant value (6.2 at Au electrode and 4.5 at KB-GCE as judged from Fig.4 (A)) at E > 0.05 V. If the author accepts the K_{M} value as 0.57 mM evaluated here, the K'_{M} value is estimated as 8.7 (at Au electrode) and 6.5 mM (at KB-GCE) with eqns. (6) and (15). Since the K'_{M} value is larger than the saturated H_2-concentration (0.74 mM), it seems to be difficult to avoid the anaerobic inactivation in immersion system. This prediction is supported by the fact given in Fig 1 (B) as a solid line. As described previously, the author has already avoided the inactivation with a gas-diffusion system.[27] The author can say that the effect is due to the increasing H_2-concentration achieved by high-speed H_2-supply to MBH over the K'_{M} value.

3.5 MBH-adsorbed gas-diffusion-type bioanode

An MBH-adsorbed KB-CPE was fabricated as a gas-diffusion-type bioanode. CVs of the MBH-adsorbed KB-CPEs were recorded under quiescent (passive) and H_2-atmospheric conditions and are depicted in Fig. 7 as a solid line. The current density is as large as about 10 mA cm^{-2} at 0 V. Not

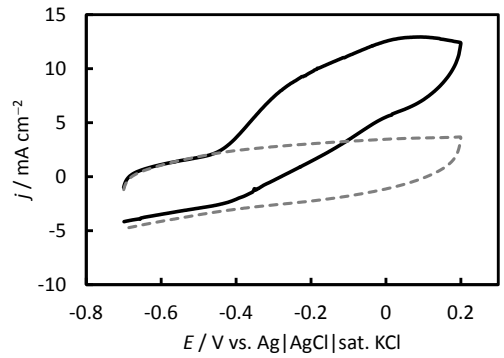

Figure 7
CVs of catalytic H_2-oxidation of MBH-adsorbed KB-CPE under H_2-(solid line) and Ar-(broken line) flow in the gas phase. The measurements were carried out in 100 mM phosphate buffer (pH 6) deaerated by Ar at 40 ± 2 °C. The scan rate was 20 mV s^{-1}.

only the inactivation is avoided, but the value is larger than that observed by MBH-adsorbed KB-GCE under stirred conditions as shown in Fig. 1(B).

In near future, a one-compartment dual gas-diffusion and DET-type H_2/O_2 biofuel cell will be constructed. The new type of H_2/O_2 biofuel cell allows us to supply H_2 and O_2 separately, thus enables us to get rid of the following problems. One is the risk of explosion, and the other is competitive limitation of dissolved gas-concentration governed by p_{H_2} and p_{O_2}.

4. Conclusion

The author has evaluated the rate constants of the inactivation and reactivation processes of the anaerobic inactivation and the K_M value for H_2 of MBH immobilized on the electrode based on steady-state electrochemical analysis. The inactivation process is independent of the electrode potential at least at $E > -0.1$ V, while the rate-determining step of the reactivation process seems to be the one-electron reduction of the Ni(III) atom in the [NiFe] center. The K'_M value (8.7 mM at Au electrode and 6.5 mM at KB-GCE) based on a competitive inhibition-like reaction is larger than the saturated H_2-concentration (0.74 mM), indicating that the adsorbed MBH is subject to the inhibition even in H_2-saturated solutions, as evidenced by the experimental results presented here. Thus, it is effective and necessary for avoiding the inactivation to utilize the gas-diffusion system. The gas-diffusion-type bioanode (MBH-adsorbed KB-GCE) have recorded the highest H_2-oxidation current (10 mA cm^{-2}) even under the quiescent conditions and it would dramatically improve the performance of DET-type H_2/O_2 biofuel cell.

5. References

1 K.A. Vincent and F.A. Armstrong, *Chem. Rev.*, 2007, **107**, 4366-4413.

2 F. A. Armstrong, N. A. Belsey, J. A. Cracknell, G. Goldet, A. Parkin, E. Reisner, K. A. Vincent and A. F. Wait, *Chem. Soc. Rev.*, 2009, **38**, 36-51.

3 A. K. Jones, E. Sillery, S. P. J. Albracht and F. A. Armstrong, *Chem. Commun.*, **8**, 2002, 866-867.

4 R. Bashyam and P. Zelenay, *Nature*, 2006, **443**, 63-66.

5 M. Guiral, L. Prunetti, C. Aussignargues, A. Ciaccafava, P. Infossi, M. Ilbert, E. Lojou and M Giudici-Orticoni, *Adv. Microb. Physiol.*, 2012, **61**, 125-194.

6 T. Yagi and Y. Higuchi, *Proc. Jpn. Acad. Ser. B*, 2013, **89**, 16-32.

7 H. S. Shafaat, O. Rüdiger, H. Ogata and W. Lubitz, *Biochimca et Biophysica Acta*, 2013, **1827**, 986-1002.

8 A. A. Karyakin, *Bioelectrochemistry*, 2012, **88**, 70-75.

9 M. J. Moehlenbrock and S. D. Minteer, *Chem. Soc. Rev*., 2008, **37**, 1188-1196.

10 N. Mano, F. Mao and A. Heller, *ChemBioChem*, 2004, **5**, 1703-1705.

11 D. Leech, P. Kavanagha and W. Schuhmann, *Electrochim. Acta*, 2012, **84**, 223-234.

12 S. C. Barton, J. Gallaway and P. Atanassov, *Chem. Rev.*, 2004, **104**, 4867-4886.

13 S. Kawai, T. Yakushi, K. Matsushita, Y. Kitazumi, O. Shirai and K. Kano, *Electrochem. Commun.*, 2014, **38**, 28-31.

14 K. So, S. Kawai, Y. Hamano, Y. Kitazumi, O. Shirai, M. Hibi, J. Ogawa and K. Kano, *Phys. Chem. Chem. Phys.*, 2014, **16**, 4823-4829.

15 E. I. Solomon, U. M. Sundaram and T. E. Machonkin, *Chem. Rev.*, 1996, **96**, 2563-2605.

16 Y. Miura, S. Tsujimura, S. Kurose, Y. Kamitaka, K. Kataoka, T. Sakurai and K. Kano, *Fuel Cells*, 2009, **9**, 70-78.

17 S. Shleev, J. Tkac, A. Christenson, T. Ruzgas, A. I. Yaropolov, J. W. Whittaker and L. Gorton, *Biosens. Bioelectron.*, 2005, **20**, 2517-2554.

18 A. D. Poulpiquet, A. Ciaccafava, R. Gadiou, S. Gounel, M. T. Giudici-Orticoni, N. Mano and E. Lojou, *Electrochem. Commun.*, 2014, **42**, 72-74.

19 L. Xu and F. A. Armstrong, *Energy Environ. Sci.*, 2013, **6**, 2166-2171.

20 H. Sakai, T. Nakagawa, H. Mita, H. Kumita and Y. Tokita, *217th Electrochemical Society Meet. Abstr. – Electrochem. Soc.*, 2010, **1001**, 396.

21 R. M. Evans, A. Parkin, M. M. Roessler, B. J. Murphy, H. Adamson, M. J. Lukey, F. Sargent, A. Volbeda, J. C. Fontecilla-Camps and F. A. Armstrong, *J. Am. Chem. Soc.*, 2013, **135** 2694-2707.

22 M. Pandelia, W. Nitschke, P. Infossi, M. Giudici-Orticoni, E. Bill and W. Lubitz, *Proc. Natl. Acad. Sci. USA*, 2011, **108**, 6097-6102.

23 M. Ludwig, J. A. Cracknell, K. A. Vincent, F. A. Armstrong and O. Lenz, *J. Biol. Chem.*, 2009, **284**, 465-477.

24 Y. Shomura, K. S. Yoon, H. Nishihara and Y. Higuchi, *Nature*, 2011, **479**, 253-257.

25 A. A. Hamdan, B. Burlat, O. Gutiérrez-Sanz, P. Liebgott, C. Baffert, A. L. D. Lacay, M. Rousset, B. Guigliarelli, C. Léger and S. Dementin, *Nat. Chem. Biol.*, 2013, **9**, 15-18.

26 A. K. Jones, S. E. Lamle, H. R. Pershad, K. A. Vincent, S. P. J. Albracht and F. A. Armstrong, *J. Am. Chem. Soc.*, 2003, **125**, 8505-8514.

27 K. So, Y. Kitazumi, O. Shirai, K. Kurita, H. Nishihara, Y. Higuchi and K. Kano, *Chem. Lett.*, in press. DOI:10.1246/cl.140622.

28 C. Lau, E. R. Adkins, R. P. Ramasamy, H. R. Luckarift, G. R. Johnson and P. Atanassov, *Adv. Energy Mater.*, 2012, **2**, 162-168.

29 G. P. M. K. Ciniciato, C. Lau, A. Cochrane, S. S. Sibbett, E. R. Gonzalez and P. Atanassov, *Electrochim. Acta*, 2012, **82**, 208-213.

30 T. Nakagawa, H. Mita, H. Kumita, H. Sakai, Y. Tokita and S. Tsujimura, *Electrochem. Commun.*, 2013, **36**, 46-49.

31 K. S. Yoon, K. Fukuda, K. Fujisawa and H. Nishihara, *Int. J. Hydrogen Energy*, 2011, **36**, 7081-7088.

32 O. Rüdiger, J. M. Abad, E. C. Hatchikian, V. M. Fernandez and A. L. D. Lacey, *J. Am. Chem. Soc.*, 2005, **127**, 16008-16009.

33 C. Baffert, K. Sybirna, P. Ezanno, T. Lautier, V. Hajj, I. Meynial-Salles, P. Soucaille, H. Bottin and C. Léger, *Anal. Chem.*, 2012, **84**, 7999-8005.

34 P. Allongue, M. Delamar, B. Desbat, O. Fagebaume, R. Hitmi, J. Pinson and J. Savéant, *J. Am. Chem. Soc.*, 1997, **119**, 201-207.

35 D. Sehgal and I. K. Vijay, *Anal. Biochem.*, 1994, **218**, 87-91.

36 A. D. Poulpiquet, H. Marques-Knopf, V. Wernert, M. T. Giudici-Orticoni, R. Gadiou and E. Lojou, *Phys. Chem. Chem. Phys.*, 2014, **16**, 1366-1378.

37 V. Fourmond, P. Infossi, M. T. Giudici-Orticoni, P. Bertrand and C. Léger, *J. Am. Chem. Soc.*, 2010, **132**, 4848-4857.

38 J. A. Koutecky and V. G. Levich, *Zhurnal Fizicheskoi Khimii USSR*, 1958, **32**, 1565-1575.

39 A. Nagashima, *J. Phsy. Chem. Ref. Data*, 1977, **6**, 1133-1166.

40 D. R. Lide, Ed., *HANDBOOK OF CHEMISTRY and PHYSICS, 90th Ed.*, CRC press, New York, 2009.

41 C. L. Young, Ed., *IUPAC Solubility Data Series*, Vol. 5/6, Pergamon Press, Oxford, 1981.

42 C. Léger, S. Dementin, P. Bertrand, M. Rousset and B. Guigliarelli, *J. Am. Chem. Soc.*, 2004, **126**, 12162-12172.

43 L. Michaelis and M. L. Menten, *Biochem. Z.*, 1913, **49**, 333.

2-4. Bioelectrochemical analysis of thermodynamics of the catalytic cycle and kinetics of the oxidative inactivation of oxygen-tolerant [NiFe]-hydrogenase

Abstract

Membrane-bound [NiFe]-hydrogenase from *Hydrogenovibrio marinus* (*Hm*MBH) is an O_2-tolerant enzyme and allows direct electron transfer (DET)-type bioelectrocatalysis for the H_2 oxidation. Very fast interfacial electron transfer occurs between the [NiFe]-active site of *Hm*MBH and the electrode, and the potential dependence of the steady-state DET-type catalytic current has been analyzed on a thermodynamic model of a two-step one-electron transfer to get a Pourbaix diagram of the catalytic center. A reversible and oxidative inactivation that occurs when the [NiFe]-hydrogenases are suffered from the oxidative stress at high electrode potentials or high solution potentials has been kinetically analyzed for the time-dependence of the steady-state catalytic current as a measure. The kinetic analysis has shown that the rate-determining step of the oxidative inactivation is not electrochemical but chemical process and that the rate of the reductive reactivation is determined by the electrochemical process. The observed catalytic waves, especially the dependence of the waves on the scan rate and the hydrogen concentration, have been well reproduced by simulation with the thermodynamic and kinetic parameters evaluated here.

1. Introduction

Hydrogenases catalyze the H_2 oxidation and H_2 evolution [1-3]. There are three main classes of hydrogenases based on their active site metals: [Fe] enzymes with only one iron atom in the active site, [FeFe] enzymes with two iron atoms in the active site, and [NiFe] enzymes that possess a heterobimetallic active site. Although most of the [Fe] and [FeFe] proteins are known to be extremely O_2-sensitive, the [NiFe] proteins are not only O_2-sensitive but O_2-resistant or O_2-tolerant [1-3]. Generally, the [NiFe]-hydrogenases comprise a large subunit that incorporates the [NiFe]-active site and a small subunit that houses an electron relay chain of [FeS]-clusters, and they are located in the periplasmic space and are often associated with a membrane. In periplasmic space, the hydrogenases may be anchored to the membrane via *b*-type cytochrome that mediates the electron transfer from H_2 to the respiratory chain quinone pool [1-3].

Many spectroscopic studies have revealed that the [NiFe]-active site stays in several states such as Ni-SI (active silent state), Ni-R (H_2-reduced state), Ni-C (one-electron-oxidized state of Ni-R), Ni-A (inactive-state with high kinetic barrier for reactivation, also known as “unready” state), and Ni-B (reversible inactive-state with low kinetic barrier for reactivation, also known as “ready” state) [1-3]. As summarized in Scheme 1, for the H_2 oxidation, the H_2-binding to the Ni-SI state is the first step and subsequently the catalytic cycle proceeds in the Ni-R, Ni-C and Ni-SI states in turn. In the

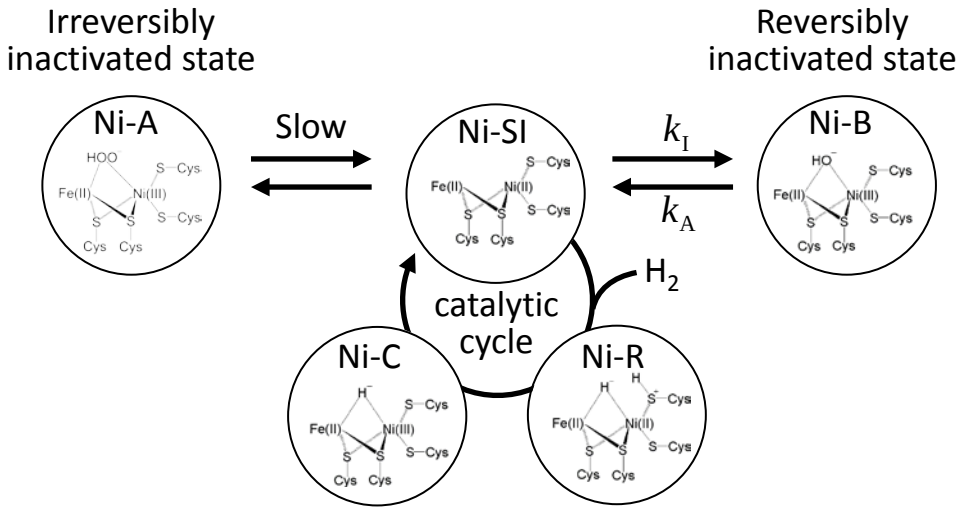

Scheme 1
The reaction scheme of the H_2 oxidation catalytic cycle, the irreversible inactivation and the reversible inactivation (oxidative inactivation). Ni-SI, Ni-R, Ni-C, Ni-A, and Ni-B are, respectively, the active silent state of [NiFe]-hydrogenases, H_2-reduced state of the Ni-SI state, one electron-oxidized state of the Ni-R state, the state caused by the irreversible inactivation, and the state caused by the oxidative inactivation.

case of the standard [NiFe]-hydrogenases, however, the Ni-SI state changes to the Ni-A and Ni-B states on the oxidative stress. The Ni-A state seems to be produced by one-electron oxidation of the Ni-SI state, in which a peroxide ligand is considered to be coordinated to the Ni atom in the bridging position with respect to the Fe(II). However, there has been much debate about oxygenation of sulfurs near the active site in recent literature [4]. The Ni-B state is produced also by one-electron oxidation of the Ni-SI state, in which, in contrast to the Ni-A state, a hydroxide ligand is coordinated to the Ni atom in the bridging position with respect to the Fe(II) [1-3]. Among the [NiFe]-hydrogenases, O_2-tolerant and membrane-bound hydrogenases from *Ralstonia species* [5,6], *Aquifex aeolicus* [7,8], *Escherichia coli* [9,10] and *Hydrogenovibrio marinus* [11,12] have been found, and they have the unique property of catalyzing the H_2 oxidation in the sustained presence of O_2. The O_2-tolerant mechanism has been considered due to the presence, close to the active site, of a unique [FeS]-cluster (a [4Fe-3S]-cluster coordinated by six Cys residues rather than a [4Fe-4S]-cluster coordinated by four Cys residues as to other [NiFe]-hydrogenases) that transfers two electrons rapidly to the active site when the hydrogenase is attacked by O_2 and thus can protect the enzyme against damaging intermediate reduction products of O_2 [6,7,9,11]. Consequently, the ability is very useful and convenient for us in utilization of the hydrogenases for practical applications.

Bioelectrocatalysis as a coupled reaction of the enzymatic catalytic reaction and the electrode reaction is classified into two types in accordance with the electric connection systems [13-18]. One is the mediated electron transfer (MET)-type, in which artificial redox mediators shuttle electrons between enzymes and electrodes to reduce the kinetic hindrance in the interfacial electron

transfer. The other is the direct electron transfer (DET)-type, in which enzymes can directly transfer electrons to or from electrodes. Biofuel cells can be constructed based on bioelectrocatalysis. The recent advances of biofuel cells are summarized by Minteer's group [19]. The device is very secure since it can operate under mild conditions (room temperature, atmospheric pressure and neutral pH). Accordingly, it is also possible to be utilized as micro-electronic power devices that can extract energy from biological sources [20-23]. There are limited number of redox enzymes capable of direct communication with electrodes, but some of hydrogenases are known as DET-type enzymes [1,13,18]. This feature enables us to construct H_2-oxidating bioanodes for DET-type biofuel cells that are very simple and compact due to minimum components (only enzyme, electrode and electrolyte) [24-27]. For O_2 reduction, several multi-copper oxidases (MCOs) such as laccase, bilirubin oxidase, and Cu efflux oxidase work as DET-type enzymes and are used in O_2-reducing biocathodes [28-30]. By utilizing hydrogenases and MCOs, a DET-type H_2/O_2 biofuel cell can be constructed. Since the electric power device does not need platinum, it might solve the platinum-depletion-problem concerning H_2/O_2 fuel cells. In fact, Lojou's group and Armstrong's group have reported power devices with a power density of 1.5 mW cm^{-2} (at 60 °C with MBH from *A. aeolicus* and BOD from *B. pumilus*) [24] and 1.67 mW cm^{-2} (at 25 °C with MBH from *E. coli* and BOD from *M. verrucaria*; noting here that the surface area of the cathode is 3 times larger than that of the anode and the power density is calculated on the basis of the surface area of the anode) [25], respectively.

In addition to the aforementioned redox enzymes (hydrogenases and MCOs), fructose dehydrogenase [31,32] and cellobiose dehydrogenase [33,34] are also known as DET-type enzymes. Catalytic voltammograms on DET-type enzyme-modified electrode tell us the characteristics of the enzymes [18]. Most of DET-type enzymes produce catalytic voltammograms with quasi-reversible or irreversible characteristics of the electron transfer between the enzymes and electrode. Unfavorable orientation of the modified enzyme leads to high overpotentials, and the steady-state catalytic current in voltammograms continues to increase linearly with the potential (called as "residual slope") after the sigmoidal increase [35]. This phenomenon has been theoretically explained by Léger *et al.*, in which they have considered effects of a dispersion on the interfacial electron transfer rate by assuming the random disorder of the distance between the electrode and the active site [35]. In this model (called dispersion model), they have taken into account the distribution of the distance from the active site of the enzyme to the electrode. Subsequently, the interfacial electron transfer rate constant is expressed based on a relation in which the electron transfer rate constant decreases exponentially with the tunneling distance between the electrode and the active site of the enzyme [36]. Finally, quasi-reversible or irreversible catalytic voltammograms can be interpreted with several factors concerning the redox potential, the standard electron transfer rate constant, and the enzyme orientation.

Hydrogenases often give sigmoidal steady-state catalytic voltammograms with the residual slope. Léger *et al*. analyzed voltammograms of the catalytic H_2 oxidation and H_2 evolution with

reversible characteristics obtained at [NiFe]-hydrogenase (from *A. vinosum*)-adsorbed electrode on a model of the two-step one-electron transfer (corresponding to the redox reaction of the Ni-SI, Ni-R and Ni-C states) by using the aforementioned dispersion model [35,37]. To get an acceptable fitting, they used an assumption that the redox potential of the Ni-R/Ni-C couple is far more negative than the potentials range investigated. More sophisticated analysis has also been reported by Léger's group [38] based on the same dispersion model. Although it may be considered that the residual slope is ascribed to the interfacial electron transfer kinetic-controlled catalytic reaction due to unfavorably oriented hydrogenases on the electrode, the sigmoidal part of the catalytic wave may be ascribed predominantly to favorably oriented enzymes and can be explained on a thermodynamic model.

On the other hand, the Ni-B state (the inactive state with low kinetic barrier for reactivation) is produced, when [NiFe]-hydrogenases are suffered from the highly oxidative stress at electrodes and by oxidized dyes and O_2 [1,37,39]. This reaction is called as the oxidative inactivation and is an obstacle for constructing an aforementioned bioelectrochemical device for H_2 energy conversion. Several kinetic studies have been reported [40-42]. In addition, there are two reports to overcome this reaction [43,44]. Schuhmann's and Lubitz's groups have proposed that a new concept to protect hydrogenases against the oxidative inactivation by exploiting a specifically designed viologen-based redox hydrogel [43]. The electron transfer between the polymer-bound viologen moieties controls the potential near the active site of the hydrogenase and thus insulates the enzyme from excessive oxidative stress [43]. On the other hand, the author has focused on the reaction mechanism and considered the oxidative inactivation as a competitive inhibition-like reaction against the H_2 binding to the Ni-SI state [44]. As far as we know, this is the first report on a description of the pseudo-steady-state current of the oxidative inhibition as a function of the electrode potential and the Michaelis constant. In the dissolved system, the saturated H_2 concentration is 740 μM at 40 °C [45], which is only slightly larger than the Michaelis constant (K_M = 570 μM) evaluated in DET-type bioelectrocatalysis [41]. To achieve the high H_2 concentration, the author has constructed a gas-diffusion-type electrode, which can directly supply H_2 gas to the enzyme layer on the solution-side of the anode. As a result, the high-speed (non-equilibrated but a steady-state)-H_2-supply enhances the H_2 concentration around the hydrogenase and thus makes it possible to overcome the oxidative inactivation [41,44].

The inactivation was sometimes analyzed from the thermodynamic point of view, and E_{switch} is often used as a practical parameter, which is defined as a potential to produce bioelectrocatalytic voltammogram with the maximum slope on the in the reductive activation process (that is, the half-wave potential of bioelectrocatalytic voltammogram in the reductive activation process) [46]. Although the parameter E_{switch} includes kinetic characteristics as well as thermodynamic ones [40], it was used as a physical index of the oxidative inactivation potential [46]. Therefore, it seems to be important to understand the characteristics of E_{switch} from the kinetic viewpoints.

In this study, the author uses an O_2-tolerant and membrane-bound [NiFe]-hydrogenase from *Hydrogenovibrio marinus* (*Hm*MBH) [11,12] for thermodynamic and kinetic analysis. First, the author has considered the H_2-binding to the [NiFe]-active site and the two-step one-electron transfer mechanism in the catalytic cycle for analysis of Nernstian response of DET-type catalytic voltammograms of the H_2 oxidation. Second, the author has kinetically examined the oxidative inactivation by focusing the time dependence of the steady-state catalytic current in potential-step measurements. Here the author uses a new model based on the competitive inhibition. Similar to the conclusion on the other reports, the inactivation rate constant does not depend on the electrode potential, and the reactivation rate constant depends on the electrode potential. In other words, the rate-determining steps (r.d.s.) of the inactivation and the reactivation are a chemical process and an electron transfer process, respectively. Here, the author also shows that the rate constant decreases by immobilizing the enzyme. Based on the kinetics, the author will discuss the redox potential concerning the oxidative inactivation. Finally, the author has simulated the bioelectrocatalytic cyclic voltammograms of *Hm*MBH with thermodynamic and kinetic parameters evaluated here. The simulation has well reproduced the fundamental feature of the oxidative inactivation, especially the dependence of the catalytic waves on the scan rate and the hydrogen concentration.

2. Experimental

2.1. Materials

N-Hydroxy-succinimide (98%, NHS) was purchased from Sigma-Aldrich Co. (USA). 1-Ethyl-3-(3-dimethylaminopropyl)-carbodiimide hydrochloride (EDC) was purchased from Dojindo Laboratory (Japan). *Hm*MBH was purified according to the literature [12]. All other chemicals used in this study were of analytical grade and all solutions were prepared with distilled water.

2.2. Preparation of HmMBH-adsorbed electrode

Gold (Au) electrodes (3 mm in diameter, BAS) were polished with alumina slurry (Buehler, 1 μm), sonicated, and washed with distilled water. A fifteen-μL aliquot of an *Hm*MBH solution (7 μM dissolved in 10 mM phosphate buffer of pH 6) was applied on the Au electrodes, and the electrodes were kept in water-saturated atmosphere for 2 h at room temperature to slowly dry the solvent (1 L = 1 dm^{-3}, 1 M = 1 mol dm^{-3}).

2.3 Immobilization of HmMBH on Au electrode

*Hm*MBH adsorbed on Au electrode was chemically immobilized via amide-linkage [47]. After preparing the Au electrode described as in section 2.2, 15-μL of an *Hm*MBH/reagent solution (7 μM HmMBH, 12 mM EDC, and 6 mM NHS dissolved in 10 mM phosphate buffer of pH 6) was applied on the Au electrode. The electrodes were kept in water-saturated atmosphere for 2 h at room temperature to slowly dry the solvent.

2.4 Electrochemical measurements

Cyclic voltammetry and chronoamperometry were performed on electrochemical analyzers BAS CV-50W and ALS 714C. An Ag|AgCl|sat. KCl electrode and a Pt wire were used as a reference electrode and a counter electrode, respectively. Measurements described in sections 3.1, 3.2 and 3.3 were carried out in McIlvaine buffer (pH 5–7) at 25 ± 2 °C, while measurements described in section 3.4 were carried out in 100 mM phosphate buffer (pH 6) at 40 ± 2 °C.

2.5 Digital simulation

Digital simulation of the DET-type bioelectrocatalysis on *Hm*MBH-adsorbed electrode were carried out using a commercial FEM package called COMSOL® Multiphysics 5.0 on a workstation equipped with two Intel Xeon processors and 64 GB RAM.

3. Results and discussion

3.1 Rate-determining step of HmMBH-catalyzed H_2 oxidation in DET-type bioelectrocatalysis

Fig. 1 (solid line) shows cyclic voltammograms (CVs) of dissolved H_2 at an *Hm*MBH-adsorbed Au electrode at several scan rates (v). Judging from the comparison with a wave under Ar-atmospheric conditions (broken line), the Faradaic wave is ascribed to the *Hm*MBH-catalyzed H_2 oxidation. The H_2 oxidation current began to sigmoidally increase from about –0.5 V. However, the current decreased in the electrode potential range more positive than about –0.2 V and recovered in the reverse scan, most notably at deceased scan rates, for example at v = 5 mV s^{-1}. The phenomenon is ascribed to the oxidative inactivation to generate the Ni-B state and the reductive reactivation (the author will discuss this reaction later).

In order to verify the O_2-tolerant characteristics of *Hm*MBH, the effects of the O_2 addition on the enzyme activity were monitored with chromoamperometry at –0.2 V. The steady-state current

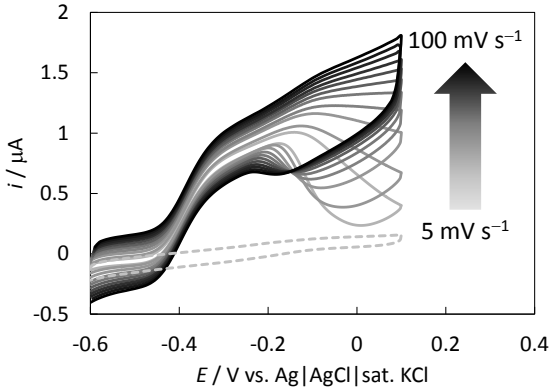

Figure 1
CVs of the *Hm*MBH-adsorbed Au electrode in H_2-(solid line) and Ar-saturated (broken line) buffer solution under quiescent conditions. The scan rates of solid lines were 5–100 mV s^{-1} from bottom to top (grey to black). The scan rate of a broken line was 10 mV s^{-1}. The measurements were carried out in McIlvaine buffer (pH 5.5) at 25 ± 2 °C.

of the catalytic H_2 oxidation decreases immediately after the addition of O_2 due to the oxidative inactivation (data not shown). The decreased current gradually recovers to the original level by the H_2-flushing. The characteristics are coincident with those of the typical O_2-tolerant hydrogenases [1].

Here, let us consider the r.d.s. of the DET-type bioelectrocatalysis with *Hm*MBH. The bioelectrocatalysis is composed of three steps in series: the substrate diffusion, the enzyme reaction, and the electrode reaction. Concerning the substrate diffusion, the author examined the effects of the electrode-rotating rate (ω) on the catalytic H_2 oxidation current. The electrode rotation causes no effects on the CV shape, and the steady-state current is independent of ω. These facts show that the mass transfer is much faster than other processes.

Concerning the enzyme reaction and the electrode reaction, it is difficult to simply separate the contributions of these reactions on the current. The gradual increase (called the residual slope) in the catalytic current (at potentials more positive than –0.3 V in Fig. 1) is ascribed to *Hm*MBH unfavorably oriented for DET [35,37,38]. Léger's group has considered the effect of a dispersion of the interfacial electron transfer rates on the voltammograms by assuming the uniform disorder of the distance between the electrode and the active site of the enzyme [35,37,38]. Based on this model, they have analyzed the voltammograms with residual slopes and have succeeded in evaluation of enzyme characteristics.

The sigmoidal part in the catalytic steady-state CV (–0.5 to –0.3 V in Fig. 1) is predominantly ascribed to the favorably oriented *Hm*MBH and that the part may be simply analyzed from the thermodynamic viewpoint [18, 35]. Here, the author considers a model similar to that of Léger's group [18]. In the model, it is assumed that spherical enzymes are "randomly" adsorbed on an electrode with one-step electron transfer site. Appendix A summarizes the derivation of Eq. (A.8) which can describe the shapes of the steady-state catalytic wave. The sigmoidal part becomes quite

clear as an increase in $k^{\circ}_{\max}/k_c$, where $k^{o}_{\max}$ and k_c are the standard rate constant for the electrode reaction at a distance of the closest approach and the catalytic constant of the enzyme, respectively. Here, let us consider the contributions of the catalytic reaction by the favorably oriented enzymes on the sigmoidal part at a large $k^{\circ}_{\max}/k_c$. The author tentatively selected the enzymes with θ' in a range of $0 \leq \theta' \leq \pi/4$ as the favorably oriented ones, where θ' is the angle between the vertical axis and the line from the center of the enzyme to the redox center. The other part of the randomly oriented enzymes with $\pi/4 \leq \theta' \leq \pi$ were considered as the unfavorably oriented enzymes. The total value of the steady-state catalytic current was divided into two contributions from the favorably oriented enzymes and the unfavorably oriented enzymes. The sigmoidal part of the voltammogram is predominantly contributed from the favorably oriented enzymes with a very large $k^{\circ}_{\max}/k_c$. Therefore, as the first approximation, the author can assume that the sigmoidal part of the steady-state catalytic CV (in the potential range from –0.5 to –0.3 V in CV in Fig. 1) is predominantly produced by the catalytic reaction of the favorably oriented enzymes which can reversibly communicate with the electrode. This consideration means that the redox states of the favorably oriented *Hm*MBH is completely governed by the electrode potential, and that the catalytic current is proportional to the Michaelis complex formed from the Ni-SI state and H_2 on the electrode surface.

3.2 Nernst analysis on the [NiFe]-active site of HmMBH

The author performs the Nernst analysis for the voltammograms of the *Hm*MBH-catalyzed H_2 oxidation in the potential range from –0.5 to –0.3 V, where the oxidative inactivation does not occur (or the inactivation may be ignored, if any). For the H_2 oxidation, the catalytic cycle can be written, as shown in Scheme 2. Since the binding positions between Ni and Fe atoms of the Ni-R and Ni-C states are occupied, H_2 seems to bind to the Ni-SI state only [1-3]. The Ni-SI:H_2 complex corresponds the Michaelis complex essentially used in the enzyme kinetics. B. L. Greene *et al*. have also assumed the presence of H_2-complex with Ni-SI state in the enzyme kinetic analysis [48]. Considering the Ni-SI:H_2 complex formation and a steady-state approximation, the steady-state catalytic current of the *Hm*MBH-catalyzed H_2 oxidation (i_{cat}) in the presence of excess amounts of H_2 can be expressed by Eq. (1)

$$i_{cat} = nFAk_c\Gamma_{\text{Ni-SI:H}_2} \quad (1)$$

Where *n*, *F*, *A*, and $\Gamma_{\text{Ni-SI:H}_2}$ are, respectively, the number of electrons (2 in this case), the Faraday constant, the projected electrode surface area, and the surface concentration of the active Ni-SI:H_2 state. The limiting catalytic current (i_{lim}) is given by Eqs. (2) and (3) similar to the Michaelis-Menten

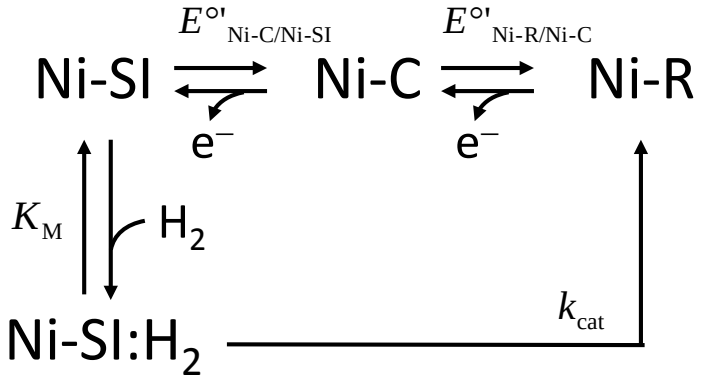

Scheme 2

The reaction scheme of the H_2 oxidation catalytic cycle for Nernst analysis. K_M, k_{cat}, $E^{\circ\prime}_{\text{Ni-C/Ni-SI}}$, and $E^{\circ\prime}_{\text{Ni-R/Ni-C}}$ are, respectively, the Michaelis constant for H_2, the catalytic constant, the formal redox potentials of Ni-C/Ni-SI and Ni-R/Ni-C redox couples.

equation

$$i_{\text{lim}} = \frac{nFAk_c\Gamma_{\text{total}}}{1+\frac{K_M}{c_{H_2}}} \tag{2}$$

while Γ_{total} is the total surface concentration of the effective *Hm*MBH given by

$$\Gamma_{\text{total}} = \Gamma_{\text{Ni-SI:H}_2} + \Gamma_{\text{Ni-SI}} + \Gamma_{\text{Ni-C}} + \Gamma_{\text{Ni-R}} \tag{3}$$

where K_M, c_{H_2}, $\Gamma_{\text{Ni-SI}}$, $\Gamma_{\text{Ni-C}}$, and $\Gamma_{\text{Ni-R}}$ are, respectively, the Michaelis constant, the concentration of dissolved H_2, and the surface concentrations of the Ni-SI, Ni-C and Ni-R states. The Nernstian distribution of the Ni-SI, Ni-C, and Ni-R states (Eqs. (4) and (5)) and the distribution ratio of Ni-SI and Ni-SI:H_2 complex (Eq. (6)) are given as follows:

$$\frac{\Gamma_{\text{Ni-SI}}}{\Gamma_{\text{Ni-C}}} = \exp\left\{\frac{F}{RT}\left(E - E^{\circ\prime}_{\text{Ni-C/Ni-SI}}\right)\right\} \equiv e_{\text{Ni-C/Ni-SI}} \tag{4}$$

$$\frac{\Gamma_{\text{Ni-C}}}{\Gamma_{\text{Ni-R}}} = \exp\left\{\frac{F}{RT}\left(E - E^{\circ\prime}_{\text{Ni-R/Ni-C}}\right)\right\} \equiv e_{\text{Ni-R/Ni-C}} \tag{5}$$

$$\frac{\Gamma_{\text{Ni-SI}}}{\Gamma_{\text{Ni-SI:H}_2}} = \frac{K_M}{c_{H_2}} \tag{6}$$

where R, T, E, $E^{\circ\prime}_{\text{Ni-C/Ni-SI}}$, and $E^{\circ\prime}_{\text{Ni-R/Ni-C}}$ are, respectively, the gas constant, the absolute temperature, the electrode potential, and the formal redox potentials of the Ni-C/Ni-SI and Ni-R/Ni-C redox couples. Therefore, the normalized steady-state catalytic current ($i_{\text{cat}}/i_{\text{lim}}$) can be expressed by:

$$\begin{aligned}\frac{i_{\text{cat}}}{i_{\text{lim}}} &= \frac{\Gamma_{\text{Ni-SI:H}_2}\left(1+\dfrac{K_{\text{M}}}{c_{\text{H}_2}}\right)}{\Gamma_{\text{total}}} \\ &= \frac{\Gamma_{\text{Ni-SI:H}_2}\left(1+\dfrac{K_{\text{M}}}{c_{\text{H}_2}}\right)}{\Gamma_{\text{Ni-SI:H}_2}+\Gamma_{\text{Ni-SI}}+\Gamma_{\text{Ni-C}}+\Gamma_{\text{Ni-R}}} \\ &= \frac{1+\dfrac{K_{\text{M}}}{c_{\text{H}_2}}}{1+\dfrac{K_{\text{M}}}{c_{\text{H}_2}}\left(1+\dfrac{1}{e_{\text{Ni-R/Ni-C}}}+\dfrac{1}{e_{\text{Ni-R/Ni-C}}e_{\text{Ni-C/Ni-SI}}}\right)}\end{aligned} \tag{7}$$

A normalized Faradaic voltammogram is given in Fig. 2 as open circles by pre-subtracting the charging current from the voltammogram (Fig. 1, forward scan, v = 5 mV s^{-1}) and normalizing the current with i_{lim}. Eq. (7) was fitted to the data with $E^{\circ\prime}_{\text{Ni-C/Ni-SI}}$ and $E^{\circ\prime}_{\text{Ni-R/Ni-C}}$ as the adjustable parameters by using a non-linear regression program Gnuplot®. The regression yielded the result that $E^{\circ\prime}_{\text{Ni-C/Ni-SI}} = -364 \pm 1\,\text{mV}$ and that $E^{\circ\prime}_{\text{Ni-R/Ni-C}} = -466 \pm 9\,\text{mV}$, and the regression curve is given in Fig. 2 as a solid line. The similar analysis was performed for the other voltammograms

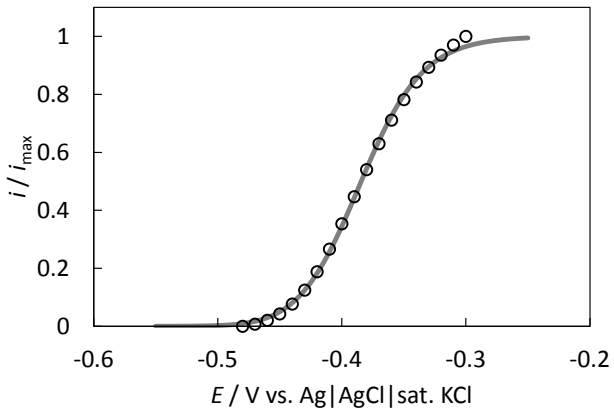

Figure 2
Nernst analysis on the *Hm*MBH-catalyzed H_2 oxidation current. Background-pre-subtracted and normalized voltammograms (forward scan of CV in Figure 1, $v = 5\,\text{mV s}^{-1}$) were shown in open circles. The solid curve was evaluated by a non-linear regression analysis based on Eq. (7).

measured at various pHs (5–7), and the results are collected in Fig. 3. This is the first report on the Nernst analysis of the sigmoidal part in the catalytic wave of hydrogenases.

The redox potentials of O_2-tolerant [NiFe]-hydrogenase from *A. aeolicus* were reported in the literature [42]. At pH 6, $E^{\circ\prime}_{\text{Ni-R/Ni-C}}$ of *Hm*MBH (= –510 ± 20 mV vs. Ag|AgCl|sat. KCl) is similar to that of [NiFe]-hydrogenase from *A. aeolicus* (= –489 mV). On the other hand, $E^{\circ\prime}_{\text{Ni-C/Ni-SI}}$ of *Hm*MBH (= –381 ±1 mV) is different from that of [NiFe]-hydrogenase from *A. aeolicus* (–421 mV). The discrepancy is due to the difference in the models used for the analysis. Note that the author has simply analyzed the voltammograms with Nernst equation on a new model of two-step electron transfer without interfacial electron transfer kinetic contribution, but by considering the H_2-binding.

3.3 Pourbaix diagram of the Ni-SI, Ni-C, and Ni-R

The closed triangles in Fig. 3 indicate the half-wave potential in the sigmoidal response (Fig. 2). The pH dependence seems to be about –30 mV/pH as a whole. This suggests that number of the proton (*m*) in the overall $2e^-$ transfer is one as judged from the theoretical value 2.303(*RT*/*F*)(*m*/*n*) (*n* being the number of electron of the total process, *n* = 2 in this case). However, as shown in Fig. 3, both of $E^{\circ\prime}_{\text{Ni-C/Ni-SI}}$ and $E^{\circ\prime}_{\text{Ni-R/Ni-C}}$ depend on pH. Therefore, the author has to consider the pH

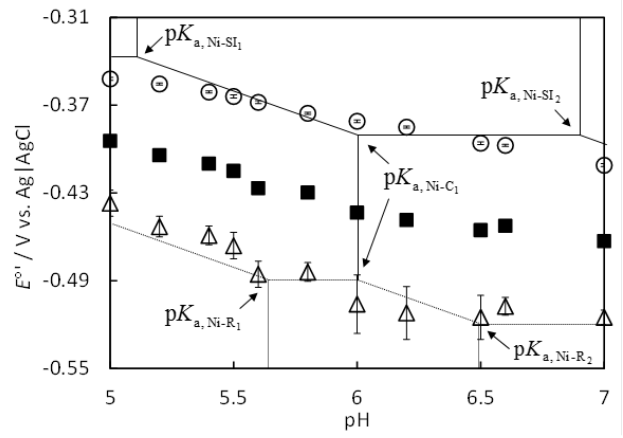

Figure 3
Pourbaix diagrams of Ni-C/Ni-SI (open circles) and Ni-R/Ni-C (open triangles) redox couples. The solid line was generated by linearization of the regression curve based on Eq. (8) with slopes of 2.303(*RT*/*F*)(*m*/*n*) (*m* = 0 or 1, *n* = 1 in this case) by considering the acid dissociations of the Ni-SI and Ni-C states. The dotted line was generated by linearization of the regression curve based on Eq. (9) with slopes of the theoretical values of 2.303(*RT*/*F*)(*m*/*n*) (*m* = 0 or 1, *n* = 1 in this case) by considering the acid dissociations of the Ni-C and Ni-R states. The error bars are given as the asymptotic standard error obtained by the non-linear regression analysis of the voltammograms (see Fig. 2). The closed triangles indicate the half-wave potential in the sigmoidal response (see Fig. 2)

dependence of $E^{\circ\prime}_{\text{Ni-C/Ni-SI}}$ and $E^{\circ\prime}_{\text{Ni-R/Ni-C}}$ as a combination of lines with slopes of –60 mV/pH and 0 mV/pH (m =1 or 0, n = 1). This means that the two one-electron transfer processes are coupled with the acid dissociation of the Ni-SI, Ni-C and Ni-R states. Since the Ni-C state is involved in both of the redox couples, the acid dissociation constant of the Ni-C state affects both of the formal redox potential of the Ni-C/Ni-SI and Ni-R/Ni-C redox couples. For this reason, the author first analyzed the Ni-C/Ni-SI redox couple. As judged from Fig. 3 (open circle), it is reasonable to assume that at least two acid dissociations for the Ni-SI state and one acid dissociation for the Ni-C state are involved in the electron transfer. Under the assumption, the pH dependence of the formal redox potential of the Ni-C/Ni-SI redox couple ($E^{\circ\prime}_{\text{Ni-C/Ni-SI, app}}$) is expressed by

$$E^{\circ\prime}_{\text{Ni-C/Ni-SI, app}} = \frac{2.303RT}{F}\left\{\begin{array}{l}\log\left(1+10^{\text{pH}-\text{p}K_{\text{a, Ni-C}_1}}\right)\\ -\log\left(1+10^{\text{pH}-\text{p}K_{\text{a, Ni-SI}_1}}+10^{2\text{pH}-\text{p}K_{\text{a, Ni-SI}_1}-\text{p}K_{\text{a, Ni-SI}_2}}\right)\end{array}\right\}+C_1 \quad (8)$$

where $\text{p}K_{\text{a, S}i}$ is the ith dissociation constant for the state S (S = Ni-SI, Ni-C, or Ni-R). Eq. (8) was fitted to the $E^{\circ\prime}_{\text{Ni-C/Ni-SI, app}}$ vs. pH profile evaluated by the non-linear regression analysis of the steady-state catalytic voltammograms with three dissociation constants ($\text{p}K_{\text{a, Ni-C}_1}$, $\text{p}K_{\text{a, Ni-SI}_1}$ and $\text{p}K_{\text{a, Ni-SI}_2}$) and C_1 as the adjustable parameters. The data are well reproduced by Eq. (8), as shown in Fig. 3. The refined parameters are: $\text{p}K_{\text{a, Ni-C}_1} = 6.0 \pm 0.1$, $\text{p}K_{\text{a, Ni-SI}_1} = 5.1 \pm 0.1$ and $\text{p}K_{\text{a, Ni-SI}_2} = 6.9 \pm 0.1$.

Similar analysis was performed to the formal potential of the Ni-R/Ni-C redox couple ($E^{\circ\prime}_{\text{Ni-R/Ni-C, app}}$). As judged from Fig. 3 (open triangle), the author may assume that at least one acid dissociation for the Ni-C state and two acid dissociations for the Ni-R state are involved in the electron transfer. The corresponding equation of the pH dependence of $E^{\circ\prime}_{\text{Ni-R/Ni-C, app}}$ is given by:

$$E^{\circ\prime}_{\text{Ni-R/Ni-C, app}} = \frac{2.303RT}{F}\left\{\begin{array}{l}\log\left(1+10^{\text{pH}-\text{p}K_{\text{a, Ni-R}_1}}+10^{2\text{pH}-\text{p}K_{\text{a, Ni-R}_1}-\text{p}K_{\text{a, Ni-R}_2}}\right)\\ -\log\left(1+10^{\text{pH}-\text{p}K_{\text{a, Ni-C}_1}}\right)-\text{pH}\end{array}\right\}+C_2 \quad (9)$$

Since $\text{p}K_{\text{a, Ni-C}_1}$ can be set as 6.0 as evaluated in the analysis of $E^{\circ\prime}_{\text{Ni-C/Ni-SI, app}}$, $\text{p}K_{\text{a, Ni-R}_1}$, and $\text{p}K_{\text{a, Ni-R}_2}$ values were evaluated by non-linear regression analysis to get about 5.6 and 6.5, respectively.

Since the electron density of the amino acid residues around the [NiFe]-active site will increase with the reduction proceeds, the pK_a of the given site should increase on the reduction. Therefore, the author may assign $pK_{a,\,Ni\text{-}SI_1}$, $pK_{a,\,Ni\text{-}C_1}$, and $pK_{a,\,Ni\text{-}R_2}$ to one identical amino acid residue. In contrast, $pK_{a,\,Ni\text{-}SI_2}$ and $pK_{a,\,Ni\text{-}R_1}$ seem to be assigned to different amino acid residues, respectively. Although it is difficult to clearly distinguish and assign them at this stage, one of possible candidates of the amino acid residue around the [NiFe]-active site is the Cys residues coordinating to the Ni or Fe atoms [49]. This is the first report on the Pourbaix diagram of the Ni-SI, Ni-C, and Ni-R states based on the thermodynamic theory.

3.4 Kinetic analysis on the oxidative inactivation

As described in Introduction, the author has performed kinetic analysis on the oxidative inactivation of *Hm*MBH adsorbed on Au electrode and meso-porous carbon electrode (Ketjen Black is used as an electrode material) [41]. In this study, the author performed the same analysis on *Hm*MBH chemically immobilized on Au electrode. *Hm*MBHs on the Au electrode were bound with each other through amide-linkage. According to a previous study [41], the author assumed a reversible (two-way) first-order reaction between the active (Ni-SI) and inactive (Ni-B) states of the enzyme with two rate constants (k_I and k_A), as shown in Scheme 1, k_I and k_A being the apparent rate constants of inactivation and reactivation, respectively. The initial potential (E_1) was set at –0.2 V, where the oxidative inactivation does not occur (or can be ignored) at pH 6 and the maximum catalytic current (i_0) was defined. After the potential was stepped at t = 0 to a given potential (E_2), at which the oxidative inactivation proceeds. The open circles in Fig. 4 indicate a CA of the H_2 oxidation current at the chemically immobilized *Hm*MBH-modified Au electrode at E_2 = –0.02 V. The data just after the potential step involve the charging current and then were eliminated from the present analysis. As shown in previous studies [40-42], the decay of the catalytic current is given by

$$i_{cat}(t) = i_0\left\{\frac{k_I}{k_I + k_A}\exp\left[-\left(k_I + k_A\right)t\right] + \frac{k_A}{k_I + k_A}\right\} \qquad (10)$$

Eq. (10) was fitted to the data in Fig. 4 with i_0, k_I, and k_A as the adjustable parameters by using Gnuplot®. The regression curve is shown in Fig. 4 as a solid curve. The similar analysis was conducted at several E_2 values, and the potential dependence of k_I and k_A is given in Fig. 5 as triangles. The open circles correspond to the results obtained at *Hm*MBH-adsorbed Au electrode.

Comparing the results of two *Hm*MBH-modified Au electrodes, the evaluated values of k_I are independent of the electrode potential (E). The fact indicates that the r.d.s. of the inactivation is

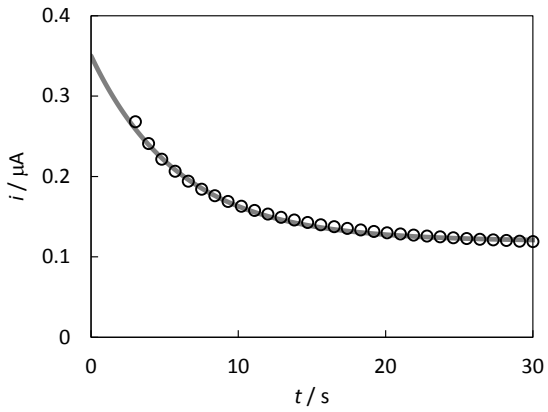

Figure 4
CA of the chemically immobilized *Hm*MBH-adsorbed Au electrode at −0.02 V under H_2-atmospheric conditions. The measurements were carried out in 100 mM phosphate buffer (pH 6) at 40 ± 2 °C. The solid curve was evaluated by a non-linear regression analysis based on Eq. (10). The best fit was obtained with the parameters: $i_0 = 0.35\,\mu\mathrm{A}$, $k_\mathrm{I} = 0.11\,\mathrm{s}^{-1}$ and $k_\mathrm{A} = 0.057\,\mathrm{s}^{-1}$.

non-electron transfer chemical process. In addition, the chemical immobilization decreases the rate constant of the chemical process. Similar decrease in k_I was observed by adsorption of *Hm*MBH on meso-porous material [41]. The chemical immobilization as well as adsorption on meso-porous material seems to cause the deceleration of the hydroxide ligand coordination to the [NiFe]-active site (the coordination of water on it and the succeeding deprotonation). The incorporation of water or the some kind of conformational changes seems to be the r.d.s. in the hydroxide ligand coordination. As to the latter reaction, the possible rate-determining chemical reaction seems to be the conformational change around the [NiFe]-active site. On the other hand, it is known that the unique proximal [FeS]-cluster of the O_2-tolerant hydrogenase changes to the superoxidation state on the attack of O_2 to overcome the irreversible inactivation (formation of the Ni-A state) and to form the Ni-B state [11]. Therefore, the rate-determining chemical process may be also related to the conformational change around the [FeS]-clusters.

In contrast, the logarithmic values of k_A decrease linearly with an increase in E and reach a corresponding limiting value at high potentials ($E > 0.05\,\mathrm{V}$). The k_A values in the exponential

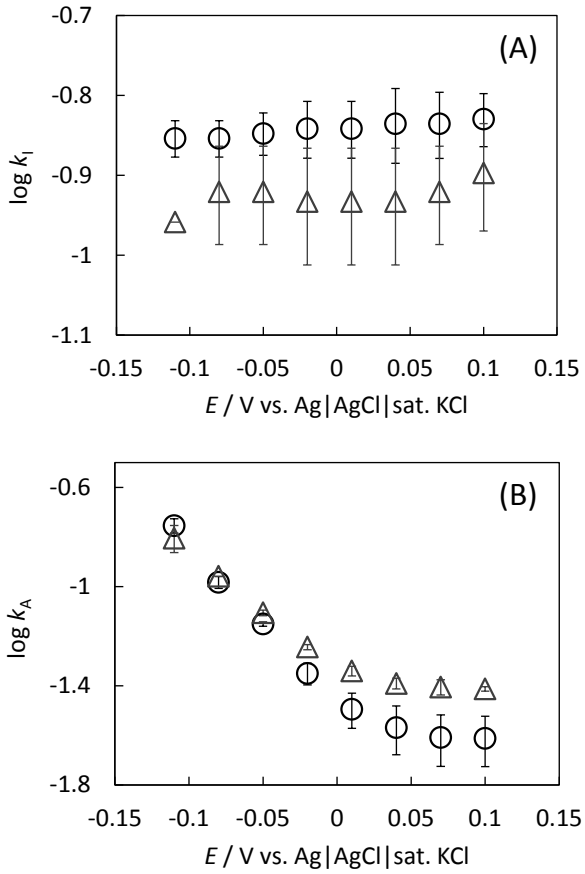

Figure 5
The potential dependence of the apparent rate constants of the inactivation (panel A) and the reactivation (panel B). The open circles and triangles correspond to the results obtained at *Hm*MBH-adsorbed Au electrode and chemically immobilized *Hm*MBH-adsorbed Au electrode, respectively. The data for the *Hm*MBH-adsorbed Au electrode are almost identical with those in Fig. 4 in Ref. 41. The error bars were evaluated by the Student *t*-distribution at 90% confidence level.

dependence against E (–0.12 V < E < –0.05 V) are not affected by the chemical immobilization. The author can say that the r.d.s. of the reactivation is one-electron reduction of the Ni(III) atom in the Ni-B state.

Concerning the dependence of k_I and k_A on the electrode potential, similar discussion has been demonstrated for O_2-tolerant [NiFe]-hydrogenase from *A. aeolicus* [42]. For instance, k_I and k_A of the [NiFe]-hydrogenase are, respectively, around 0.002 s^{-1} and 0.02s^{-1} at E = 0.1 V vs. SHE (–0.1 V vs. Ag|AgCl|sat. KCl) (note that the experience was carried out at pH 6, 1 atm H_2, and 40 °C). Consequently, the author can say that k_I (= 0.14 s^{-1}) and k_A (= 0.16 s^{-1}) of *Hm*MBH at E = –0.1V (vs. Ag|AgCl|sat. KCl) shown in Fig. 5 are much larger than those of [NiFe]-hydrogenase from *A. aeolicus*. However, the author cannot elucidate the differences at this stage.

As discussed in the above paragraphs, the oxidative inactivation is composed of two

processes: the electron transfer process (one-electron oxidation of the Ni atom) and non-electron transfer chemical process (coordination of hydroxide ligand on the [NiFe]-active site). Consequently, k_I and k_A can be expressed by Eqs. (11) to (14)

$$\frac{1}{k_I} = \frac{1}{k_{I,elec}(E)} + \frac{1}{k_{I,chem}} \tag{11}$$

$$k_I \approx k_{I,chem}\ (E > -0.2\ V) \tag{12}$$

$$\frac{1}{k_A} = \frac{1}{k_{A,elec}(E)} + \frac{1}{k_{A,chem}} \tag{13}$$

$$k_A \approx k_{A,elec}(E)\ (-0.02\ V > E > -0.2\ V) \tag{14}$$

where $k_{I,elec}(E)$, $k_{I,chem}$, $k_{A,elec}(E)$, and $k_{A,chem}$ are the rate constants of the electron transfer reaction and the chemical (non-electron transfer) reaction of the inactivation or reactivation, respectively.

Here, the author assumes a model reaction, as shown in Scheme 3. The parameters k_1 and k_{-1} are, respectively, the forward and backward rate constants of the H_2-binding, and are defined as

$$K_M = \frac{k_{-1}}{k_1} \tag{15}$$

According to our competitive inhibition-like model (Scheme 3), the parameters k_2 and k_{-2} are, respectively, the true rate constants of the inactivation and reactivation, and are defined as [41]

$$k_2 = k_I \tag{16}$$

$$k_{-2} = \frac{k_A}{1 + \frac{c_{H_2}}{K_M}} \tag{17}$$

Here, the author can reasonably assume that the true rate constant of the electrochemical oxidation of Ni-SI ($k_{2,elec}$) is equal to that of the reduction of Ni-B ($k_{-2,elec}$) at the formal potential of the oxidative inactivation ($E^{\circ\prime}_{Ni\text{-}SI/Ni\text{-}B}$) Therefore,

$$\frac{k_{2,elec}}{k_{-2,elec}} \equiv \frac{k_{I,elec}}{k_{A,elec}}\left(1 + \frac{c_{H_2}}{K_M}\right) = 1 \tag{18}$$

However, it is difficult to evaluate the value of $E^{\circ\prime}_{Ni\text{-}SI/Ni\text{-}B}$, since the author cannot get $k_{I,elec}(E)$

at this stage. According to the definition of E_{switch} [46] (see also Introduction), E_{switch} is evaluated as –0.12 V in our case, as judged from the CV at v = 5 mV s^{-1} in Fig. 1. The value of log k_A in Fig. 5 (B) is extrapolated to about –0.7 at –0.12 V. When the author uses 0.57 mM for K_M in the case of *Hm*MBH and 0.74 mM for the saturated c_{H_2} at 40 °C [45], log $k_{I,elec}$ can be estimated to be about –1.0 at –0.12 V by using Eqs. (14) and (18). This value is much smaller than that of log k_I (≈ –0.85) at –0.12 V (Fig. 5 (A)). The situation does not satisfy Eq. (12) (note that the r.d.s. of the inactivation is the non-electron transfer chemical process). To satisfy Eq. (12), $k_{I,elec}$ should be much larger than $k_{I,chem}$. Such situation will be realized at more negative potentials than –0.12 V (= E_{switch}). For example, log k_A in Fig. 5 (B) is extrapolated to about –0.2 at –0.2 V, and then log $k_{I,elec}$ should be about –0.5 at –0.2 V by using Eq. (18). This situation can satisfy Eq. (12) and $E^{\circ\prime}_{Ni\text{-}SI/Ni\text{-}B}$ will locate around –0.2 V. In conclusion, $E^{\circ\prime}_{Ni\text{-}SI/Ni\text{-}B}$ is more negative than E_{switch}. This conclusion is in consistence with that in the literature [40]

3.5 Digital simulation of bioelectrocatalytic CVs with HmMBH

As mentioned in Introduction, it is reasonable to consider the oxidative inactivation as a competitive inhibition-like reaction. *Hm*MBH adsorbed on the electrode has several states affected by, for instance, the electrode potential and the substrate concentration. Under such conditions, the shape of bioelectrocatalytic CVs with adsorbed *Hm*MBH results in the complicated one, as shown in Fig. 1 (solid line). On the other hand, Léger's group simulated the CVs of [NiFe]-hydrogenase from *A. aeolicus* on the dispersion model with apparent rate constants of the inactivation and reactivation [42]. Since the author has evaluated the thermodynamic property of the catalytic cycle ($E^{\circ\prime}_{Ni\text{-}C/Ni\text{-}SI,app}$ and $E^{\circ\prime}_{Ni\text{-}R/Ni\text{-}C,app}$) and the true kinetic property of the reversible inactivation (k_2 and k_{-2}) in the above sections, the author attempted to simulate the CV based on the above analysis. The parameters k_3, k_{-3}, k_4 and k_{-4} in Scheme 3 are, respectively, the electrode reaction rate constants of Ni-C/Ni-SI and Ni-R/Ni-C redox couples, and are expressed by Butler-Volmer equation (by assuming the transfer coefficient as 0.5) as:

$$k_3 = k^\circ \exp\left[\frac{F}{2RT}\left(E - E^{\circ\prime}_{\text{Ni-C/Ni-SI}}\right)\right] \tag{19}$$

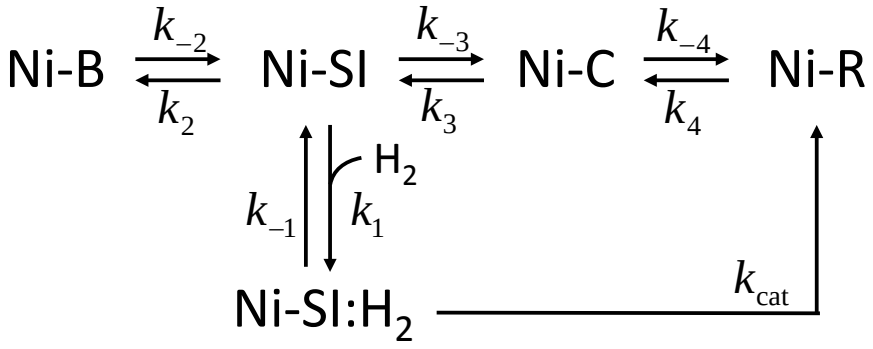

Scheme 3
The reaction scheme of the catalytic H_2 oxidation for digital simulation. k_1, k_{-1}, k_2, k_{-2}, k_3, k_{-3}, k_4, k_{-4} and k_{cat} are, respectively, the forward and backward rate constants of the H_2-binding, the true rate constants of inactivation and reactivation, the electrode reaction rate constants of Ni-C/Ni-SI and Ni-R/Ni-C redox couples and the catalytic constant.

$$k_{-3} = k^\circ \exp\left[\frac{-F}{2RT}\left(E - E^{\circ\prime}_{\text{Ni-C/Ni-SI}}\right)\right] \tag{20}$$

$$k_4 = k^\circ \exp\left[\frac{F}{2RT}\left(E - E^{\circ\prime}_{\text{Ni-R/Ni-C}}\right)\right] \tag{21}$$

$$k_{-4} = k^\circ \exp\left[\frac{-F}{2RT}\left(E - E^{\circ\prime}_{\text{Ni-R/Ni-C}}\right)\right] \tag{22}$$

Since the interfacial electron transfer process of the favorably oriented *Hm*MBH is reversible (Nernst response) as mentioned in section 3.1, the author assumed the very fast electron transfer by tentatively setting the standard rate constant (k°) as 10000 s^{-1}. Furthermore, the author also tentatively set k_{-1} as 100 s^{-1}, which is much larger than the value of k_c to achieve the rapid equilibrium in the H_2-binding reaction to the Ni-SI state. Note that the value of k_{cat} is tentatively set to satisfy that $k^\circ >> k_{cat}$, because the current is simply proportional to $k_{cat}\Gamma$. In other words, here, the author only focused on the shape of CVs in this simulation. Concerning the k_2 and k_{-2}, the author estimated the values from the analytical results (Fig. 5). $k_I = 10^{-0.85}\ s^{-1}$ calculated from Fig. 5 (A),

and $k_A = 10^{-8E-1.6}\ s^{-1}$ calculated from the linear range of Fig. 5 (B) (–0.11 to –0.08 V).

Under the aforementioned conditions, the author simulated the H_2 oxidation of the DET-type bioelectrocatalysis with adsorbed *Hm*MBH at pH 6. Simulated CVs (from –0.6 to 0 V) with several scan rates are shown in Fig. 6. The simulated CVs can well reproduce the experimental CVs. The scan rate-independent sigmoidal increase in the catalytic wave (of which the characteristics show that $k°$ is high enough to realize Nernst response) and the hysteresis in the reversible oxidative inactivation are well reproduced, although the "residual slope" after the sigmoidal increase was ignored in the present analysis. In addition, the reductive reactivation is notable at $v = 5\ mV\ s^{-1}$. The results support the validity of the present analysis of the thermodynamics of the catalytic cycle and the kinetics of the oxidative inactivation in DET-type bioelectrocatalysis with adsorbed *Hm*MBH.

The author also examined effects of the H_2-concentrarion on the shapes of CVs. The simulated CVs with several H_2-concentraitons are shown in Fig. 7. The author can predict that the increase in the H_2-concentration is effective for avoiding the oxidative inactivation. As mentioned in Introduction, the author has already shown that the gas-diffusion-type electrode is effective for avoiding the inactivation. The maximum concentration evaluated here is 47.4 mM, which is almost as same as that of the H_2 gas (by assuming the H_2 gas as an ideal gas). Although it is very difficult to

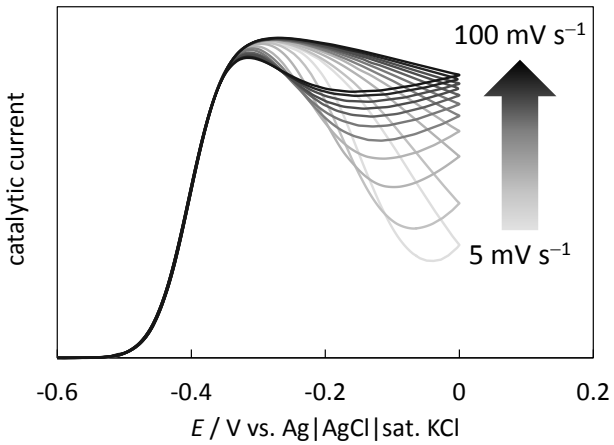

Figure 6
Simulated CVs of the *Hm*MBH-adsorbed electrode under H_2-saturated conditions. The scan rates were 5 – 100 mV s^{-1} from bottom to top (grey to black). The parameters were estimated from the results measured at pH 6.

define the H_2-concentration around the enzyme in the gas-diffusion-type electrode, the simulated CVs (Fig. 7) will be great help for further understanding in the electrochemical phenomena near and on the electrode surface.

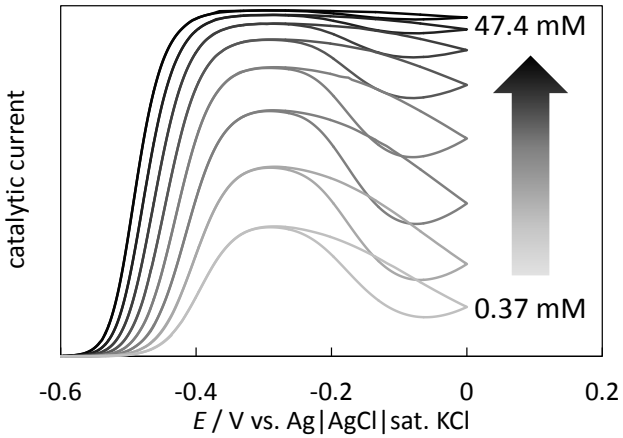

Figure 7
Effects of the H_2-concentration on simulated CVs of the *Hm*MBH-adsorbed electrode. The scan rate is 10 mV s^{-1}. The H_2-concentrations are 0.37, 0.74, 1.48, 2.96, 5.92, 11.8, 23.7, and 47.4 mM from bottom to top (grey to black). The important parameters used are those estimated in this work.

4. Conclusions

Nernst analysis has been successfully performed for the CVs of *Hm*MBH-catalyzed H_2 oxidation by considering the situations that it proceeds in a two-step one-electron transfer mechanism and that the substrate-enzyme complex (Ni-SI:H_2) is assumed as in the steady-state enzyme kinetics. The results have shown that at least three acid dissociation reactions around the [NiFe]-active site are involved in the catalytic cycle. In addition, the author has discussed the kinetics of the oxidative inactivation. Based on the kinetic analysis, it can be concluded that the inactivation rate constant is independent of E, whereas the reactivation is dependent on E. The rate-determining and potential-independent inactivation process seems to be the hydroxide ligand coordination to the [NiFe]-active site. The author has shown that the electrode potential (or solution potential) and the H_2-concentration near the enzyme strongly affects the inactivation kinetics, and that the inactivation rate constant can be reduced by restricting the enzyme movement by chemical immobilization on planer electrodes as well as physical adsorption on porous electrodes. This means that since the reactivation rate constant is almost independent of the atmosphere around the enzyme, the inhibition constant can be decreased by restricting the enzyme movement, which is very useful in application of this enzyme to bioelectrochemical devices [24-26,41]. The author has also given some thermodynamic discussions

on the oxidative inactivation at the present stage. Furthermore, by utilizing the resultant thermodynamic and kinetic parameters, the author has successfully simulated the bioelectrocatalytic CVs at *Hm*MBH-adsorbed electrode. Finally, the author has also shown that the increase in the H_2-concentration is effective for avoiding the oxidative inactivation.

5. Appendix

Theory of steady-state wave catalyzed by randomly oriented sphere enzymes with one-step electron transfer site

The enzyme adsorbed on the electrode is simplified as a sphere. A polar coordinate system (r, θ, φ) is introduced with the coordinate origin at the center of the enzyme (Fig. A1) in a way similar to that of the literature [18]. The rotation axes of θ and φ are arranged parallel and vertical to the electrode, respectively. Probability distribution with respect to the presence of the active site on the polar coordinate system is defined as the probability density function f. When the enzyme is randomly adsorbed in the range of $0 \le \theta \le \theta'$ and $0 \le \varphi \le 2\pi$, f is written as follows.

$$f = \frac{\delta(r - r_0)\zeta(\theta')}{2\pi r_0^2(1-\cos\theta')} \tag{A.1}$$

where r_0, $\delta(r - r_0)$, and $\zeta(\theta')$ are, respectively, the distance between the center of the enzyme and the active site, Dirac delta function, and the unstandardized distribution function about θ. $\zeta(\theta')$ is equal to 1 in $0 \le \theta \le \theta'$ and is equal to 0 in $\theta \le \theta'$. The denominator of the right side of Eq. (A.1) is normalization constant derived from the stochastic convergence.

In addition, the catalytic steady-state current (i_s) caused by the DET-type bioelectrocatalysis is written as Eq. (A.2) [50,51].

$$i_s = \frac{i_s^{lim}}{1 + \frac{k_c}{k_f} + \frac{k_b}{k_f}} \tag{A.2}$$

where i_s^{lim}, k_f, and k_b are, respectively, the catalytic current under kinetically-controlled limiting current conditions (without substrate concentration polarization), and forward and backward rate constants for the electrode reaction. k_f and k_b can be expressed with Butler-Volmer equations as follows,

$$k_f = k^\circ \exp\left\{-\frac{\alpha n'_E F}{RT}\left(E - E^{\circ\prime}{}_E\right)\right\} \tag{A.3}$$

$$k_b = k^\circ \exp\left\{-\frac{(1-\alpha) n'_E F}{RT}\left(E - E^{\circ\prime}{}_E\right)\right\} \tag{A.4}$$

where k^o, $E^{\circ\prime}$, n'_E, and α are, respectively, the standard rate constant for the electrode reaction, the

formal redox potential of the enzyme, the number of electrons, and the transfer coefficient.

Here, the author considers the steady-state catalytic current caused by the enzymes which are randomly adsorbed (i_{sr}) in the range of $0 \leq \theta \leq \theta'$. DET-type bioelectrocatalytic current with the enzyme at a certain situation (r_1, θ_1, φ_1) can be expressed by the product of $i_s(r_1, \theta_1, \varphi_1)$ and $f(r_1, \theta_1, \varphi_1)$. Therefore, i_{sr} is equal to the integral value of $i_s f$ in the total space, according to Eq. (A.5).

$$i_{sr} = \int_V i_s f \mathrm{d}V = \iiint i_s f r \sin\theta \mathrm{d}r\mathrm{d}\theta\mathrm{d}\phi \tag{A.5}$$

In order to solve Eq. (A.5), the dependence of r, θ and φ on i_s is needed. The author defines d as the increase in the distance between the active site and the electrode in accordance with the change in θ. It is known that the long electron transfer rate constant decreases exponentially on the distance between electron donor and acceptor. The relation between k^o and d can be expressed by Eq. (A.6).

$$k^\circ = k^\circ{}_{\max} \exp(-\beta d) \tag{A.6}$$

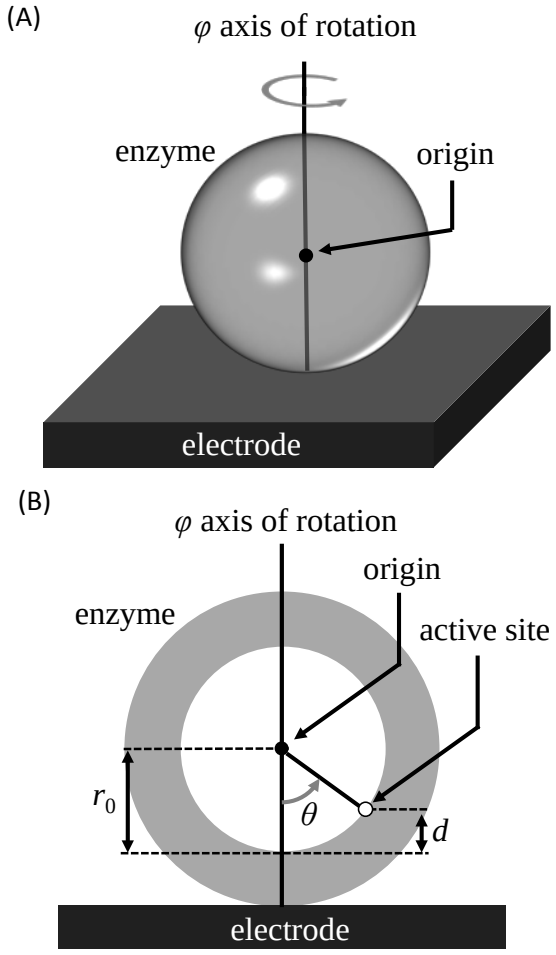

Figure A1
(A) Illustration of the spherical enzyme adsorbed on the electrode.
(B) Sectional view of the adsorbed enzyme on the electrode across the ϕ axis.
Student t-distribution at 90% confidence level.

where k^{o}_{max} is k^{o} at a distance of the closest approach and the β is a decay constant. In our model (Fig. A1), d can be expressed with r_0 and θ as follows,

$$d = r_0\left(1-\cos\theta\right) \tag{A.7}$$

Substitution of Eqs. (A.3, A.4, A.6, A.7) for Eq. (A.2) elucidates the dependences of r, θ and φ on i_s. Integration in Eq. (A.5) gives the following equation,

$$i_{sr} = \frac{i_s^{lim}}{\beta r_0\left(1-\cos\theta'\right)\left[1+\exp\left\{-\frac{n'_E F}{RT}\left(E-E^{\circ\prime}{}_E\right)\right\}\right]}$$

$$\times \ln\left|\frac{k_c\exp\left\{\frac{\alpha n'_E F}{RT}\left(E-E^{\circ\prime}{}_E\right)\right\}+k^{\circ}{}_{max}\left[1+\exp\left\{\frac{n'_E F}{RT}\left(E-E^{\circ\prime}{}_E\right)\right\}\right]}{k_c\exp\left\{\frac{\alpha n'_E F}{RT}\left(E-E^{\circ\prime}{}_E\right)\right\}+k^{\circ}{}_{max}\exp\left\{-\beta r_0\left(1-\cos\theta'\right)\right\}\left[1+\exp\left\{\frac{n'_E F}{RT}\left(E-E^{\circ\prime}{}_E\right)\right\}\right]}\right| \tag{A.8}$$

Assuming the parameters: $r_0 = 3\ \mathrm{nm}$, $\theta' = \pi$, $n'_E = 1$, $\alpha = 0.5$, $\beta = 14\ \mathrm{nm^{-1}}$, and $E^{\circ\prime}{}_E = -0.3\ \mathrm{V}$, the author can consider the dependence of $k^{\circ}{}_{max}/k_c$ on the voltammograms (Fig. A2). In addition, the author also divided the current contributions from the enzymes in the range of $0 \le \theta' \le \pi/4$ (as the favorably oriented enzymes) and $\pi/4 \le \theta' \le \pi$ (as the unfavorably oriented enzymes) on

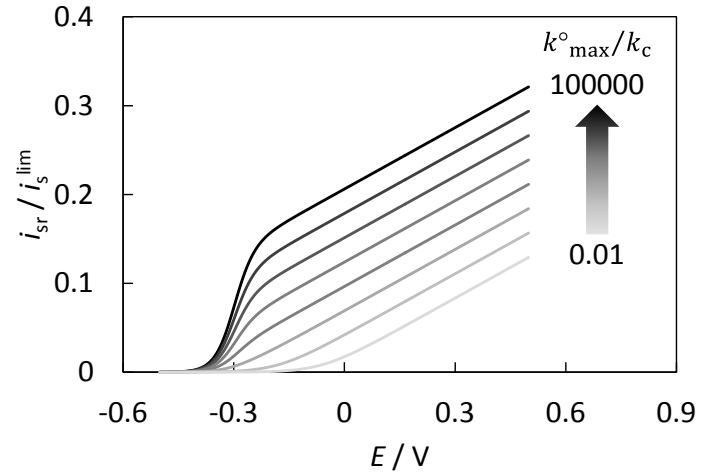

Figure A2
Dependence of $k^{\circ}{}_{max}/k_c$ on the voltammograms calculated with Eq. (A.8). The parameters are: $r_0 = 3\ \mathrm{nm}$, $\theta' = \pi$, $n'_E = 1$, $\alpha = 0.5$, $\beta = 14\ \mathrm{nm^{-1}}$, and $E^{\circ\prime}{}_E = -0.3\ \mathrm{V}$.

the voltammograms (broken line and dotted line, respectively, shown in Fig. A3).

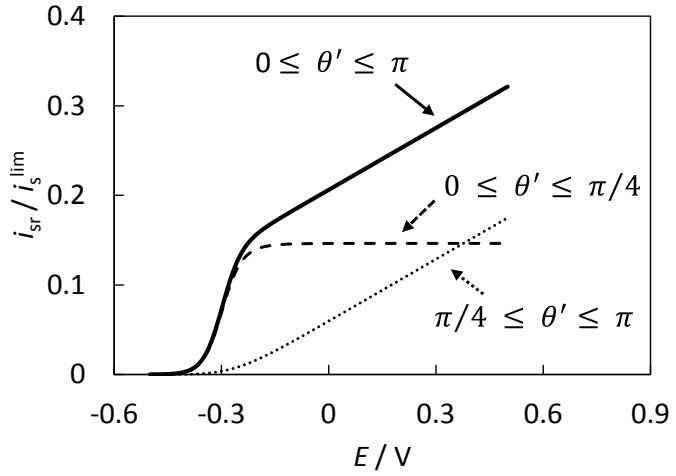

Figure A3
The current contributions from the favorably oriented enzymes with θ' in the range of $0 \leq \theta' \leq \pi/4$ and the unfavorably oriented enzymes with θ' in the range of $\pi/4 \leq \theta' \leq \pi$ to the total current of the voltammograms. The solid, broken, and dotted lines are, respectively, the steady-state voltammograms catalyzed by the enzymes with θ' in the range of $0 \leq \theta' \leq \pi$, $0 \leq \theta' \leq \pi/4$, and $\pi/4 \leq \theta' \leq \pi$. The parameters are: $r_0 = 3$ nm, $k^{\circ}{}'_{\max}/k_c = 100000$, $n'_E = 1$, $\alpha = 0.5$, $\beta = 14\ \mathrm{nm}^{-1}$, and $E^{\circ\prime}{}_E = -0.3$ V.

6. References

[1] K. A. Vincent, A. Parkin, F. A. Armstrong, Investigating and Exploiting the Electrocatalytic Properties of Hydrogenases, Chem. Rev. 107 (2007) 4366-4413.

[2] H. S. Shafaat, O. Rüdiger, H. Ogata, W. Lubitz, A common active site for hydrogen metabolism under diverse conditions, Biochim. Biophys. Acta 1827 (2013) 986-1002.

[3] T. Yagi, Y. Higuchi, Studies on hydrogenase, Proc. Jpn. Acad., Ser. B 89 (2013) 16-33.

[4] A. Volbeda, L. Martin, P. Liebgott, A. D. Lacey, J. C. Fontecilla-Camps, [NiFe]-hydrogenases revisited: nickel-carboxamido bond formation in a variant with accrued O_2-tolerance and a tentative re-interpretation of Ni-SI states, Metallomics 7 (2015) 710-718.

[5] J. Fritsch, P. Scheerer, S. Frielingsdorf, S. Kroschinsky, B. Friedrich, O. Lenz, C. M. T. Spahn, The crystal structure of an oxygen-tolerant hydrogenase uncovers a novel iron-sulphur centre, Nature 479 (2011) 249-252.

[6] T. Goris, A. F. Wait, M. Saggu, J. Fritsch, N. Heidary, M. Stein, I. Zebger, F. Lendzian, F. A. Armstrong, B. Friedrich, O. Lenz, A unique iron-sulfur cluster is crucial for oxygen tolerance of a [NiFe]-hydrogenase, Nat. Chem. Biol. 7 (2011) 310-318.

[7] M. Pandelia, W. Nitschke, P. Infossi, M. Giudici-Orticoni, E. Bill, W. Lubitz, Characterization of a unique [FeS] cluster in the electron transfer chain of the oxygen tolerant [NiFe] hydrogenase from Aquifex aeolicus, Proc. Natl. Acad. Sci. 108 (2011) 6097-6102.

[8] M. Pandelia, V. Fourmond, P. Tron-Infossi, E. Lojou, P. Bertrand, C. Léger, M. Giudici-Orticoni, W. Lubitz, Membrane-Bound Hydrogenase I from the Hyperthermophilic Bacterium *Aquifex aeolicus*: Enzyme Activation, Redox Intermediates and Oxygen Tolerance, J. Am. Chem. Soc. 132 (2010) 6991-7004.

[9] M. M. Roessler, R. M. Evans, R. A. Davies, J. Harmer, F. A. Armstrong, EPR Spectroscopic Studies of the Fe–S Clusters in the O_2-Tolerant [NiFe]-Hydrogenase Hyd-1 from *Escherichia coli* and Characterization of the Unique [4Fe–3S] Cluster by HYSCORE, J. Am. Chem. Soc. 134 (2012) 15581-15594.

[10] J. A. Cracknell, A. F. Wait, O. Lenz, B. Friedrich, F. A. Armstrong, A kinetic and thermodynamic understanding of O_2 tolerance in [NiFe]-hydrogenases, Proc. Natl. Acad. Sci. 106 (2009) 20681-20686.

[11] Y. Shomura, K. S. Yoon, H. Nishihara, Y. Higuchi, Structural basis for a [4Fe-3S] cluster in the oxygen-tolerant membrane-bound [NiFe]-hydrogenase, Nature 479 (2011) 253-257.

[12] K. S. Yoon, K. Fukuda, K. Fujisawa, H. Nishihara, Purification and characterization of a highly thermostable, oxygen-resistant, respiratory [NiFe]-hydrogenase from a marine, aerobic hydrogen-oxidizing bacterium *Hydrogenovibrio marinus*, Int. J. Hydrogen Energy 36 (2011) 7081-7088.

[13] J. A. Cracknell, K. A. Vincent, F. A. Armstrong, Enzymes as Working or Inspirational Electrocatalysts for Fuel Cells and Electrolysis, Chem. Rev. 108 (2008) 2439-2461.

[14] M. J. Moehlenbrock, S. D. Minteer, Extended lifetime biofuel cells, Chem. Soc. Rev. 37 (2008) 1188-1196.

[15] N. Mano, F. Mao, A. Heller, A Miniature Membrane-less Biofuel Cell Operating at +0.60 V under Physiological Conditions, ChemBioChem 5 (2004) 1703-1705.

[16] D. Leech, P. Kavanagha, W. Schuhmann, Enzymatic fuel cells: Recent progress, Electrochim.

Acta 84 (2012) 223-234.

[17] S. C. Barton, J. Gallaway, P. Atanassov, Enzymatic Biofuel Cells for Implantable and Microscale Devices, Chem. Rev. 104 (2004) 4867-4886.

[18] C. Léger, P. Bertrand, Direct Electrochemistry of Redox Enzymes as a Tool for Mechanistic Studies, Chem. Rev. 108 (2008) 2379-2438.

[19] M. Rasmussen, S. Abdellaoui, S. D. Minteer, Enzymatic biofuel cells: 30 years of critical advancements, Biosens. Bioelectron. 76 (2016) 91-102.

[20] M. Rasmussen, R. E. Ritzmann, I. Lee, A. J. Pollack, D. Scherson, An Implantable Biofuel Cell for a Live Insect, J. Am. Chem. Soc. 134 (2012) 1458-1460.

[21] A. Szczupak, J. Halámek, L. Halámková, V. Bocharova, L. Alfonta, E. Katz, Living battery – biofuel cells operating in vivo in clams, Energy Environ. Sci. 5 (2012) 8891-8895.

[22] A. Zebda, S. Cosnier, J.-P. Alcaraz, M. Holzinger, A. Le Goff, C. Gondran, F. Boucher, F. Giroud, K. Gorgy, H. Lamraoui, P. Cinquin, Single Glucose Biofuel Cells Implanted in Rats Power Electronic Devices, Sci. Rep. 3 (2013) 1516.

[23] E. Katz, K. MacVittie, Implanted biofuel cells operating in vivo – methods, applications and perspectives – feature article, Energy Environ. Sci. 6 (2013) 2791-2803.

[24] A. D. Poulpiquet, A. Ciaccafava, R. Gadiou, S. Gounel, M. T. Giudici-Orticoni, N. Mano, E. Lojou, Design of a H_2/O_2 biofuel cell based on thermostable enzymes, Electrochem. Commun. 42 (2014) 72-74.

[25] L. Xu, F. A. Armstrong, Optimizing the power of enzyme-based membrane-less hydrogen fuel cells for hydrogen-rich H_2–air mixtures, Energy Environ. Sci. 6 (2013) 2166-2171.

[26] A. D. Poulpiquet, D. Ranava, K. Monsalve, M. T. Giudici-Orticoni, E. Lojou, Biohydrogen for a New Generation of H_2/O_2 Biofuel Cells: A Sustainable Energy Perspective, ChemElectroChem 1 (2014) 1724-1750.

[27] N. Lalaoui, A. D. Poulpiquet, R. Haddad, A. L. Goff, M. Holzinger, S. Gounel, M. Mermoux, P. Infossi, N. Mano, E. Lojou, S. Cosnier, A membraneless air-breathing hydrogen biofuel cell based on direct wiring of thermostable enzymes on carbon nanotube electrodes, Chem. Commun. 51 (2015) 7447-7450.

[28] E. I. Solomon, U. M. Sundaram, T. E. Machonkin, Multicopper Oxidases and Oxygenases, Chem. Rev. 96 (1996) 2563-2606.

[29] K. So, S. Kawai, Y. Hamano, Y. Kitazumi, O. Shirai, M. Hibi, J. Ogawa, K. Kano, Improvement of a direct electron transfer-type fructose/dioxygen biofuel cell with a substrate-modified biocathode, Phys. Chem. Chem. Phys. 16 (2014) 4823-4829.

[30] N. Mano, L. Edembe, Bilirubin oxidases in bioelectrochemistry: Features and recent findings, Biosens. Bioelectron. 50 (2013) 478-485.

[31] S. Kawai, M. Tsutsumi, T. Yakushi, K. Kano, K. Matsushita, Heterologous Overexpression and Characterization of a Flavoprotein-cytochrome c Complex Fructose Dehydrogenase of *Gluconobacter japonicus* NBRC3260, Appl. Environ. Microbiol. 79 (2013) 1654-1660.

[32] S. Kawai, T. Yakushi, K. Matsushita, Y. Kitazumi, O. Shirai, K. Kano, The electron transfer pathway in direct electrochemical communication of fructose dehydrogenase with electrodes, Electrochem. Commun. 38 (2014) 28-31.

[33] A. Lindgren, L. Gorton, T. Ruzgas, U. Baminger, D. Haltrich, M. Schülein, Direct electron transfer of cellobiose dehydrogenase from various biological origins at gold and graphite electrodes, J. Electroanal. Chem. 496 (2001) 76-81.

[34] V. Fridman, U. Wollenberger, V. Bogdanovskaya, F. Lisdat, T. Ruzgas, A. Lindgren, L. Gorton, F. W. Scheller, Electrochemical investigation of cellobiose oxidation by cellobiose dehydrogenase in the presence of cytochrome c as mediator, Biochem. Soc. Trans. 28 (2000) 63-70.

[35] C. Léger, A. K. Jones, S. P. J. Albracht, F. A. Armstrong, Effect of a Dispersion of Interfacial Electron Transfer Rates on Steady State Catalytic Electron Transport in [NiFe]-hydrogenase and Other Enzymes, J. Phys. Chem. B 106 (2002) 13058-13063.

[36] C. C. Page, C. Moser, X. Chen, P. L. Dutton, Natural engineering principles of electron tunnelling in biological oxidation–reduction, Nature 402 (1999) 47-52.

[37] C. Léger, A. K. Jones, W. Roseboom, S. P. J. Albracht, F. A. Armstrong, Enzyme Electrokinetics: Hydrogen Evolution and Oxidation by Allochromatium vinosum [NiFe]-Hydrogenase, Biochemistry 41 (2002) 15736-15746.

[38] V. Fourmond, C. Baffert, K. Sybirna, T. Lautier, A. A. Hamdan, S. Dementin, P. Soucaille, I. Meynial-Salles, H. Bottin, C. Léger, Steady-State Catalytic Wave-Shapes for 2-Electron Reversible Electrocatalysts and Enzymes, J. Am. Chem. Soc. 135 (2013) 3926-3938.

[39] A. A. Hamdan, B. Burlat, O. Gutiérrez-Sanz, P. Liebgott, C. Baffert, A. L. D. Lacey, M. Rousset, B. Guigliarelli, C. Léger, S. Dementin, O_2-independent formation of the inactive

states of NiFe hydrogenase, Nat. Chem. Biol. 9 (2013) 15-17.

[40] A. A. Hamdan, P. Liebgott, V. Fourmond, O. Gutiérrez-Sanz, A. D. Lacey, P. Infossi, M. Rousset, S. Dementin, C. Léger, Relation between anaerobic inactivation and oxygen tolerance in a large series of NiFe hydrogenase mutants, Proc. Natl. Acad. Sci. 109 (2012) 19916-19921.

[41] K. So, Y. Kitazumi, O. Shirai, K. Kurita, H. Nishihara, Y. Higuchi, K. Kano, Kinetic Analysis of Inactivation and Enzyme Reaction of Oxygen-Tolerant [NiFe]-Hydrogenase at Direct Electron-Transfer Bioanode, Bull. Chem. Soc. Jpn. 87 (2014) 1177-1185.

[42] V. Fourmond, P. Infossi, M. Giudici-Orticoni, P. Bertrand, C. Léger, "Two-Step" Chronoamperometric Method for Studying the Anaerobic Inactivation of an Oxygen Tolerant NiFe Hydrogenase, J. Am. Chem. Soc. 132 (2010) 4848-4857.

[43] N. Plumeré, O. Rüdiger, A. A. Oughli, R. Williams, J. Vivekananthan, S. Pöller, W. Schuhmann, W. Lubitz, A redox hydrogel protects hydrogenase from high-potential deactivation and oxygen damage, Nat. Chem. 6 (2014) 822-827.

[44] K. So, Y. Kitazumi, O. Shirai, K. Kurita, H. Nishihara, Y. Higuchi, K. Kano, Gas-diffusion and Direct-electron-transfer-type Bioanode for Hydrogen Oxidation with Oxygen-tolerant [NiFe]-hydrogenase as an Electrocatalyst, Chem. Lett. 43 (2014) 1575-1577.

[45] C. L. Young, Ed. Hydrogen and Deuterium. IUPAC Solubility Data Series, Vol. 5/6, Pergamon Press Oxford, England, 1981.

[46] A. K. Jones, S. E. Lamle, H. R. Pershad, K. A. Vincent, S. P. J. Albracht, F. A. Armstrong, Enzyme Electrokinetics: Electrochemical Studies of the Anaerobic Interconversions between Active and Inactive States of *Allochromatium vinosum* [NiFe]-hydrogenase, J. Am. Chem. Soc. 125 (2003) 8505-8514.

[47] D. Sehgal, I. K. Vijay, A method for the high efficiency of water-soluble carbodiimide-mediated amidation, Anal. Biochem. 218 (1994) 87-91.

[48] B. L. Greene, C. Wu, P. M. McTernan, M. W. W. Adams, R. B Dyer, Proton-Coupled Electron Transfer Dynamics in the Catalytic Mechanism of a [NiFe]-Hydrogenase, J. Am. Chem. Soc. 137 (2015) 4558-4566.

[49] A. L. D. Lacey, E. C. Hatchikian, A. Volbeda, M. Frey, J. C. Fontecilla-Camps, V. M. Fernandez, Infrared-Spectroelectrochemical Characterization of the [NiFe] Hydrogenase of *Desulfovibrio gigas*, J. Am. Chem. Soc. 119 (1997) 7181-7189.

[50] T. Ikeda, D. Kobayashi, F. Matsushita, T. Sagara, K. Niki, Bioelectrocatalysis at electrodes coated with alcohol dehydrogenase, a quinohemoprotein with heme c serving as a built-in mediator, J. Electroanal. Chem. 361 (1991) 221-228.

[51] S. Tsujimura, T. Nakagawa, K. Kano, T. Ikeda, Kinetic study of direct bioelectrocatalysis of dioxygen reduction with bilirubin oxidase at carbon electrodes, Electrochemistry 72 (2004) 437-439.

Chapter 3

Development of Dual Gas Diffusion-Type Biofuel Cells

3-1. Direct electron transfer-type dual gas diffusion H_2/O_2 biofuel cells

Abstract

H_2/O_2 biofuel cells utilizing hydrogenases and multicopper oxidases as bioelectrocatalysts are clean, sustainable, and environmentally friendly power devices. In this study, the author constructed a novel gas diffusion bioelectrode with a sheet of waterproof carbon cloth as the electrode base and optimized the hydrophilicity/hydrophobicity of the electrode for both high gas permeability and high direct electron transfer bioelectrocatalytic activity. The electrode exhibited a large current density of about 10 mA cm^{-2} in the steady state for both H_2 oxidation and O_2 reduction. The biocathode and the bioanode were coupled to construct a gas diffusion H_2/O_2 biofuel cell. The dual gas diffusion system allowed the separate supply of gaseous substrates (H_2 and O_2) to the bioanode and biocathode, with consequent suppression of the oxidative inhibition of the hydrogenases. The cell exhibited a maximum power density of 8.4 mW cm^{-2} at a cell voltage of 0.7 V under quiescent conditions.

1. Introduction

Biofuel cells are energy conversion systems in which enzymes are utilized as biocatalysts.[1-8] Due to the characteristics of the enzyme reaction, the power device can operate under very mild and safe conditions, e.g., at neutral pH, room temperature, and atmospheric pressure.[1-8] Moreover, the active sites in enzymes consist of nonprecious metals (e.g., Cu, Ni, Fe, Mo, and W) or organic compounds (e.g., nicotinamide adenine dinucleotide, flavin adenine dinucleotide, and quinones).[7-11] Although conventional polymer electrolyte H_2/O_2 fuel cells are known as clean and efficient energy conversion devices, they usually require Pt catalysts, which are expensive.[12-14] By utilizing hydrogenases[11,15,16] and multicopper oxidases (MCOs)[10] as catalysts for H_2 oxidation and O_2 reduction, respectively, a sustainable and environmentally friendly H_2/O_2 biofuel cell may be constructed.[2,6,17-25]

Bioelectrocatalysis, in which an enzyme reaction and an electrode reaction is coupled, is a key process for biofuel cells.[1-8] The reaction is classified into two types: mediated electron transfer (MET) and direct electron transfer (DET). In the MET-type system, an artificial redox mediator shuttles electrons between an electrode and an enzyme. Regarding performance of biofuel cells, mediators can minimize the kinetic barrier in the electron transfer between redox enzymes and electrodes. However, this often incurs a thermodynamic loss in order to create a driving force for the

electron transfer between an enzyme and an electrode, and thus often decreases the operating potential of biofuel cells.[1-8]

Conversely, in DET-type systems, an enzyme directly communicates with an electrode. This makes it possible to construct a compact and simple biofuel cell and to minimize the thermodynamic loss in the electron transfer between an enzyme and an electrode.[1-8] Hydrogenase,[11,15] fructose dehydrogenase (FDH),[26,27] glucose dehydrogenase,[28] and cellobiose dehydrogenase[29,30] are known to be enzymes capable of DET-type bioelectrocatalysis at bioanodes, and MCOs including bilirubin oxidase (BOD),[31-33] laccase,[34,35] and Cu efflux oxidase[36,37] are known to be DET-type enzymes for biocathodes. However, there are two major problems with DET-type biofuel cells: 1) Only a limited number of enzymes are suitable for DET-type bioelectrocatalysis; and 2) interfacial electron transfer kinetics between an enzyme and an electrode often becomes a kinetic bottleneck inducing large overpotentials.[4,38-42] Since the interfacial electron transfer rate constant decreases exponentially with an increase in the tunneling distance between the active site of an enzyme and an electrode[43,44], the orientation of an adsorbed enzyme is one of the most important factors in controlling the interfacial electron transfer kinetics.[4,38-42] Several approaches to realizing favorable enzyme orientation have been proposed, such as genomic enzyme modification,[45,46] electrode modification,[42,47-58] and screening of suitable electrode materials.[59-62]

Generally, MCOs have four Cu atoms as active sites (labeled as types I, II, and III based on their spectroscopic and magnetic properties).[10] Type I Cu and type II-III Cu clusters are known as the electron-accepting site and the catalytic site for $4e^-$ reduction of O_2, respectively.[10,63,64] Among the MCOs, BOD is a promising enzyme for DET-type biocathodes.[31-33] BOD has high bioelectrocatalytic-activity even at neutral pH, and its formal potential ($E°'_E$ = 0.46V vs. Ag|AgCl|sat. KCl at pH 7) is relatively close to that of the $2H_2O/O_2$ redox couple ($E°'_O$ = 0.62 V vs. Ag|AgCl|sat. KCl at pH 7).[65] The modification of electrodes and utilization of compatible electrode materials have been reported as effective methods to improve the interfacial electron transfer of BODs.[42,54-58,60,61] These methods include covalent modification by diazonium coupling[54] or oxidation of amines,[42] physical adsorption of bilirubin[55-57] or other aromatic compounds,[58] and utilization of functionalized carbon nanotubes (CNTs) such as pyrene-functionalized CNTs[60] and water-soluble CNTs with lengths of 1–4 μm.[61]

O_2-tolerant and O_2-sensitive [NiFe]-hydrogenases are often utilized for DET-type bioanodes.[2,6,17-25] In H_2 oxidation, H_2 binding to the Ni-SI state (active silent state) is the first step, and subsequently the catalytic cycle proceeds to the Ni-R (H_2-reduced state), Ni-C (one-electron-oxidized state of Ni-R), and Ni-SI states in turn.[11,15,16] In the presence of O_2, however, [NiFe]-hydrogenases become inactive.[11,15,16] Ni-A state (also termed the "unready" or irreversible inactive state) and Ni-B state (also termed the "ready" or reversible inactive state) have been reported.[11,15,16] The Ni-A state seems to be produced by one-electron oxidation of the Ni-SI state, in which a peroxide ligand is thought to coordinate to the Ni atom in the bridging position with respect to Fe(II).[11,15,16] However,

there has been much debate concerning the oxygenation of sulfur atoms near the active site in recent literature.[66] The Ni-B state is also produced by one-electron oxidation of the Ni-SI state, in which, in contrast to the Ni-A state, a hydroxide ligand is coordinated to the Ni atom in the bridging position with respect to Fe(II).[11,15,16] The O_2-tolerant mechanism has been considered due to the presence of a unique [FeS]-cluster close to the active site (i.e., a [4Fe-3S]-cluster coordinated by six Cys residues rather than a [4Fe-4S]-cluster coordinated by four Cys residues, as in other [NiFe]-hydrogenases) that transfers two electrons rapidly to the active site when the hydrogenase is attacked by O_2.[67-70] This property seems to enable O_2-tolerant [NiFe]-hydrogenases to form the Ni-B inactive state only under oxidative conditions.[11,39,71] Conversely, O_2-sensitive [NiFe]-hydrogenases form both of the inactive states (Ni-A and Ni-B states) under oxidative conditions.[11,15,16]

With regard to DET-type bioelectrocatalysis of hydrogenases, O_2-tolerant [NiFe]-hydrogenase[72-75] is specialized to H_2 oxidation and needs an overpotential for bioelectrochemical H_2-oxidation. Conversely, O_2-sensitive [NiFe]-hydrogenase[76,77] can realize a reversible and bidirectional catalytic reaction (H_2 oxidation and H^+ reduction), and the zero-current potential of the electrode is almost identical to the equilibrium potential of the $H_2/2H^+$ couple.[39]

Generally, electrode potentials that are high compared with the formal potential of the enzymes are required for bioanodes to achieve high-speed and enzyme-kinetics-controlled DET-type bioelectrocatalysis.[78] However, [NiFe]-hydrogenases suffer from high oxidative stress at such high potentials and inactive states (Ni-A and Ni-B states) are produced. This phenomena is called oxidative inactivation,[41,79-81] and causes power decay in H_2/O_2 biofuel cells. Schuhmann et al. and Lubitz et al. have proposed a new strategy to protect hydrogenases against oxidative inactivation in MET-type systems using a specifically designed viologen-based redox hydrogel.[82] Electron transfer between the polymer-bound viologen moieties controls the potential near the active site of the hydrogenase, and thus the redox hydrogel insulates the enzyme from excessive oxidative stress.[82]

Combining a MCO-adsorbed biocathode and [NiFe]-hydrogenase-adsorbed bioanode, we can construct a DET-type H_2/O_2 biofuel cell.[2,6,17-25] The low solubility of the gaseous substrates (H_2 and O_2) frequently causes a power decline. To solve this problem, a gas diffusion electrode that can supply a gaseous substrate to an enzyme from the gas phase has been proposed.[25,56,80,83-87] In addition, the gas diffusion electrode can maintain high substrate concentrations near the active enzyme on the electrode. This system is also useful for avoiding the aforementioned oxidative inactivation of [NiFe]-hydrogenases, since the inactivation is thought to compete with H_2 binding to the Ni-SI state.[80,85] Furthermore, the gas diffusion electrode allows independent supply of gaseous substrates to the bioanode and the biocathode, thus avoiding the risk of explosion on mixing of H_2 with and O_2, as reported in the literature.[19]

In this study, the author investigated waterproof carbon material as an electrode base in order to realize high gas permeability and created a new type of gas diffusion electrode. BOD and two kinds

of [NiFe]-hydrogenases (O_2-tolerant and O_2-resistant) were used to modify the electrode, and the resulting electrochemical properties were assessed. Finally, the author constructed a DET-type dual gas diffusion H_2/O_2 biofuel cell system, which is the first example of such in the field of biofuel cells.

2. Experimental

2.1 Chemicals

Waterproof carbon cloth (WPCC, EC-CC1-060T) was purchased from Toyo Corp., (Japan), and Ketjen black EC300J (KB) was kindly donated by Lion Corp., (Japan). Poly(1,1,2,2-tetrafluoroethylene) (PTFE, 6-J) fine powder was purchased from DuPont-Mitsui Fluorochemicals Co., Ltd., (Japan). Bilirubin was purchased from Wako Pure Chemical (Japan) and was dissolved in 30 mM NaOH aqueous solution. BOD (EC 1.3.3.5) from *Myrothecium verrucaria* was donated by Amano Enzyme Inc. (Japan) and used without further purification. O_2-tolerant membrane-bound [NiFe]-hydrogenase from *Hydrogenovibrio marinus* (*Hm*MBH) and O_2-sensitive [NiFe]-hydrogenase from *Desulfovibrio vulgaris* Miyazaki F (*Dv*MF) were purified according to the literature.[75,88] All other chemicals used in this study were of analytical grade unless otherwise specified, and all aqueous solutions were prepared with distilled water.

2.2 Electrode preparation

The gas diffusion electrode was prepared as follows: KB powder (40 mg) was mixed with PTFE and homogenized in 3.5 mL of 2-propanol for 3 min at 0 °C to prepare a KB slurry. Then, about 1.0 mL of the KB slurry was applied to one side of a 1.4 cm^2 piece of WPCC and dried. This electrode is termed KB/PTFE/WPCC. Bilirubin modification of KB/PTFE/WPCC was carried out according to the literature with minor modifications.[56] Briefly, 0.3 mL of bilirubin solution (1 mM) was applied to a KB/PTFE/WPCC electrode, which was previously dried at 60 °C, and the surface was washed with 10 mM phosphate buffer (pH 7) five times. The bilirubin-modified electrode is termed BL/KB/PTFE/WPCC.

A 0.3 mL aliquot of BOD solution (20 mg mL^{-1}) dissolved in 10 mM phosphate buffer (pH 7) was applied to the surface of a KB/PTFE/WPCC electrode and a BL/KB/PTFE/WPCC electrode. A 0.3 mL aliquot of *Hm*MBH solution (5 mg mL^{-1}) dissolved in 10 mM phosphate buffer (pH 7, containing 0.2 M NaCl and 0.025% Triton X-100) was applied to a KB/PTFE/WPCC electrode, and 0.3 mL of *Dv*MF solution (5 mg mL^{-1}) dissolved in 25 mM Tris-HCl buffer (pH 7.4) was applied to a further KB/PTFE/WPCC electrode. These electrodes were dried for 2 h under reduced pressure at room temperature.

2.3 Electrochemical measurements

Cyclic voltammetry and chronoamperometry were carried out on BAS CV50W and ALS 714C electrochemical analyzers, respectively. A handmade gas-diffusion-type electrolysis cell identical to that reported in a previous paper was used for the measurements.[56] The projected surface area of the working electrode was set to 1.0 cm^2. A Ti mesh served as a current collector. A Pt mesh and an Ag|AgCl|sat. KCl electrode were used as counter and reference electrodes, respectively. All potentials in this study are in reference to the reference electrode. The measurements were performed in 1.5 M citrate buffer (pH 5) at 40 °C under quiescent conditions, with O_2 and H_2 atmospheres at the biocathodes and bioanodes, respectively.

2.4 DET-type biofuel cells

Chronopotentiometry was carried out on an HA-151A (Hokuto Denko) electrochemical analyzer to evaluate the performance of the bioanode (*Dv*MF-adsorbed KB/PTFE/WPCC) and the biocathode (BOD-adsorbed BL/KB/PTFE/WPCC). The aforementioned gas-diffusion-type electrolysis cell identical to that reported in a previous paper[56] was used for the measurements. For practical application, it is normal to evaluate a cell performance using a one-compartment cell. However, complete separation of the H_2 and O_2 outlet gases was difficult in our experimental system. Thus, for safety, the author evaluated each of the single electrodes of the DET-type H_2/O_2 biofuel cell separately, but under the same conditions (except the flow gas, which was H_2 for the bioanode and O_2 for the biocathode).

3. Results and discussion

3.1 Optimization of KB/PTFE/WPCC with BOD

Figure 1 shows cyclic voltammograms (CVs) for the BOD-adsorbed KB/PTFE/WPCC (black line) and the BOD-adsorbed BL/KB/PTFE/WPCC (gray line) under quiescent and O_2 (solid lines) or Ar (dotted line) atmospheric conditions. The PTFE content was 50% (PTFE/PTFE+KB (wt%)) and the bilirubin concentration was 3 mM. The faradic waves are ascribed to O_2 reduction due to DET-type bioelectrocatalysis with BOD, as described in the literature.[32,42,54-58,60,61] The BOD-adsorbed BL/KB/PTFE/WPCC exhibits a clear catalytic wave with sigmoidal shape compared with the BOD-adsorbed KB/PTFE/WPCC. Modification with bilirubin is an effective way to induce a favorable orientation of the BOD,[55-57] and this characteristic indicates that the interfacial electron transfer between BOD and BL/KB/PTFE/WPCC is faster than that between BOD and

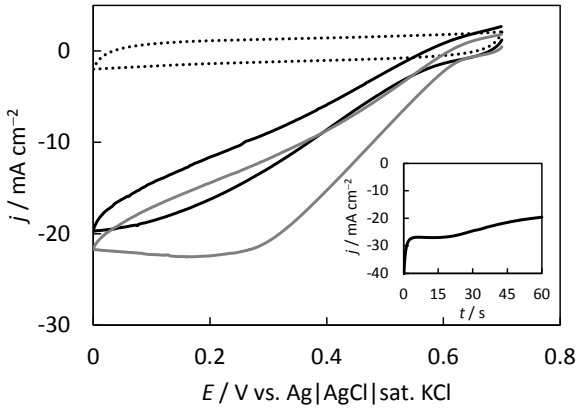

Figure 1
CVs for BOD-adsorbed KB/PTFE/WPCC (black line) and BL/KB/PTFE/WPCC (gray line). The scan rate was 10 mV s^{-1}. The inset shows CA for BOD-adsorbed KB/PTFE/WPCC. The electrode potential was 0 V. Measurements were carried out in 1.5 M citrate buffer (pH 5) at 40 °C under quiescent and O_2 (solid lines) or Ar (dotted line) atmospheric conditions. The PTFE content and the bilirubin concentration were 50% and 3 mM, respectively.

KB/PTFE/WPCC. In the case of KB/PTFE/WPCC, the most favorable BOD adsorption is realized by setting the bilirubin concentration to 3 mM (data not shown).

The inset of Fig. 1 shows a chronoamperogram (CA) at 0 V for the BOD-adsorbed KB/PTFE/WPCC. A steady-state catalytic reduction current at a current density of −25 mA cm^{-2} is obtained until about 15 s. However, the catalytic reduction current gradually decreases with time. Similar phenomena are observed even when the O_2 gas is blown forcibly onto the surface of the electrode (data not shown). These results indicate that the current decrease is not caused by O_2 depletion near the electrode surface. In addition, repeated CAs (by setting the electrode to open-circuit for 5 min before the second and third measurements) exhibit similar results (data not shown). It should be noted here that the steady-state reduction current is return to the initial value in the first chronoamperometric experiment. This indicates that the enzyme remains active for long time. The decrease in the current is most likely due to a slight change in balance of bio-three-phase balance that will be regulated by the electrode hydrophilicity/hydrophobicity and the H_2O amount (including a balance of generation and vaporization of H_2O). Since the reduction currents after 15 s in the CAs are controlled by the gas permeability, the author selected them as an index to optimize the PTFE content. The catalytic reduction current densities at the BOD-adsorbed KB/PTFE/WPCC with various PTFE contents are summarized in Fig. 2. The optimum PTFE content for the BOD-adsorbed KB/PTFE/WPCC is 50%, and the reduction current densities reach 26 ± 2 and 17 ± 3 mA cm^{-2} after 15 and 60 s, respectively (note here that the errors in this study were evaluated by the Student *t* distribution at a 90% confidence level). The performance is much better than that previously reported

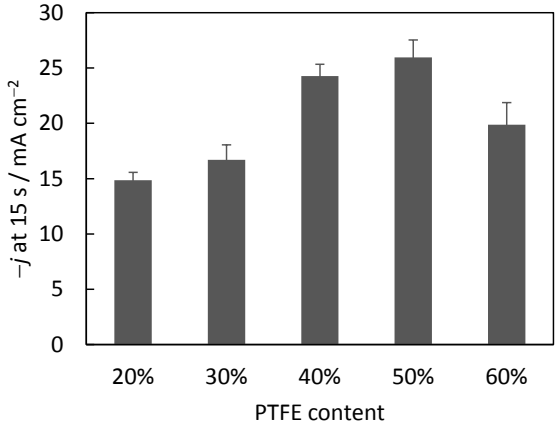

Figure 2
Effects of the PTFE content on the steady-state catalytic reduction current densities after 15 s in CA at 0 V. Measurements were carried out in 1.5 M citrate buffer (pH 5) at 40 °C under quiescent and O_2 atmospheric conditions. The error bars were evaluated by the Student *t* distribution at a 90% confidence level.

for DET-type O_2 reduction with gas-diffusion-type electrodes (about 13 mA cm^{-2}).[87] Accordingly, the author succeeded in constructing a DET-type gas diffusion bioelectrode with high gas permeability.

3.2 Gas-diffusion-type H_2-oxidation with [NiFe]-hydrogenases

The author utilized *Hm*MBH and *Dv*MF as catalysts for H_2 oxidation. Characteristic rotating disk voltammograms are observed for *Hm*MBH- and a *Dv*MF-adsorbed KB-modified electrodes (data not shown). The rotating disk mode was used to avoid concentration depletion near the electrode surface. In the case of the *Hm*MBH-adsorbed electrode (black line), an H_2-oxidation wave is observed and the current gradually decreases at positive potentials due to oxidative stress (i.e., oxidative inactivation, as discussed in the Introduction section). The apparent half-wave potential of the sigmoidal part of the steady-state wave ($E_{1/2}'$ = –0.39 V) is slightly more positive than the formal potential of the $H_2/2H^+$ redox couple at pH 6 ($E_{\mathbf{H}}°'_{pH=6}$ = −0.53 V). The overpotential (= $E_{1/2}' - E_{\mathbf{H}}°'$) is predominantly ascribed to the difference between $E_{\mathbf{H}}°'$ and the formal potential ($E_{\mathbf{E}}°'$) of the catalytic center of *Hm*MBH.[41] The *Dv*MF-adsorbed electrode (gray line) exhibits a reversible and bidirectional catalytic wave, i.e., H_2 oxidation at positive potentials and H^+ reduction at negative potentials.[77] $E_{1/2}'$ is –0.51 V and close to $E_{\mathbf{H}}°'_{pH=6}$. This means that the bioelectrocatalytic conversion between $H_2/2H^+$ does not require any overpotential. However, the oxidation current rapidly decreases at positive potentials due to oxidative inactivation.

Conversely, the author reported that the oxidative inactivation was able to be suppressed by using a gas diffusion system.[80,85] Figure 3 shows CVs of the *Hm*MBH- (black line) and the *Dv*MF-adsorbed KB/PTFE/WPCC (gray line) under quiescent and H_2 atmospheric conditions. The PTFE

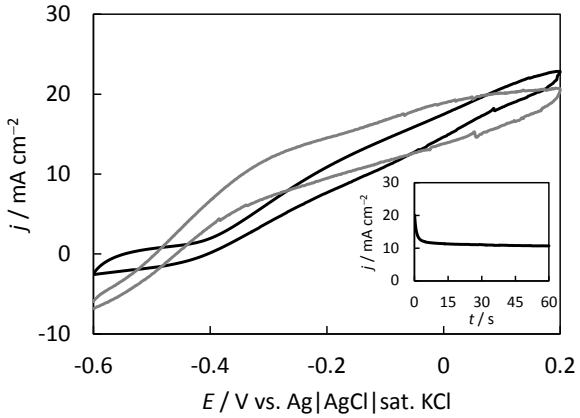

Figure 3
CVs of *Hm*MBH- and *Dv*MF-adsorbed KB/PTFE/WPCC (black and gray lines, respectively). The scan rate was 10 mV s^{-1}. The inset shows the CA of *Hm*MBH-adsorbed KB/PTFE/WPCC. The electrode potential was –0.1 V. Measurements were carried out in 1.5 M citrate buffer (pH 5) at 40 °C under quiescent and H_2 atmospheric conditions. The PTFE content was 50%.

content was set as 50%, as optimized in the above section (Fig. 2). The oxidation current densities at the *Hm*MBH-adsorbed KB/PTFE/WPCC continue to increase with the potential and reach a value of about 20 mA cm^{-2} at 0.2 V. The *Hm*MBH-adsorbed KB/PTFE/WPCC retains a large steady-state oxidation current density of 10 mA cm^{-2} at −0.1 V according to CA (Fig. 3, inset). The author can conclude that the H_2 supply is sufficient to suppress the oxidative inactivation of *Hm*MBH adsorbed on the KB/PTFE/WPCC at −0.1 V and to produce a large current density.

At the *Dv*MF-adsorbed KB/PTFE/WPCC, slight inactivation is still observed at potentials over 0.1 V (Fig. 3, gray line). However, multi-sweep CVs between −0.6 and −0.3 V show almost constant bioelectrocatalysis with a limiting current density of about 10 mA cm^{-2} (data not shown). This result suggests that the oxidative inactivation is largely prevented at the *Dv*MF-adsorbed KB/PTFE/WPCC in this potential range (up to −0.3 V). *Dv*MF (classified as O_2-sensitive) catalyzes the reversible and bidirectional H_2 oxidation and H^+ reduction and is able to catalyze electrochemical H_2 oxidation without overpotential. Consequently, the author utilized *Dv*MF (as well as BOD) to construct a DET-type H_2/O_2 biofuel cell.

3.3 DET-type dual gas-diffusion H_2/O_2 biofuel cells

The author constructed a dual gas diffusion H_2/O_2 biofuel cell with *Dv*MF-adsorbed KB/PTFE/WPCC and BOD-adsorbed BL/KB/PTFE/WPCC as the bioanode and biocathode, respectively. Normally, both the bioanode and the biocathode are placed in the biofuel cell assembly, and the polarization curve is obtained by changing the resistance between the anode and the cathode.[2,6]

However, due to possible gas leakage from the biofuel cells and the commensurate risk of explosion, it is dangerous to operate a dual gas diffusion H_2/O_2 biofuel cell in a conventional experimental situation. Thus, in this study, the performances of the bioanode and the biocathode were evaluated separately by chronopotentiometry (CP) for 15 s under the same conditions except for the flow gas (H_2 and O_2 gas were supplied to the bioanode and the biocathode, respectively). In our experience with H_2/O_2 biofuel cells, the polarization curve of a biofuel cell assembly is almost identical to that obtained when the bioanode and the biocathode are evaluated separately.[17]

Potentiograms of the *Dv*MF-adsorbed KB/PTFE/WPCC and the BOD-adsorbed BL/KB/PTFE/WPCC are measured (data not shown). Although the potentials change gradually under large current densities (e.g., 15 mA cm^{-2} for the anode and 28 mA cm^{-2} for the cathode), the potentials at lower current densities show steady-state characteristics. Figure 4 (A) shows the potentials of the bioanode and the biocathode in CP recorded 15 s after closing the circuit as a function of the current density. Figure 4 (B) shows the current density dependences of the cell voltage and the cell power

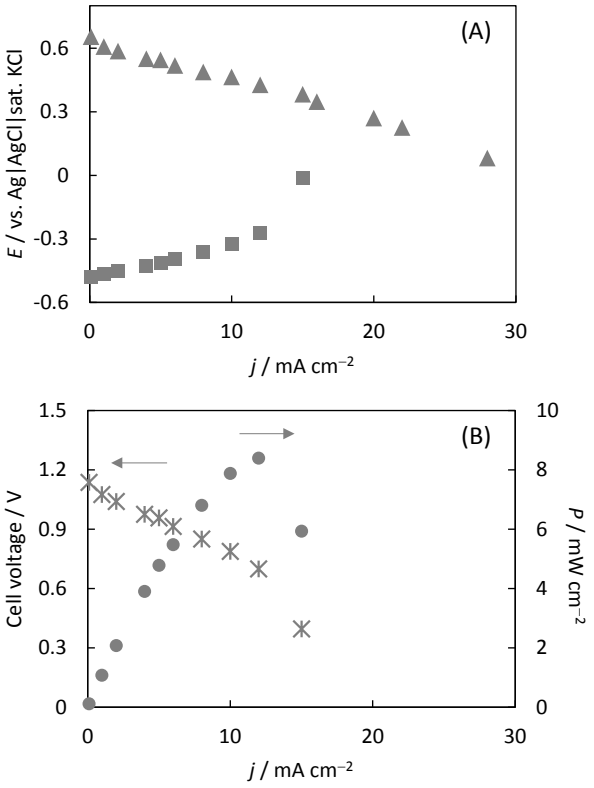

Figure 4
(A) Polarization curves of a DET-type dual gas diffusion H_2/O_2 biofuel cell. The potentials of the bioanode and the biocathode as measured in CP are plotted as functions of the current density. The measurements were carried out in 1.5 M citrate buffer (pH 5) at 40 °C under quiescent and H_2 and O_2 atmospheric conditions for the bioanode or the biocathode, respectively.
(B) The cell voltage and the power density as a function of the current density of the biofuel cell.

density calculated from the data in Fig. 4 (A). The open-circuit voltage is 1.14 ± 0.03 V and is close to the standard motive force of the ideal H_2/O_2 cell (1.23 V). The maximum power density is 8.4 ± 0.5 mW cm^{-2} at 0.7 V of the cell voltage. The power density can be compared with that of a recent polymer electrolyte H_2/O_2 fuel cell with Pt as the catalyst (68 mW cm^{-2} at 0.21 V at 1 atm, 40 °C, in a membrane-electrode assembly system with single cell).[14]

Since the effects of oxidative inactivation on the current increase for high current densities at the bioanode, it is difficult to correctly evaluate the cell performance for current densities above 15 mA cm^{-2}. However, the author can certainly report that a powerful H_2/O_2 DET-type biofuel cell with dual gas diffusion has been successfully constructed.

Figure 5 summarizes recent developments in the power densities of H_2/O_2 biofuel cells (in both MET- and DET-type systems) and DET-type biofuel cells with other fuels as reported in the literature.[2,6,89-91] The data for biofuel cells utilizing Pt as the cathode catalyst are not included, because the author attempted to comprehensively compare the performance of the biofuel cells with the bioanode and the biocathode. As judged from Fig. 5, the performance of our biofuel cell is 5.6 times better than that of the best H_2/O_2 biofuel cell in the literature and 3.2 times larger than that of DET-type biofuel cells with other fuels.

Since the concentrations of H_2 and O_2 in solution are proportional to the partial pressures of the H_2 and O_2 gases, it is impossible to realize a saturated condition for both gases without a separator in the solution.[17,20,22,24] In addition, the risk of explosion on mixing the H_2 and O_2 gases is debated.[19] Gas diffusion electrodes avoid these problems.[25] By constructing gas diffusion electrodes for the

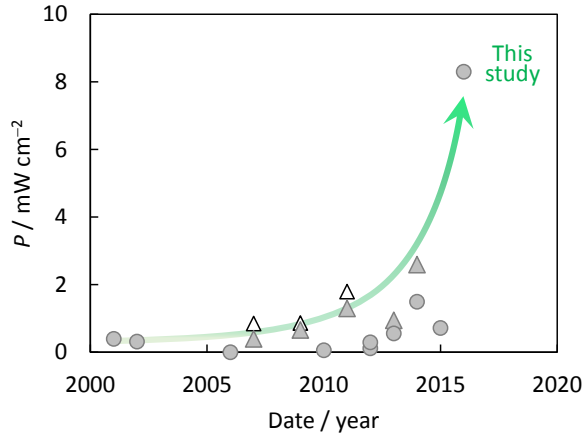

Figure 5
Recent advancement in the power density of H_2/O_2 biofuel cells and DET-type biofuel cells. The power densities of H_2/O_2 biofuel cells and DET-type biofuel cells with other fuels are indicated with circles and triangles, respectively. The open triangles are the values evaluated under stirring conditions. Power densities measured from a single-layer cell with identical bioanode and the biocathode surface areas are presented to fairly compare their performances.

bioanode and the biocathode, the author is able to completely separate the H_2 and O_2 gas inlets and realize high concentrations of the gas substrates for both the bioanode and the biocathode.

From the viewpoint of DET-type biofuel cells with other fuels, FDH is a promising catalyst for bioanodes,[56,59,83,89,90] since FDH has a high DET-type bioelectrocatalytic activity and exhibits about 40 mA cm^{-2} at porous carbon electrodes.[56] However, its maximum power density is limited to 2.6 mW cm^{-2} (6 mA cm^{-2} at 0.45 V of the cell voltage) due to a large overpotential ascribed to thermodynamic loss in the electron transfer from the substrate (D-fructose) to FDH and a kinetic barrier in the electron transfer from FDH to the electrode.[27,38]. Conversely, $E_{1/2}'$ of the catalytic wave on the *Dv*MF-adsorbed KB/PTFE/WPCC is close to $E_{\mathbf{H}}°'$ thanks to the reversible characteristics of *Dv*MF and fast interfacial electron transfer kinetics. Consequently, these characteristics contribute to the realization of high operating potential, which results in a high power density.

4. Conclusions

A novel gas diffusion bioelectrode fabricated with WPCC was created and optimized. The electrode showed a high gas permeability, which realized steady-state catalytic current densities as large as 10 mA cm^{-2} for H_2 oxidation and O_2 reduction. For the biocathode, the electron transfer between BOD and the KB/PTFE/WPCC was accelerated by bilirubin modification.[56] For the bioanode, the gas diffusion electrode greatly suppressed the oxidative inactivation of *Hm*MBH and *Dv*MF. By combining the *Dv*MF-adsorbed KB/PTFE/WPCC and the BOD-adsorbed BL/KB/PTFE/WPCC, the author succeeded in constructing a DET-type dual gas diffusion H_2/O_2 biofuel cell. This is the first report of a dual gas-diffusion system in the field of biofuel cells, and enables us to separately supply the gas substrates (H_2 or O_2) from the gas phases of the bioanode and the biocathode. Therefore, it becomes possible to independently control the substrate supply to the bioanode and the biocathode. The cell exhibited a power density of 8.4 mW cm^{-2} at 0.7 V of the cell voltage under quiescent conditions by flowing the H_2 and O_2 gases into the gas phases of the bioanode and biocathode, respectively. This value is 5.6 and 3.2 times larger than those of the best reported H_2/O_2 biofuel cell and the best DET-type biofuel cell with other fuels, respectively.

5. References

1 S. C. Barton, J. Gallaway and P. Atanassov, *Chem. Rev.*, 2004, **104**, 4867.

2 A. D. Poulpiquet, D. Ranava, K. Monsalve, M. Giudici-Orticoni and E. Lojou, *ChemElectroChem*, 2014, **1**, 1724.

3 D. Leech, P. Kavanagh and W. Schuhmann, *Electrochim. Acta*, 2012, **84**, 223.

4 C. Léger and P. Bertrand, *Chem. Rev.*, 2008, **108**, 2379.

5 N. Mano, F. Mao and A. Heller, *ChemBioChem*, 2004, **5**, 1703.
6 M. Rasmussen, S. Abdellaoui and S. D. Minteer, *Biosens. Bioelectron.*, 2016, **76**, 91.
7 J. A. Cracknell, K. A. Vincent and F. A. Armstrong, *Chem. Rev.*, 2008, **108**, 2439.
8 M. Zhou, *Electroanalysis*, 2015, **27**, 1786.
9 A. Kietzin and M. W. W. Adams, *FEMS Microbiol. Rev.*, 1996, **18**, 5.
10 E. I. Solomon, U. M. Sundaram and T. E. Machonkin, *Chem. Rev.*, 1996, **96**, 2563.
11 K. A. Vincent, A. Parkin and F. A. Armstrong, *Chem. Rev.*, 2007, **107**, 4366.
12 B. C. H. Steele and A. Heinzel, *Nature*, 2001, **414**, 345.
13 M. Z. Jacobson, W. G. Colella and D. M. Golden, *Science*, 2005, **308**, 1901.
14 M. R. Berber, T. Fujigaya, K. Sasaki and N. Nakashima, *Sci. Rep.*, 2013, **3**, 1764.
15 H. S. Shafaat, O. Rüdiger, H. Ogata and W. Lubitz, *Biochim. Biophys. Acta*, 2013, **1827**, 986.
16 T. Yagi and Y. Higuchi, *Proc. Jpn. Acad. Ser. B*, 2013, **89**, 16.
17 S. Tsujimura, M. Fujita, H. Tatsumi, K. Kano and T. Ikeda, *Phys. Chem. Chem. Phys.*, 2001, **3**, 1331.
18 M. R. Tarasevich, V. A. Bogdanovskaya, N. M. Zagudaeva and A. V Kapustin, *Russ. J. Electrochem.*, 2002, **38**, 335.
19 K. A. Vincent, J. A. Cracknell, J. R. Clark, M. Ludwig, O. Lenz, B. Friedrich and F. A. Armstrong, *Chem. Commun.*, 2006, 5033.
20 A. F. Wait, A. Parkin, G. M. Morley, L. D. Santos and F. A. Armstrong, *J. Phys. Chem. C*, 2010, **114**, 12003.
21 S. Krishnan and F. A. Armstrong, *Chem. Sci.*, 2012, **3**, 1015.
22 A. Ciaccafava, A. D. Poulpiquet, V. Techer, M. T. Giudici-Orticoni, S. Tingry, C. Innocent and E. Lojou, *Electrochem. Commun.*, 2012, **23**, 25.
23 L. Xu and F. A. Armstrong, *Energy Environ. Sci.*, 2013, **6**, 2166.
24 A. D. Poulpiquet, A. Ciaccafava, R. Gadiou, S. Gounel, M. T. Giudici-Orticoni, N. Mano and E. Lojou, *Electrochem. Commun.*, 2014, **42**, 72.
25 N. Lalaoui, A. D. Poulpiquet, R. Haddad, A. L. Goff, M. Holzinger, S. Gounel, M. Mermoux, P. Infossi, N. Mano, E. Lojou and S. Cosnier, *Chem. Commun.*, 2015, **51**, 7447.
26 S. Kawai, M. Goda-Tsutsumi, T. Yakushi, K. Kano and K. Matsushita, *Appl. Environ. Microbiol.*, 2013, **79**, 1654.
27 S. Kawai, T. Yakushi, K. Matsushita, Y. Kitazumi, O. Shirai and K. Kano, *Electrochem. Commun.*, 2014, **38**, 28.
28 V. Flexer, F. Durand, S. Tsujimura and N. Mano, *Anal. Chem.*, 2011, **83**, 5721.

29 A. Lindgren, L. Gorton, T. Ruzgas, U. Baminger, D. Haltrich and M. Schülein, *J. Electroanal. Chem.*, 2001, **496**, 76.

30 V. Fridman and U. Wollenberger, V. Bogdanovskaya, F. Lisdat, A. Lindfren, L. Gorton and F. W. Scheller, *Biochem. Soc. Trans.*, 2000, **28**, 63.

31 S. Murao and N. Tanaka, *Agric. Biol. Chem.*, 1981, **45**, 2383.

32 S. Tsujimura, T. Nakagawa, K. Kano and T. Ikeda, *Electrochemistry*, 2004, **72**, 437.

33 N. Mano and L. Edembe, *Biosens. Bioelectron.*, 2013, **50**, 478.

34 M. R. Tarasevich, A. I. Yaropolov, V. A. Bogdanovskaya and S. D. Varfolomeev, *J. Electroanal. Chem.*, 1979, **104**, 393.

35 S. Shleev, A. Jarosz-Wilkolazka, A. Khalunina, O. Morozova, A. Yaropolov, T. Ruzgas and L. Gorton, *Bioelectrochemistry*, 2005, **67**, 115.

36 K. Kataoka, H. Komori, Y. Ueki, Y. Konno, Y. Kamitaka, S. Kurose, S. Tsujimura, Y. Higuchi, K. Kano, D. Seo and T. Sakurai, *J. Mol. Biol.*, 2007, **373**, 141.

37 Y. Miura, S. Tsujimura, S. Kurose, Y. Kamitaka, K. Kataoka, T. Sakurai and K. Kano, *Fuel Cells*, 2009, **9**, 70.

38 C. Léger and A. Jones, S. P. J. Albracht and F. A. Armstrong, *J. Phys. Chem. B*, 2002, **106**, 13058.

39 C. Léger, A. K. Jones, W. Roseboom, S. P. J. Albracht and F. A. Armstrong, *Biochemistry*, 2002, **41**, 15736.

40 V. Fourmond, C. Baffert, K. Sybirna, T. Lautier, A. A. Hamdan, S. Dementin, P. Soucaille, I. Meynial-Salles, H. Bottin and C. Léger, *J. Am. Chem. Soc.*, 2013, **135**, 3926.

41 K. So, R. Hamamoto, R. Takeuchi, Y. Kitazumi, O. Shirai, R. Endo, H. Nishihara, Y. Higuchi and K. Kano, *J. Electroanal. Chem.*, 2016, **766**, 152.

42 H. Xia, Y. Kitazumi, O. Shirai and K. Kano, *J. Electroanal. Chem.*, 2016, **763**, 104.

43 C. C. Page, C. C. Moser, X. Chen and P. L. Dutton, *Nature*, 1999, **402**, 47.

44 R. A. Marcus, *Angew. Chem. Int. Ed.*, 1993, **32**, 1111.

45 V. Balland, C. Hureau, A. M. Cusano, Y. Liu, T. Tron and B. Limoges, *Chem. Eur. J.*, 2008, **14**, 7186.

46 M. Sosna, H. Boer and P. N. Bartlett, *ChemPhysChem*, 2013, **14**, 2225.

47 P. Olejnik, B. Palys, A. Kowalczyk and A. M. Nowicka, *J. Phys. Chem. C*, 2012, **116**, 25911.

48 M. T. Meredith, M. Minson, D. Hickey, K. Artyushkova, D. T. Glatzhofer and S. D. Minteer, *ACS Catal.*, 2011, **1**, 1683.

49 K. Stolarczyk, M. Sepelowska, D. Lyp, K. Zelechowska, J. F. Biernat, J. Rogalski, K. D. Farmer, K. N. Roberts and R. Bilewicz, *Bioelectrochemistry*, 2012, **87**, 154.

50 C. F. Blanford, R. S. Heath and F. A. Armstrong, *Chem. Commun.*, 2007, 1710.

51 M. Pita, C. Gutierrez-Sanchez, D. Olea, M. Velez, C. Garcia-Diego, S. Shleev, V. M. Fernandez and A. L. De Lacey, *J. Phys. Chem. C*, 2011, **115**, 13420.

52 C. Vaz-Dominguez, S. Campuzano, O. Rüdiger, M. Pita, M. Gorbacheva, S. Shleev, V. M. Fernandez and A. L. De Lacey, *Biosens. Bioelectron.*, 2008, **24**, 531.

53 V. Balland, C. Hureau, A. M. Cusano, Y. Liu, T. Tron and B. Limoges, *Chem. Eur. J.*, 2008, **14**, 7186.

54 L. D. Santos, V. Climent, C. F. Blanford and F. A. Armstrong, *Phys. Chem. Chem. Phys.*, 2010, **12**, 13962.

55 J. A. Cracknell, T. P. McNamara, E. D. Lowe and C. F. Blanford, *Dalton Trans.*, 2011, **40**, 6668.

56 K. So, S. Kawai, Y. Hamano, Y. Kitazumi, O. Shirai, M. Hibi, J. Ogawa and K. Kano, *Phys. Chem. Chem. Phys.*, 2014, **16**, 4823.

57 R. J. Lopez, S. Babanova, Y. Ulyanova, S. Singhal and P. Atanassov, *ChemElectroChem*, 2014, **1**, 241.

58 G. Göbel and F. Lisdat, *Electrochem. commun.*, 2008, **10**, 1691.

59 T. Miyake, S. Yoshino, T. Yamada, K. Hata and M. Nishizawa, *J. Am. Chem. Soc.*, 2011, **133**, 5129.

60 M. Jönsson-Niedziolka, A. Kaminska and M. Opallo, *Electrochim. Acta*, 2010, **55**, 8744.

61 K. So, M. Onizuka, T. Komukai, Y. Kitazumi, O. Shirai and K. Kano, *Electrochim. Acta*, 2016, **192**, 133.

62 C. Gutiérrez-Sánchez, M. Pita, C. Vaz-Domínguez, S. Shleev and A. L. D. Lacey, *J. Am. Chem. Soc.*, 2012, **134**, 17212.

63 S. Shleev, J. Tkac, A. Christenson, T. Ruzgas, A. I. Yaropolov, J. W. Whittaker and L. Gorton, *Biosens. Bioelectron.*, 2005, **20**, 2517.

64 K. Kataoka, R. Sugiyama, S. Hirota, M. Inoue, K. Urata, Y. Minagawa, D. Seo and T. Sakurai, *J. Biol. Chem.*, 2009, **284**, 14405.

65 S. Tsujimura, A. Kuriyama, N. Fujieda, K. Kano and T. Ikeda, *Anal. Biochem.*, 2005, **337**, 325.

66 A. Volbeda, L. Martin, P. Liebgott, A. L. D. Lacey and J. C. Fontecilla-Camps, *Metallomics*, 2015, **7**, 710.

67 T. Goris, A. F. Wait, M. Saggu, J. Fritsch, N. Heidary, M. Stein, I. Zebger, F. Lendzian, F. A. Armstrong, B. Friedrich and O. Lenz, *Nat. Chem. Biol.*, 2011, **7**, 310.

68 M. Pandelia, W. Nitschke, P. Infossi, M. Giudici-Orticoni, E. Bill and W. Lubitz, *Proc. Natl. Acad. Sci. U. S. A.*, 2011, **108**, 6097.

69 M. M. Roessler, R. M. Evans, R. A. Davies, J. Harmer and F. A. Armstrong, *J. Am. Chem. Soc.*, 2012, **134**, 15581.

70 Y. Shomura, K. Yoon, H. Nishihara and Y. Higuchi, *Nature*, 2011, **479**, 253.

71 A. A. Hamdan, B. Burlat, O. Gutiérrez-Sanz, P. Liebgott, C. Baffert, A. L. D. Lacey, M. Rousset, B. Guigliarelli, C. Léger and S. Dementin, *Nat. Chem. Biol.*, 2013, **9**, 15.

72 J. Fritsch, P. Scheerer, S. Frielingsdorf, S. Kroschinsky, B. Friedrich, O. Lenz and C. M. T. Spahn, *Nature*, 2011, **479**, 249.

73 M. Pandelia, V. Fourmond, P. Tron-Infossi, E. Lojou, P. Bertrand, C. Léger, M. Giudici-Orticoni and W. Lubitz, *J. Am. Chem. Soc.*, 2010, **132**, 6991.

74 J. A. Cracknell, A. F. Wait, O. Lenz, B. Friedrich and F. A. Armstrong, *Proc. Natl. Acad. Sci. U. S. A.*, 2009, **106**, 20681.

75 K. Yoon, K. Fukuda, K. Fujisawa and H. Nishihara, *Int. J. Hydrogen Energy*, 2011, **36**, 7081.

76 A. K. Jones, E. Sillery, S. P. J. Albracht and F. A. Armstrong, *Chem. Commun.*, 2002, 866.

77 D. Millo, P. Hildebrandt, M. Pandelia, W. Lubitz and I. Zebger, *Angew. Chemie. Int. Ed.*, 2011, **50**, 2632.

78 A. J. Bard and L. R. Faulkner, Electrochemical methods: fundamentals and applications, 2nd ed., Wiley, New York.

79 A. A. Hamdan, P. Liebgott, V. Fourmond, O. Gutiérrez-Sanz, A. L. D. Lacey, P. Infossi, M. Rousset, S. Dementin and C. Léger, *Proc. Natl. Acad. Sci. U. S. A.*, 2012, **109**, 19916.

80 K. So, Y. Kitazumi, O. Shirai, K. Kurita, H. Nishihara, Y. Higuchi and K. Kano, *Bull. Chem. Soc. Jpn.*, 2014, **87**, 1177.

81 V. Fourmond, P. Infossi, M. Giudici-Orticoni, P. Bertrand and C. Léger, *J. Am. Chem. Soc.*, 2010, **132**, 4848.

82 N. Plumeré, O. Rüdiger, A. A. Oughli, R. Williams, J. Vivekananthan, S. Pöller, W. Schuhmann and W. Lubitz, *Nat. Chem.*, 2014, **6**, 822.

83 T. Miyake, K. Haneda, S. Yoshino and M. Nishizawa, *Biosens. Bioelectron.*, 2013, **40**, 45.

84 G. Gupta, C. Lau, V. Rajendran, F. Colon, B. Branch, D. Ivnitski and P. Atanassov, *Electrochem. Commun.*, 2011, **13**, 247.

85 K. So, Y. Kitazumi, O. Shirai, K. Kurita, H. Nishihara, Y. Higuchi and K. Kano, *Chem. Lett.*, 2014, **43**, 1575.

86 S. C. Barton, *Electrochim. Acta*, 2005, **50**, 2145.

87 K. So, M. Onizuka, T. Komukai, Y. Kitazumi, O. Shirai and K. Kano, *Electrochem. Commun.*, 2016, 66, 58.

88 Y. Higuchi, N. Yasuoka, M. Kakudo,Y. Katsube, T. Yagi, and H. Inokuchi, *J. Biol. Chem.*, 1987, **262**, 2823

89 Y. Kamitaka, S. Tsujimura, N. Setoyama, T. Kajino and K. Kano, *Phys. Chem. Chem. Phys.*, 2007, **9**, 1793.

90 K. Murata, K. Kajiya, N. Nakamura and H. Ohno, *Energy Environ. Sci.*, 2009, **2**, 1280.

91 A. Zebda, C. Gondran, A. L. Goff, M. Holzinger, P. Cinquin and S. Cosnier, *Nat. Commun.*, 2011, **2**, 370.

Conclusions

In this research, the author succeeded in constructing a DET-type dual gas diffusion H_2/O_2 biofuel cell with BOD and [NiFe]-hydrogenase. This is the first report of a dual gas diffusion-type system in the field of biofuel cells, and the system overcomes several problems of previous H_2/O_2 biofuel cells such as “mass-transport limitation of substrates” and “oxidative inactivation”.

In chapter 1, the author developed some methods to enhance DET-type bioelectrocatalysis of BOD. The author also examined and compared the characteristics of BOD-adsorbed electrodes in DET-type bioelectrocatalysis for O_2 reduction. The effect of the mass-transport on the catalytic current was minimized by decreasing the BOD activity at low temperature and high pH. This operation was carried out to more accurately extract the kinetic parameters of the enzyme reaction and interfacial electron transfer steps from the voltammetric data. The electrochemical analysis revealed that the improvement obtained upon application of both methods was predominantly ascribed to an increased amount of effective enzymes (i.e., enzymes with productive orientation) and that the interfacial electron transfer remained nearly unchanged. In addition, the author successfully detected clear non-catalytic redox signals of adsorbed BOD in BOD/MWCNT/GCE and BOD/BL/MWCNT/GCE samples owing to their high $\Gamma_{\mathrm{enz,eff}}$ values.

In chapter 2, the author constructed two kinds of gas diffusion-type electrodes with KB or MWCNT as carbon materials. Optimization of the electrodes are carried out by monitoring BOD catalyzed O_2 reduction current. The electrodes showed high gas permeability, which realized steady-state catalytic current densities over 25 mA cm^{-2} under quiescent conditions. On the other hand, the author successfully simulated the bioelectrocatalytic CVs at [NiFe]-hydrogenase adsorbed electrode with thermodynamic and kinetic analysis. The author also found that the oxidative inactivation of [NiFe]-hydrogenases could be inhibited by increasing H_2 concentration. In fact, the inactivation hardly happened in gas diffusion-type system.

In chapter 3, the author created a novel DET-type dual gas diffusion H_2/O_2 biofuel cell. The system can separately supply the gas substrates (H_2 or O_2) from the gas phases of the bioanode and the biocathode. Therefore, it becomes possible to independently control the substrate supply to the bioanode and the biocathode. The cell exhibited a power density of 8.4 mW cm^{-2} at 0.7 V of the cell voltage under quiescent conditions. This value is 5.6 and 3.2 times larger than those of the best reported H_2/O_2 biofuel cell and the best DET-type biofuel cell with other fuels, respectively.

Acknowledgments

The author wishes to express his sincere and heartfelt gratitude to Dr. Kenji Kano, Professor of Kyoto University for providing him with his continuous guidance, valuable discussion, and encouragement throughout this study, and Osamu Shirai, Associate Professor of Kyoto University, for a number of helpful suggestions and criticisms. The author would like to thank Dr. Yuki Kitazumi, Assistant Professor of Kyoto University, for his kind supports and a number of critical comments.

The author is very grateful to Dr. Yoshiki Higuchi, Professor of University of Hyogo, Dr. Shun Hirota, Professor of Nara Institute of Science and Technology, Dr. Yasuhito Shomura, Associate Professor of Ibaraki University, Dr. Koji Nishikawa, Assistant Professor of University of Hyogo and Dr. Hu-lin Tai, Specially Appointed Assistant Professor of Nara Institute of Science and Technology for their continuous support and advice concerning to the research of hydrogenases.

The author shows his appreciation to Dr. Jun Ogawa, Professor of Kyoto University, Dr. Keiko Kita, Professor of Kyoto University, Dr. Tatsuo Kurihara, Professor of Kyoto University, Dr. Masaru Mato, Professor of Kyoto University, Dr. Bunzo Mikami, Professor of Kyoto University, Dr. Hisashi Miyagawa, Dr. Hideto Miyoshi, Professor of Kyoto University, Professor of Kyoto University, Dr. Yasuyoshi Sakai, Professor of Kyoto University, Dr. Kazumitsu Ueda, Professor of Kyoto University, Dr. Mitsuyoshi Ueda, Professor of Kyoto University, and Dr. Takashi Watanabe, Professor of Kyoto University for their critical comments and kind supports.

The author gratefully thanks to the members of Kano's laboratory, Mr. Katsumi Hamamoto, Dr. Tatsuo Noda, Dr. Shintaro Kubota, Dr. Chi-hua Nieh, Mr. Yu Sugimoto, Mr. Masafumi Asahi, Mr. Tsukasa Inoue, Mr. Noriyoshi Ueya, Mr. Takafumi Yamauchi, Mr. Itaru Asano, Dr. Shota Kawai, Ms. Yuko Inoue-Kikuchi, Ms. Michiko Shinmura, Mr. Yasuyuki Hamano, Mr. Kei Hichiri, Mr. Yuki Kushida, Mr. Maruyama, Mr. Hajime Yamada, Mr. Hiroki Kagohashi, Mr. Masahiro Takeshige, Mr. Rui, Hamamoto, Ms. Kanako Hamano-Chimori, Mr. Hong-qi Xia, Mr. Issei Hirata, Mr. Masahiro Hori, Mr. Keisuke Kimura, Mr. Kento Sakai, Mr. Yasunari Takano, Mr. Yuya Hibino, Mr. Masaki Motoike, Mr. Arato Suzuki, Mr. Yutaka Takeuchi, Mr. Kebin Xu, Mr. Ryutaro Katsube, Mr. Ryosuke Takeuchi, Mr. Takuya Yamaguchi, Ms. Yuko Fukao, Ms. Yukina Matsui, Mr. Eisaku Nakao, Ms. Saeko Shiraiwa, Ms. Maiko Kaji, Ms. Akiho Kojima, Ms. Yui Takahashi, Mr. Masaki Takaishi, and Ms.Toshie Koyama, for their kind support in the author's laboratory life.

Finally, the author would like to express his greatest thanks to his family for their continuous encouragement.

Keisei So

Kyoto

March 2017

List of Publications

Keisei So, Shota Kawai, Yasuyuki Hamano, Yuki Kitazumi, Osamu Shirai, Makoto Hibi, Jun Ogawa, and Kenji Kano
Improvement of a direct electron transfer-type fructose/dioxygen biofuel cell with a substrate-modified biocathode
Phys. Chem. Chem. Phys., **16** (2014) 4823-4829. (Chapter 1, 1-1)

Keisei So, Maki Onizuka, Takuji Komukai, Yuki Kitazumi, Osamu Shirai, and Kenji Kano
Significance of the Length of Carbon Nanotubes on the Bioelectrocatalytic Activity of Bilirubin Oxidase for Dioxygen Reduction
Electrochim. Acta, **192** (2016) 133-138. (Chapter 1, 1-2)

Keisei So, Yuki Kitazumi, Osamu Shirai, and Kenji Kano
Analysis of factors governing direct electron transfer-type bioelectrocatalysis of bilirubin oxidase at modified electrodes
J. Electroanal. Chem., **783** (2016) 316-323. (Chapter 1, 1-3)

Keisei So, Maki Onizuka, Takuji Komukai, Yuki Kitazumi, Osamu Shirai, and Kenji Kano
Binder/surfactant-free biocathode with bilirubin oxidase for gas-diffusion-type system
Electrochem. Commun., **66** (2016) 58-61. (Chapter 2, 2-1)

Keisei So, Yuki Kitazumi, Osamu Shirai, Kouhei Kurita, Hirofumi Nishihara, Yoshiki Higuchi, and Kenji Kano
Gas-diffusion and Direct-electron-transfer-type Bioanode for Hydrogen Oxidation with Oxygen-tolerant [NiFe]-hydrogenase as an Electrocatalyst
Chem. Lett., **43** (2014) 1575-1577. (Chapter 2, 2-2)

Keisei So, Yuki Kitazumi, Osamu Shirai, Kouhei Kurita, Hirofumi Nishihara, Yoshiki Higuchi, and Kenji Kano
Kinetic Analysis of Inactivation and Enzyme Reaction of Oxygen-Tolerant [NiFe]-Hydrogenase at Direct Electron-Transfer Bioanode
Bull. Chem. Soc. Jpn., **87** (2014) 1177-1185. (Chapter 2, 2-3)

Keisei So, Rui Hamamoto, Ryosuke Takeuchi, Yuki Kitazumi, Osamu Shirai, Ryohei Endo, Hirofumi

Nishihara, Yoshiki Higuchi, and Kenji Kano
Bioelectrochemical analysis of thermodynamics of the catalytic cycle and kinetics of the oxidative inactivation of oxygen-tolerant [NiFe]-hydrogenase
J. Electroanal. Chem., **766** (2016) 152-161. (Chapter 2, 2-4)

Keisei So, Yuki Kitazumi, Osamu Shirai, Koji Nishikawa, Yoshiki Higuchi, and Kenji Kano
Direct electron transfer-type dual gas diffusion H_2/O_2 biofuel cells
J. Mater. Chem. A, **4** (2016) 8742-8749. (Chapter 3, 3-1)